

LOCKHEED MARTIN ENERGY RESEARCH LIBRARIES



3 4456 0514902 3

CENTRAL RESEARCH LIBRARY

ORNL-TM-3969

cy. 1

FUELS AND MATERIALS DEVELOPMENT PROGRAM
QUARTERLY PROGRESS REPORT
FOR PERIOD ENDING JUNE 30, 1972

P. Patriarca

OAK RIDGE NATIONAL LABORATORY
CENTRAL RESEARCH LIBRARY
DOCUMENT COLLECTION

LIBRARY LOAN COPY

DO NOT TRANSFER TO ANOTHER PERSON

If you wish someone else to see this
document, send in name with document
and the library will arrange a loan.

UCN-7969
13 3-671



OAK RIDGE NATIONAL LABORATORY

OPERATED BY UNION CARBIDE CORPORATION • FOR THE U.S. ATOMIC ENERGY COMMISSION

This report was prepared as an account of work sponsored by the United States Government. Neither the United States nor the United States Atomic Energy Commission, nor any of their employees, nor any of their contractors, subcontractors, or their employees, makes any warranty, express or implied, or assumes any legal liability or responsibility for the accuracy, completeness or usefulness of any information, apparatus, product or process disclosed, or represents that its use would not infringe privately owned rights.

Contract No. W-7405-eng-26

METALS AND CERAMICS DIVISION

FUELS AND MATERIALS DEVELOPMENT PROGRAM QUARTERLY PROGRESS
REPORT FOR PERIOD ENDING JUNE 30, 1972

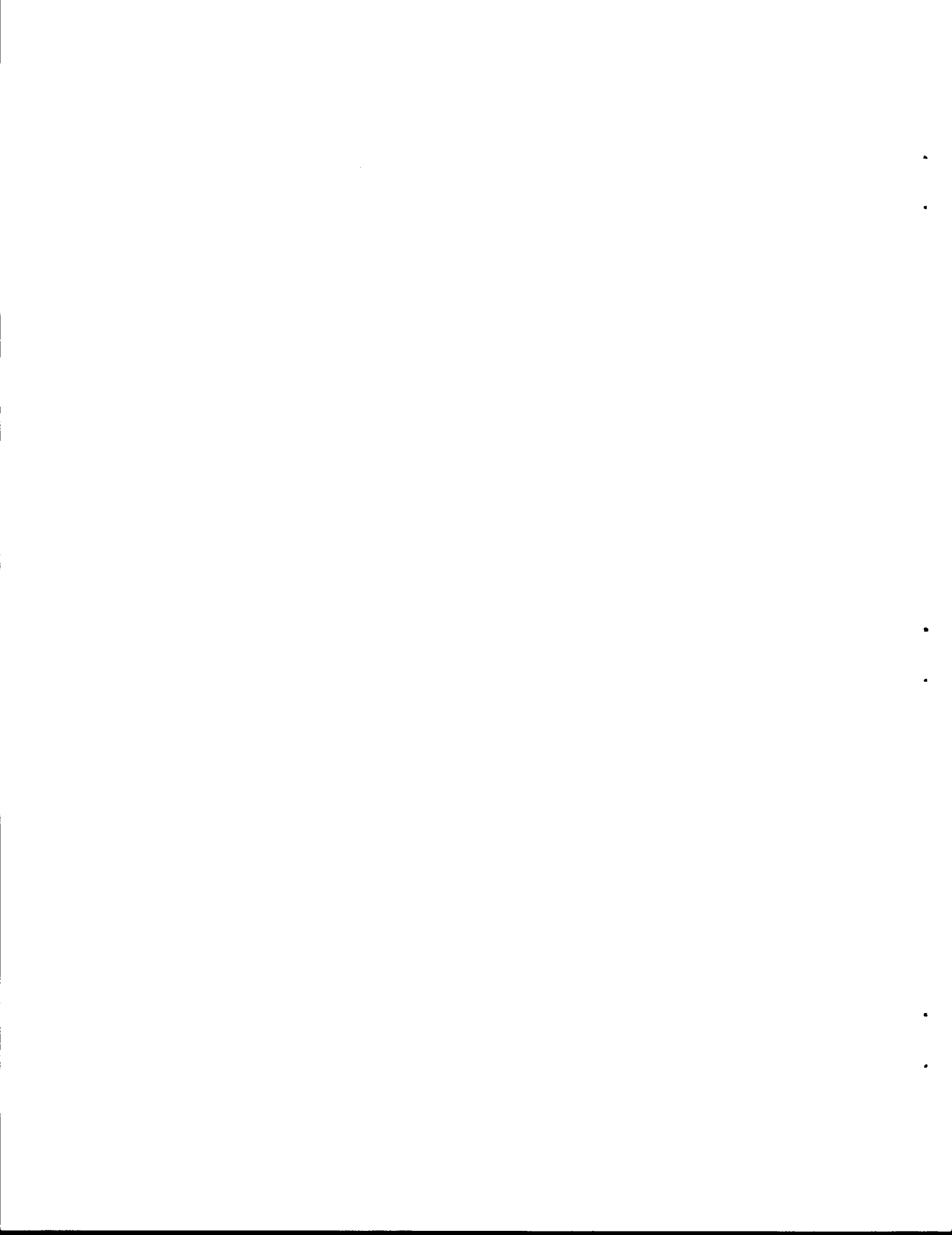
P. Patriarca

SEPTEMBER 1972

OAK RIDGE NATIONAL LABORATORY
Oak Ridge, Tennessee 37830
operated by
UNION CARBIDE CORPORATION
for the
U.S. ATOMIC ENERGY COMMISSION



3 4456 0514902 3

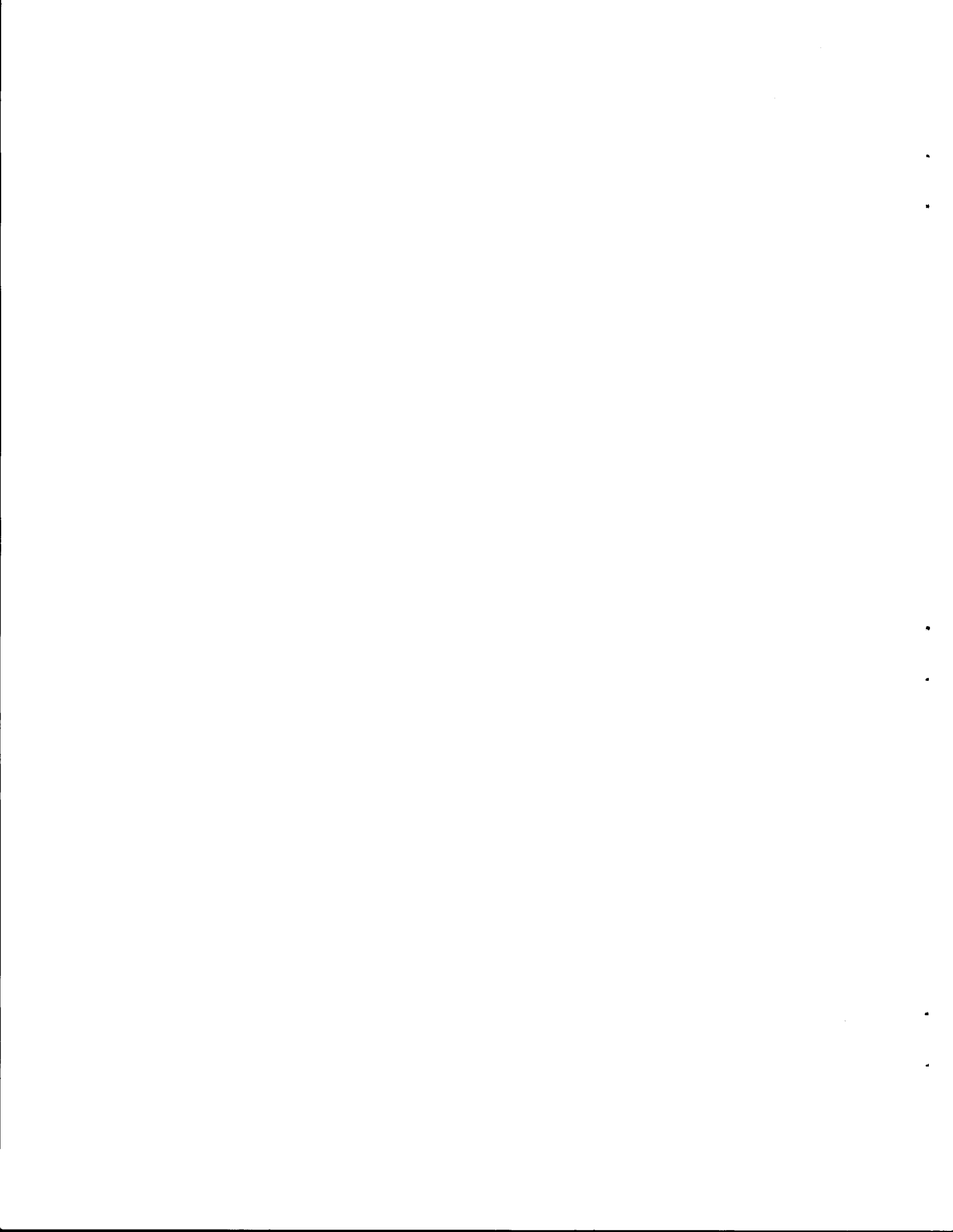


FOREWORD

This report is an excerpt from the Metals and Ceramics Division annual progress report and summarizes the research and development on nuclear fuels and materials in this division for the period July 1, 1971, through June 30, 1972. This work is either sponsored by or of particular interest to the Fuels and Materials Branch of the Division of Reactor Development and Technology.

We are publishing this report in lieu of our quarterly progress report for the period ending June 30, 1972, but will resume our regular reporting for the period ending September 30, 1972.

Progress on these programs is reported for the two major divisions of the work — Fast Reactor Technology and Space Power Technology.



CONTENTS

	<u>Page</u>
SUMMARY	ix
FAST REACTOR TECHNOLOGY	
ADVANCED FAST BREEDER REACTOR FUEL DEVELOPMENT	38
Irradiation Testing	38
Thermal Flux Tests	38
Fast Flux Tests	38
Fabrication of (U,Pu)N Fuel	39
COMPATIBILITY OF STEAM GENERATOR MATERIALS	40
Examination of Alco/BLH Steam Generator	40
Corrosion of Advanced Steam Generator Alloys	42
General Corrosion	42
Stress Corrosion	42
DEVELOPMENT OF FBR NEUTRON-ABSORBER MATERIALS	47
Irradiation Behavior of Boron Carbide	47
Microstructure of Boron Carbide after Fast-Neutron Irradiation	47
Evaluation of Fast-Reactor-Irradiated Boron Carbide Powders	49
Evaluation of Boron Carbide Pellets from EBR-II Higher Worth Control Rod	49
Evaluation of Boron Carbide Pellets from ORNL EBR-II Experiment X 099	49
Performance Modeling of Neutron Absorbers	50
Development of Vents	51
The Effect of Temperature on the Microstructure of Neutron-Irradiated Tantalum	52
Alternate Absorber Materials	53
Reactor Experiment Design and Fabrication	53
DEVELOPMENT OF FBR OXIDE FUELS	55
Development of Fabrication Processes	55
Irradiation Behavior	56
Fast Flux Irradiation Tests	56

Uninstrumented Thermal Flux Irradiations	56
ETR Instrumented Tests	58
Fuel-Cladding Mechanical Interaction Tests	58
Cladding Chemical Reactions	58
Analysis of Fuel Element Performance	61
Performance Model Development	61
Porosity, Actinide, and Oxygen Redistribution in Irradiated (U,Pu)O ₂	65
Analysis of ORR Instrumented Thermal Performance Tests	66
CASDAR: A Nuclear Data Manipulation Program	67
Chemical Modeling of Fuel-Cladding Attack in LMFBR Oxide Pins	68
Analysis of Intergranular Attack Data	68
Elimination of CO ₂ and H ₂ O as Oxygen Transport Species in Mixed Oxide Fuel Pins	69
FABRICATION DEVELOPMENT OF FAST BREEDER REACTOR CLADDING	70
Biaxial Creep Rupture of Stainless Steel Tubing with Electrodischarge Machined Notches	70
Effects of Sharp Artificial Notches on Thin-Wall Type 316 Stainless Steel Tubing	71
JOINING OF STRUCTURAL MATERIALS	73
Stainless Steels	73
Heavy Section Weldment Evaluation	73
Properties of Stainless Steel Welds with Controlled Residual Elements	74
Filler Metal Development for Pipe Welding	74
Nickel-Rich Alloys	75
Inconel 718	75
Incoloy 800	75
Ferritic Steels	76
Stabilized Grades	76
Low-Carbon Grades	76
Tube-to-Tube-Sheet Welding Studies	77

MECHANICAL PROPERTIES OF ALLOYS IN REACTOR ENVIRONMENTS	79
Swelling of Austenitic Stainless Steel	79
Annealed Type 304 Stainless Steel	79
Annealed Type 316 Stainless Steel	80
Cold-Worked Type 316 Stainless Steel	80
Titanium-Modified Type 316 Stainless Steel	81
Mechanical Properties of Austenitic Stainless Steels	82
Type 316 Stainless Steel	82
Titanium-Modified Type 316 Stainless Steel	85
MECHANICAL PROPERTIES OF STRUCTURAL ALLOYS	86
Exploratory Tests on Type 304 Stainless Steel in Support of the High-Temperature Structural Design Methods for LMFBR Components Program	86
Heat-to-Heat Variations in the Mechanical Properties of Type 304 Stainless Steel	87
Mechanical Properties of Structural Materials for Steam Generators	88
Weldments	88
Base Metal	88
NONDESTRUCTIVE TEST DEVELOPMENT	91
Nondestructive Test Development for Steam Generators	91
Radiography	91
Liquid Penetrants	91
Eddy Currents	92
Ultrasonics	92
Electromagnetic Inspection Methods	93
Ultrasonic Inspection Methods	93
Frequency Analysis	93
Ultrasonic Imaging	94
Penetrating Radiation Inspection Methods	95
CLADDING MATERIALS FOR SPACE ISOTOPIIC HEAT SOURCES*	96
New Platinum-Rhodium-Tungsten Alloys for Space Isotopic Heat Sources	96

*Sponsored by the Division of Space Nuclear Systems.

Characterization of Pt-Rh-W Alloys	97
Characterization of Iridium	97
DEVELOPMENT OF URANIUM NITRIDE FUELS FOR NASA	98
Irradiation Testing of Uranium Nitride	98
UN Fabrication Studies	99
PHYSICAL METALLURGY OF REFRACTORY METALS	100
Embrittlement of T-111 Pioneer Fuel Capsules	100
Evaluation of Pioneer Test Capsules	100
Mechanical Properties and Structure of Internally Oxidized Ta-8% W-2% Hf (T-111) Alloy	101
TUNGSTEN METALLURGY	102
Fabrication of Experimental Tungsten Materials	102
The High-Temperature Creep Properties of Chemically Vapor Deposited Tungsten	102
Low-Stress Creep Testing of Tungsten	103
Creep Properties of W-3.8% ThO ₂	103
Effect of Carburization on the Creep Properties of Tungsten Alloys	103
Radiation Damage to Refractory Metals as Related to Thermionic Applications	105
High-Temperature Fast-Neutron Irradiation of Tungsten Alloys	105

SUMMARY

FAST REACTOR TECHNOLOGY

Advanced Fast Breeder Reactor Fuel Development

Two capsules were placed in the ETR to determine the irradiation behavior of (U,Pu)N fuel. One was removed after a burnup of 5% FIMA at 30 kW/ft linear heat rating and is being examined at Los Alamos Scientific Laboratory (LASL). Radiography showed pellet cracking, but the fuel pins were dimensionally stable, and gamma scanning indicated a normal distribution of fission products.

We completed the fabrication of seven fuel pins, also containing (U,Pu)N pellets, for irradiation in EBR-II. Some difficulty was encountered in sodium bonding the pellets using ultrasonic vibration, which had previously proven satisfactory for UN pellets. The pins were shipped first to Battelle Columbus Laboratory, where a satisfactory bond was obtained by centrifugation, and then to LASL, who is now responsible for this program.

Work on the fabrication and characterization of mixed nitride fuel for the LMFBR was stopped at the end of FY 1972. We completed a report on the characterization of (U,Pu)N fuels to be irradiated in EBR-II and returned the residual materials from the nitride fuel development to AEC recovery centers.

Compatibility of Steam Generator Materials

Examination of the Alco/BLH steam generator after its failure at the Liquid Metal Engineering Center has revealed (1) fabrication difficulties associated with some tube-to-tube-sheet fillet welds, (2) lower tube sheet stress-corrosion cracks associated primarily with type 316 stainless steel sections and having at least three alternative explanations, (3) upper tube sheet stress-corrosion cracking caused by caustic formed in water-sodium reactions, (4) heavy corrosion of shell-side tube surfaces in the sodium vapor-argon gas space immediately below the top tube sheet, and (5) no evidence of significant general or stress-assisted corrosion for

surfaces exposed exclusively to sodium. Our program to examine general and stress-assisted corrosion phenomena under steam environments at an operating power plant has continued with emphasis on chloride stress-corrosion cracking for wide ranges of temperatures, materials, and oxygen impurity contents.

Development of FBR Neutron-Absorber Materials

Boron carbide powders and pellets irradiated in the fast flux of the EBR-II were examined. Transmission electron microscopy revealed crystallographically oriented cavities with high strain fields. These are assumed to be helium-filled bubbles generated by the $^{10}\text{B}(n,\alpha)^7\text{Li}$ reaction. After irradiation above about 500°C, a denuded zone free of bubbles was observed adjacent to grain boundaries. However, at these temperatures bubbles are concentrated in grain boundaries, on dislocations, and on stacking faults. Upon irradiation at about 750°C or upon post-irradiation annealing at higher temperatures these bubbles coalesced, causing grain separations, reflected in pellet cracking and fragmentation. Lattice contractions and expansions were observed coincident with bubble formation. Upon postirradiation annealing the lattice parameters returned to their preirradiation values as the strain fields associated with the helium bubbles were relieved. Scanning electron microscopy of surfaces fractured after annealing reveals particles, which may be a result of lithium precipitation during the anneal.

Stainless steel and molybdenum disks were fabricated with controlled porosity by powder metallurgy for potential use as vents in boron-containing control rods. Methods were developed for joining these disks to stainless steel housings.

Tantalum irradiated in the EBR-II in the range 425 to 1050°C showed voids by transmission electron microscopy. Peak swelling of 2.4% was observed at 585°C with a void concentration of 1.9×10^{17} voids/cm³.

Methods of fabricating tantalum borides, which are attractive because of their high reactivity worth, were developed. These materials have been characterized in preparation for testing in the EBR-II.

A materials variables irradiation testing program encompassing boron carbide, tantalum and its alloys, and tantalum borides is under way. This program consists of 21 capsules in three EBR-II subassemblies. One subassembly (X 099A) is presently at the EBR-II, and the others are scheduled for insertion in September and November.

Development of FBR Oxide Fuels

The oxide fuels development program was a five-year program to advance the technology of $(U,Pu)O_2$ as a fast breeder reactor fuel. The objectives were to establish the performance characteristics and limitations of $(U,Pu)O_2$ fuels fabricated by different processes, to obtain a fundamental understanding of the mechanisms involved in the irradiation behavior of fuel elements incorporating these fuels, to develop economical techniques to fabricate a product with optimized performance, and to develop analytical models sufficiently accurate to optimize experimental design and predict fuel element response to fast reactor conditions.

Previously developed processes for loading fuel pins by the Sphere-Pac process or making pellets from sol-gel precursor material and for adjusting fuel composition to meet specifications were used to prepare fuel and load fuel pins for irradiation tests. The ability to Sphere-Pac fuels to controlled densities of 81 to 84% of theoretical was demonstrated. The ability to fabricate pellets from sol-gel material was demonstrated, and techniques were developed for control of the various specified parameters, including density and stoichiometry.

The irradiation program has had as its objective the determination of in-reactor properties and performance of $(U,Pu)O_2$ fuel pins as functions of fabrication form, porosity distribution, stoichiometry, and irradiation condition. The program has included both fast and thermal flux irradiations and steady-state, cyclic, and transient power conditions.

The principal results were that Sphere-Pac fuels perform as well as pellet fuels, they exhibit better compatibility with cladding, and they have better fuel-cladding thermal conductance. In our fast flux tests in EBR-II, two Sphere-Pac $(U,Pu)O_2$ fuel pins were examined after achieving a peak burnup of 6% FIMA and had performed very satisfactorily. Three

similar pins have continued irradiation in EBR-II and are now at a peak calculated burnup level of 8.1% FIMA. A 37-pin subassembly for EBR-II, consisting of 19 pins from ORNL and 18 from the Babcock & Wilcox Company, was irradiated to a peak burnup level of approximately 3.8% FIMA. It contains Sphere-Pac and pellet fuels derived from the sol-gel process and pellets and Vi-Pac shards processed from coprecipitated powders. One fuel pin containing (U,Pu)O₂ Sphere-Pac fuel was irradiated to 11.3% FIMA without any abnormal effect, but the peak cladding temperature was low (< 400°C). The irradiation of two ETR instrumented capsules was completed with a calculated burnup of approximately 8% FIMA maximum.

A highly instrumented capsule was irradiated in the ORR to measure in-reactor axial extension of the fuel column and cladding and the internal gas pressure developed during operation under prototypic LMFBR power and temperature conditions. Almost daily power cycles simulated load-following conditions in a power reactor. Gas release was continuous as burnup increased at power and was not significantly changed by power transients. The fuel column grew as a result of thermal expansion during heatup, shortened during early constant power operation, probably because of creep or restructuring, and expanded slowly in accordance with expected fission product swelling.

When solution-treated type 316 stainless steel tubing was exposed to a controlled oxidation potential, matrix oxidation and intergranular attack were often localized in areas having discrete temperatures of operation. For example, localized increased attack was observed in the range 585 to 605°C out of the total temperature range tested, 560 to 650°C. A greater change in wall thickness of the tubing used was indicated above 660°C. We postulate that this oxidation in specific temperature regimes is due to the morphology of the carbide present in the stainless steel. Additional work may explain observations on intergranular attack in (U,Pu)O₂ fuel pins clad with stainless steel.

We incorporated a sophisticated fuel-cladding gap conductance model in the FMODEL fuel performance code and also refined the model for thermal-gradient-induced redistribution of porosity and fuel components during irradiation of PuO₂ fuel. The principal modeling effort was detailed analysis of sensitivity of predicted fuel pin performance to uncertainties

in physical and mechanical properties of the fuel and cladding. The uncertainties examined included thermal expansion of both fuel and cladding, fuel thermal conductivity, mechanical properties of fuel and cladding, and cladding swelling characteristics as a function of fast neutron fluence and temperature. A statistical analysis was done to further confirm that the central temperature ($^{\circ}\text{C}$) of Sphere-Pac fuel under irradiation is always cooler than that in pellet fuel by $11.7 \pm 1.2\%$ at the 99% confidence level. Additional analyses included modeling of chemical attack between mixed oxide and stainless steel cladding and a thermodynamic study that showed that CO_2 and H_2O do not transport oxygen in mixed oxide fuel pins.

Fabrication Development of Fast Breeder Reactor Cladding

Two types of artificial defects in type 316 stainless steel tubing reduced creep strengths and ductility. Stress concentrations occur at the defects.

Joining of Structural Materials

We are studying the elevated-temperature properties of austenitic stainless steel weldments for application to LMFBR vessels and components, particularly piping. Included in the program are the shielded metal-arc, gas tungsten-arc, submerged-arc, gas metal-arc, and electroslag welding processes. The serious lack of long-term ductility in conventional weldments has led to the development of filler metals having improved strength and ductility.

We have participated in the preparation of a program plan to determine the weldability and properties of Inconel 718, an age-hardenable nickel-chromium alloy. Weld-metal fissuring in Incoloy 800 is intergranular and is probably related to large columnar grains. We developed a filler metal that has the nominal composition of Incoloy 800 but does not produce large columnar grains. The cracking propensity of this composition is reduced, and we are attempting further improvements to eliminate the problem.

Niobium-stabilized 2 1/4 Cr-1 Mo-1/2 Ni steels are prone to hot cracking during welding because a liquid phase is present in the heat-affected zone and, in multipass welds, in the weld metal. The presence of this phase, however, does not deleteriously affect the tensile and impact properties of the weldment. Hardness studies of the low-, medium-, and high-carbon 2 1/4 Cr-1 Mo steels showed that the base metal is the weakest zone in a weldment. We developed a technique to simulate the bore-side weld in a flat-plate configuration that will permit the preparation of specimens for mechanical properties and nondestructive testing. Moreover, we devised a double-torch technique that permits the simulation across an entire weldment of the overlap region in a weld.

Mechanical Properties of Alloys in Reactor Environments

Microstructural changes that occur as a result of fast neutron irradiation over a wide range of temperature and neutron fluence were studied in types 304 and 316 stainless steel. Of particular importance is the observation that preirradiation structure has a pronounced effect on void formation and swelling. Ductility is the most adversely affected mechanical property. The loss of ductility appears to result from a combination of matrix hardening and helium effects.

Mechanical Properties of Structural Alloys

Before the deformation behavior of type 304 stainless steel can be predicted under complicated loading conditions for reactor components, the creep law predicting strain under variable loads must be determined. Our tests to date support a strain-hardening rule for cumulative creep rather than a time-hardening rule.

In design, average mechanical property data are customarily used with minimum strength properties sometimes available. For the critical analyses of components operating in the creep range, it is necessary to validate those average properties and establish the expected heat-to-heat variation in creep properties. Thus far our effort has shown that the variation in creep properties at 593°C is greater than anticipated.

We are collecting mechanical property data for steam generator materials. Our program involves the Croloy and Incoloy 800 alloys, both wrought and weld metal. To date, our work has been primarily directed toward determining the influence of carbon on the properties of 2 1/4 Cr-1 Mo alloy in the normalized and tempered condition. In general, the strength increases with carbon content.

Nondestructive Test Development

We are developing new methods, techniques, and equipment for non-destructively inspecting materials and components for the LMFBR, with emphasis on problems related to steam generators.

The primary problem being investigated for steam generators is the tube-to-tube-sheet welded joint. Studies have begun on radiography using a small-rod-anode x-ray unit. Preliminary techniques were examined for application of liquid penetrants with viewing by closed-circuit television. Computer design of optimum eddy-current coils for the tubular configuration is in progress. A prototype ultrasonic system was developed for quantitative recording of flaws in flat-weld simulations of the tubular joint.

We continued computer analysis of eddy-current test systems with emphasis on applied problems such as optimum design for reflection coils, reduction of noise and temperature drift, improved capability for measurement of thickness, and measurement of liquid level. The experimental program included construction of equipment to confirm and apply the above, including measurement of the degree of cold work in stainless steel.

Significant progress was made in the ability to characterize flaws of different configurations by ultrasonic frequency analysis. Improvements in the optical imaging system for ultrasound increased its frequency response and power and allowed studies of stainless steel welds by schlieren techniques. Preliminary studies were performed on interferometric and Bragg diffraction methods.

SPACE POWER TECHNOLOGY

Cladding Materials for Space Isotopic Heat Sources

Alloys of platinum with rhodium and tungsten, including modifications with small amounts of hafnium and titanium, were prepared in sufficient quantities for properties determinations. In toughness at 1316°C, Pt-30% Rh-8% W-1.0% Hf-0.2% Ti was superior to refractory materials such as iridium, TZM, and T-111. Forming studies have also been initiated. In general, the alloys continue to show great promise for use as container materials in space applications of isotopic power fuels.

Development of Uranium Nitride Fuels for NASA

Three capsules were irradiated throughout the year without serious difficulty. Neutron radiographs showed that the pins contained in the capsules were dimensionally stable although some pellet cracking occurred. Leakage of 10^{-5} of the fission product gas was detected in the blanket gas of two capsules. The principal operational difficulty was the failure of cladding thermocouples, which required the use of heat-generation measurements to control the capsules.

Two methods were developed to fabricate 85%-dense UN pellets that are thermally stable to 2300°C. One method involved preconditioning of UN powders before pressing and sintering; the second involved the use of $UN_{1.74}$ as starting material.

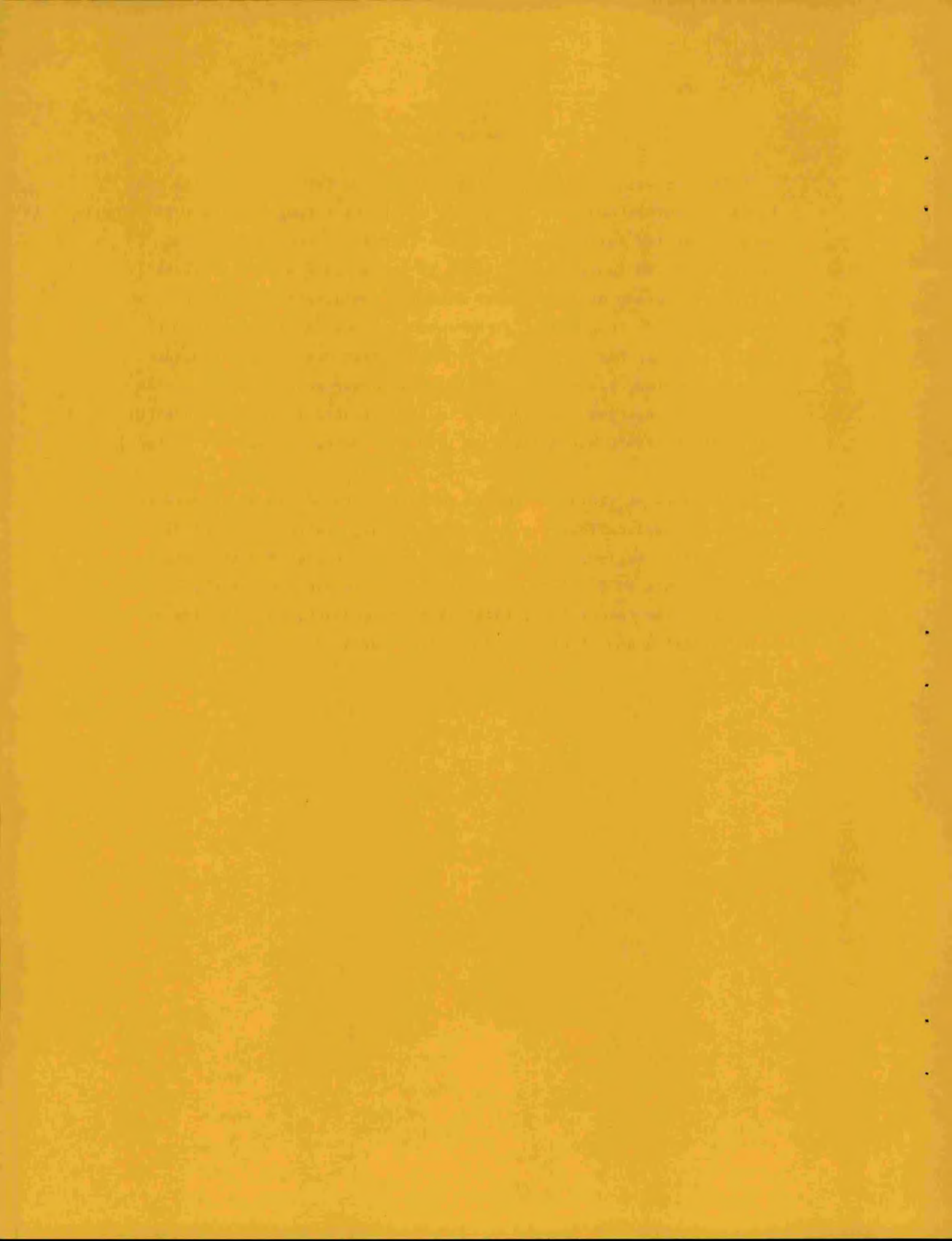
Physical Metallurgy of Refractory Alloys

The failure of T-111 containers of $^{238}\text{PuO}_2$ fuel in test Pioneer radioisotope thermoelectric generators was traced to oxygen contamination. Sources of the oxygen were identified and suggestions made for diminishing the problem. The rates of oxygen contamination, the degree of sensitivity, and mechanism for embrittlement were determined for T-111 under simulated operating and reentry situations. The mechanical properties of T-111 Pioneer test capsules were measured to determine the effectiveness of the engineering "fix" for this problem.

Tungsten Metallurgy

Experimental tungsten materials including CVD tungsten with controlled fluorine contents and tubing of arc-cast tungsten and W-2% ThO₂ were fabricated for evaluation in the thermionic reactor program. Deposits of CVD tungsten containing 15 to 25 ppm F were significantly stronger in creep at 1650°C than deposits containing 5 to 10 ppm. We are testing CVD tungsten at stresses to produce 1% creep in 1000 to 50,000 hr using highly accurate optical strain measuring techniques. In creep-rupture tests W-3.8% ThO₂ was stronger and more stable than W-2% ThO₂. The creep strength of tungsten tested in low-pressure CH₄ is lower at 1800°C but greater at 1650°C compared to material tested in vacuum.

A review of radiation damage to refractory metals as related to thermionic applications was completed. A high-temperature irradiation experiment on various tungsten materials was completed after achieving a peak fluence of 8×10^{21} neutrons/cm². Determination of the effect of irradiation temperature, fabrication processing, and alloying on the void formation and electrical properties began.



Reprinted from
METALS AND CERAMICS DIVISION ANNUAL PROGRESS REPORT
FOR PERIOD ENDING JUNE 30, 1972
ORNL-4820 (pp. 38-105)

Part II. Fast Reactor Technology

12. Advanced Fast Breeder Reactor Fuel Development

J. L. Scott

The goals of this program are to investigate the properties and behavior of those uranium- and plutonium-base ceramic fuels that we term conductors — such as the mononitrides, carbonitrides, and monocarbides — and to compare their potential as liquid-metal fast breeder reactor (LMFBR) fuel with that of $(U,Pu)O_2$, which by comparison is an insulator. Since the thermal conductivity of the ceramic conductors is about ten times that of $(U,Pu)O_2$, one could theoretically operate a conductor at ten times the power density with the same central temperature. In practice, heat transfer limitations, thermal stresses in the cladding, and high rates of swelling at high temperatures limit the power density to about two or three times that of $(U,Pu)O_2$ — still a challenging improvement. Additionally, the margins for transient overpower are much higher in the ceramic conductors than in $(U,Pu)O_2$.

To evaluate the true potential of these fuels, we need to define the structures, composition, and quality control required to achieve 150,000 MWd/metric ton at peak linear heat ratings of 30 to 50 kW/ft. We must also demonstrate the possibility of a low-cost fuel cycle for manufacturing fuel with the needed properties. Our work is oriented primarily toward demonstrating the irradiation performance of $(U,Pu)N$ at high burnups and high heat ratings. Therefore, much of our effort is devoted to fabricating and characterizing fuel for irradiation testing.

Other work on nitride fuels is reported in Chap. 22.

IRRADIATION TESTING

T. N. Washburn

Thermal Flux Tests

The initial series of irradiation tests are two noninstrumented capsules of four pins each in the ETR.

These "screening" tests are to determine the performance of nitride fuel synthesized from metal. The peak linear heat rating is 30 kW/ft to burnups of 50,000 and 100,000 MWd/metric ton. The fuel is cold-pressed and sintered pellets with densities from 86 to 91% of theoretical, and the fuel pins have a 0.010-in. radial gap between the fuel pellet and cladding, filled with NaK-19 to enhance heat transfer.

Capsules 43-N1 and 43-N2 were inserted into ETR in December 1970; 43-N1 continues in irradiation, and 43-N2 was removed from the reactor in January 1972 after achieving a burnup level of about 5% fissions per initial actinide metal atom (FIMA). Capsule 43-N2 is currently in postirradiation examination at Los Alamos Scientific Laboratory (LASL). Betatron radiographs of the irradiated capsule showed the only significant change from the preirradiation neutron radiograph to be numerous cracked pellets in each fuel pin, an entirely expected condition from operation at 30 kW/ft linear heat rate. Gamma scanning, both for gross activity and for several radionuclides of interest, revealed only normal fission product distribution. Diameters of the fuel pins showed negligible deviations from preirradiation values. All information obtained to date indicates that the fuel pins performed very satisfactorily.

The postirradiation examination of capsule 43-N2 will be continued at LASL in FY 1973, and technical responsibility for capsule 43-N1, which is still being irradiated, was transferred to LASL on June 30, 1972.

Fast Flux Tests

E. J. Manthos T. N. Washburn

Fabrication was completed on seven unencapsulated fuel pins, five for testing in EBR-II and two as spares or replacements. Test parameters and description of these

fuel pins were previously reported.¹ All aspects of the fabrication were satisfactory except that the sodium bond between the fuel pellets and cladding showed evidence, by eddy-current testing, of voids in excess of the established $\frac{1}{16}$ -in.-diam. standard. The sodium bonding was performed by ultrasonic vibration, which had proven to be satisfactory for bonding UN fuel pellets in both development pins and two UN-fueled dummy pins loaded at the same time as the (U,Pu)N fuel pins. We were not able to establish why there was a difference in the quality of sodium bond with (U,Pu)N instead of UN pellets. Since this program was being phased out, the pins were shipped to Battelle Columbus Laboratory for bonding by their established centrifuging technique. After centrifuging, the bond quality was satisfactory, and the fuel pins were shipped to LASL, who has been assigned responsibility for this program.

FABRICATION OF (U,Pu)N FUEL

E. S. Bomar

This program was terminated, and work during this period was limited to writing the results of examina-

tions to characterize fuel pellets for EBR-II irradiation tests and to disposing of the residual fuel materials.

We had residual fuel in three forms: arc-cast uranium-plutonium ingots, sintered pellets, and powder. Since the powder is pyrophoric, it was necessary to convert it to a stable form before shipping to a recovery point. On the assumption that the nitride powder would oxidize readily, we treated several batches in argon plus oxygen or air mixtures at temperatures to 750°C. The results varied from one batch of powder to another and ranged from complete oxidization in some instances to only superficial oxidation in others. Since use of the available furnaces did not assure the formation of a stable oxide powder, we therefore dissolved the nitride powders in nitric acid. About 1.5 kg of nitride powder was treated in this manner. All of the residual fuel materials were then shipped to recovery sites.

1. E. J. Manthos, M. K. Preston, and J. H. Erwin, *Metals and Ceramics Div. Annu. Progr. Rep. June 30, 1971*, ORNL-4770, p. 61.

13. Compatibility of Steam Generator Materials

P. Patriarca J. R. Weir, Jr.

Two programs are under way to investigate the behavior of steam generator materials under potential service conditions in an LMFBR heat transport system. One program concerns the post-test examination of a failed sodium-to-steam steam generator, and the second involves the corrosion testing of representative materials in steam, with and without chloride and caustic as contaminants.

EXAMINATION OF ALCO/BLH STEAM GENERATOR

J. H. DeVan G. M. Slaughter

We have investigated the chemical and metallurgical condition of the Alco/BLH steam generator¹ following its removal from the Sodium Components Test Installation at the Liquid Metal Engineering Center. Our examination centered around the upper tube sheet, which was the site of three tube failures, and the lower tube sheet, which was extensively cracked.

Our preliminary findings² can be summarized as follows:

1. The Alco/BLH steam generator was fabricated with procedures adequate to obtain good quality of construction. However, numerous tube-to-tube-sheet fillet welds exhibited small weld cracks, and the weld throat thickness was marginal (Fig. 13.1).

2. Cracks in the lower tube sheet are almost totally confined to type 316 stainless steel sections and appear to have been caused by stress corrosion. As shown in Fig. 13.2, one system of cracks linked several tube crevices that had contained sodium with a small opening into the water side of the tube sheet. Another system of cracks appeared to enter from the air side of

the tube sheet and to connect with the former crack system.

3. Tube leaks in the upper tube sheet were caused by caustic stress-corrosion cracking, which initiated in the sodium-filled tube crevices. We believe that the stress-corrosion conditions were set up by leakage of water into the tube crevices through defective tube-to-tube-sheet fillet welds.

4. Our examination revealed heavy corrosion of shell-side tube surfaces in the sodium vapor-argon gas space immediately below the top tube sheet. The corrosion was associated with the collection of sodium-steam reaction products (Fig. 13.3) and consumed up to 0.040 in. of the type 316 stainless steel surfaces.

5. Steam generator surfaces that had been exposed to liquid sodium showed no evidence of either general or stress-assisted corrosion.

Referring to Fig. 13.2, there are at least three alternative explanations for the onset of stress-corrosion conditions in the lower tube sheet. The water side of the tube sheet was protected by a $\frac{3}{8}$ -in.-thick Inconel



Fig. 13.1. Tube-to-tube-sheet weld in upper tube sheet, showing weld-bead cracking. 8.5X. Etchant: hydrochloric and nitric acids. Reduced 34%.

1. G. M. Slaughter, R. H. Jones, J. H. DeVan, and P. Patriarca, *Metals and Ceramics Div. Annu. Progr. Rep. June 30, 1971*, ORNL-4770, pp. 97-98.

2. G. M. Slaughter, J. H. DeVan, and R. H. Jones, "Post-Test Examination of the LMEC Alco/BLH Steam Generator," *Trans. Amer. Nucl. Soc.* 14, 787-88 (1971).

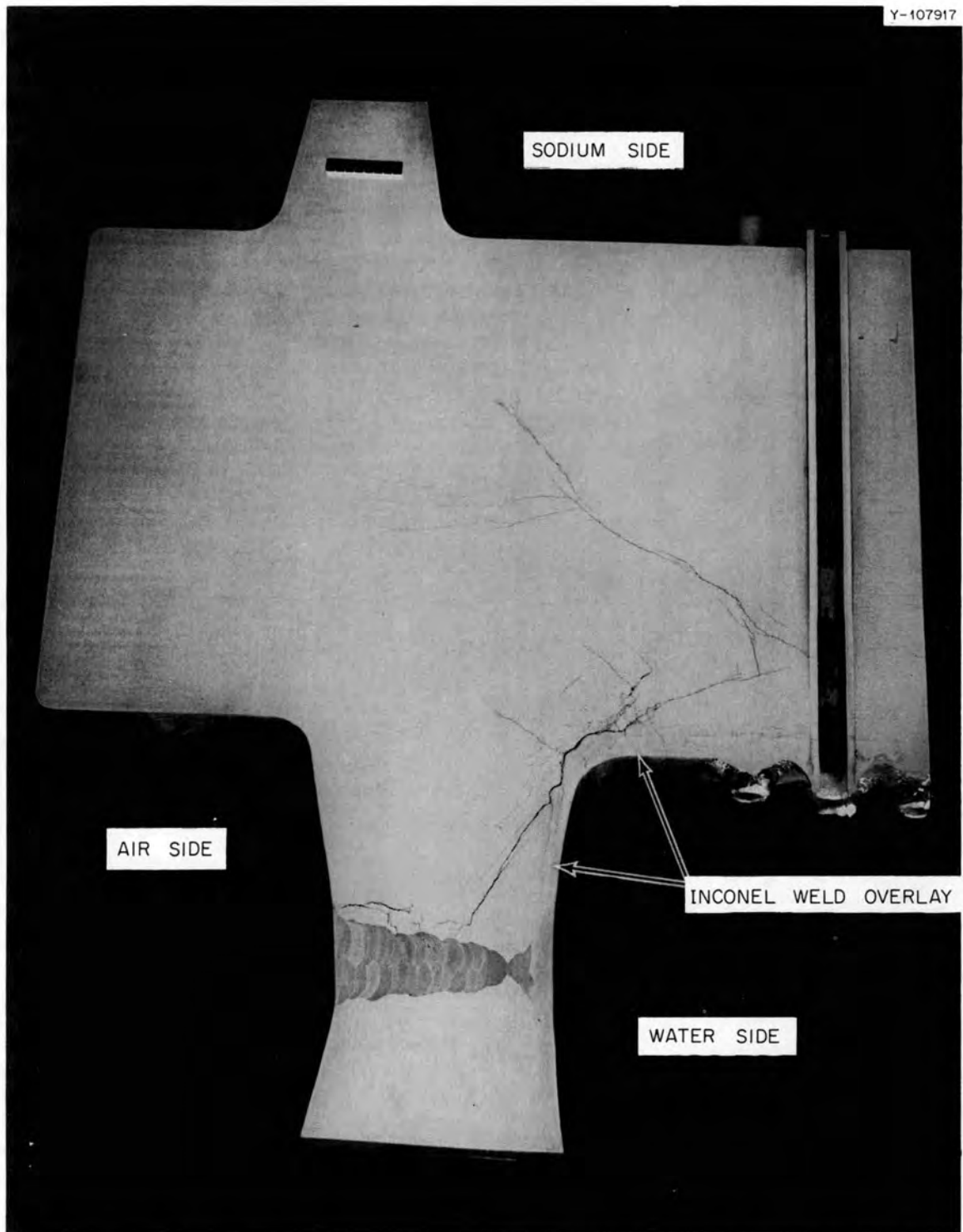


Fig. 13.2. Cross section along radius plane of lower tube sheet of Alco/BLH steam generator. Note system of stress-corrosion cracks, which interconnect tube crevices with the outside surface of tube sheet.



Fig. 13.3. Corrosion products observed in argon cover gas region in Alco/BLH steam generator, formed by reaction of steam with condensed sodium.

weld overlay, and water reached the crack networks through a small hole in this overlay. Assuming that the overlay was cracked at this point before operation, chloride impurities may have induced both the system of cracks that ran to the air side of the tube sheet and those leading to the sodium-filled crevices. Alternatively, as in the case of the top tube sheet, defects in the tube-to-tube-sheet fillet welds may have provided a path for water to reach the tube crevices. In this case, caustic cracking would have proceeded from the crevices to the Inconel overlay and thence toward the air side of the tube sheet. Thirdly, cracking may have originated at the air side of the steam generator as a consequence of chloride impurities and moisture contained in the thermal insulation surrounding the generator. The cracking patterns are such that none of these explanations can be disregarded.

CORROSION OF ADVANCED STEAM GENERATOR ALLOYS

J. P. Hammond G. M. Slaughter

This program concerns the corrosion behavior of steam generator alloys in steam, primarily as weldments. The actual testing is performed under sub-contract by Southern Nuclear Engineering, Inc., at the Bartow Plant of Florida Power Corporation. It includes two areas of investigation: (1) general corrosion (uniform scaling, including pitting and localized attack at fusion lines) at 480, 595, and 650°C (900, 1100, and 1200°F) and (2) stress-corrosion cracking (induced by chloride or caustic as contaminants) at 282 to 595°C (540 to 1100°F).

General Corrosion

The general corrosion specimens of similar- and dissimilar-alloy weldments examined at 595 and 650°C for advanced gas-cooled reactor applications³ were removed from tests after exposures to 23,000 hr, and the test loop was reconditioned to enable tests at 480 and 595°C on materials of special interest for LMFBR application. The findings of the former investigation, which included exposures to 16,000 hr, were promulgated.⁴ The study of materials for LMFBR use includes specimens of Incoloy 800, Super 12 Cr (HT-9), 2¼ Cr-1 Mo steel, and various intermediate and highly alloyed ferritic steels, in both ground and electro-polished surface conditions. These materials are being studied by the weight-loss and weight-gain methods, making determinations at intervals to 12,000 hr.

Stress Corrosion

Chloride. During the past year, runs 6 and 7 were completed and run 8 begun in the chloride-injection corrosion loop. All of these runs were conducted under identical cyclic operating conditions (20 ppm O₂ injected continuously and 10 ppm NaCl added during the saturation phase of cycling only). Because large numbers of specimens and such a wide variety of materials were represented, studies were made to establish more precisely the environmental conditions that prevailed as a function of time and location within

3. J. P. Hammond, *Metals and Ceramics Div. Annu. Progr. Rep. June 30, 1971*, ORNL-4770, pp. 90-94.

4. J. P. Hammond, "Corrosion of Nickel Base Alloy Weldments in Steam at 1100 and 1200°F (595 and 650°C)," paper presented at American Welding Society 52nd Annual Meeting, San Francisco, April 26-30, 1971 (submitted for publication).

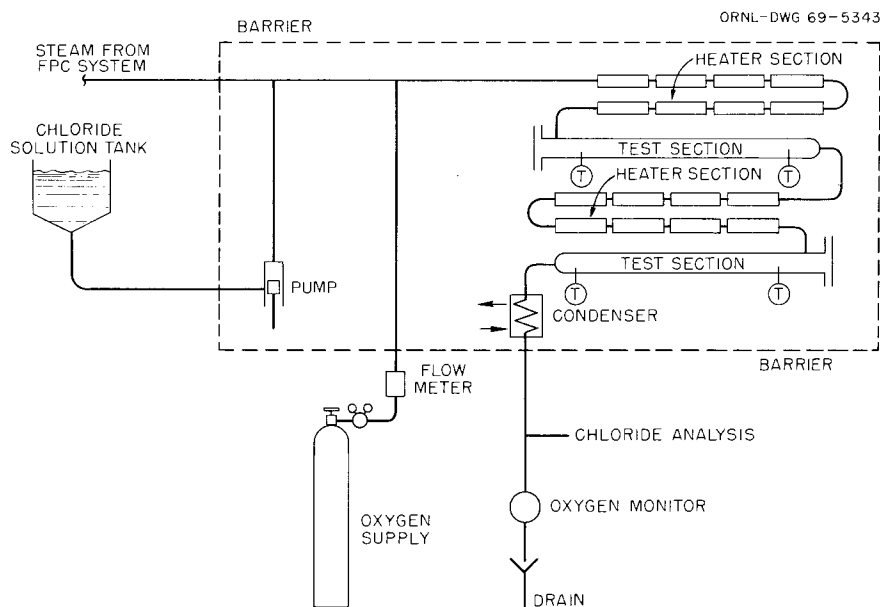


Fig. 13.4. Chloride and oxygen additive loop, schematic.

the test autoclaves. To more closely simulate steam generator components, a stress-corrosion test employing a tubular specimen was developed to complement the present U-bend test.

Environmental analyses. The objectives of the environmental analyses were to (1) determine the amount and location of moisture in the test autoclaves as a function of time during test, (2) establish water levels accumulating in the bottom of the autoclaves, and (3) assess the chloride concentrations in the saturated steam and accumulated water. The experimental procedures and detailed findings of these analyses were reported earlier.⁵ The findings are summarized below along with information on the loop operating conditions.

A schematic of the chloride-injection steam corrosion loop is reproduced in Fig. 13.4. Operating conditions of the loop during runs 6 through 8, for which the analyses were made, were as follows:

Test cycles	Three per week between superheated and saturated conditions
Saturation periods	24 hr each, followed by 24 hr at superheat (except 48 hr on weekends)
Superheat temperature	427°C (800°F)
Steam-saturation temperature	282°C (540°C)
Oxygen content (continuous)	20 ppm
Sodium chloride content (during saturation phase of cycle only)	10 ppm
Steam flow (at saturation temperature)	100 lb/hr
Loop pressure	900 psig

The oxygen and chloride contents were deliberately maintained at high levels to permit evaluation of material behavior under off-design conditions and to permit a screening study in which failures would occur in reasonable times. Subsequent tests will be designed to incorporate test conditions of decreasing severity.

Several conclusions were reached by these analyses. The amount of moisture formed during the saturation phase of the cycling averaged about 25%. However, because the velocity of the steam flow in the autoclaves (devoid of specimens) was very low (≈ 2 fps), this moisture manifested itself largely as water that collected at the bottom of the autoclaves (1.9-in.-ID pipes) and flowed on through the loop. This water begins to collect just as the autoclaves reach the saturation temperature and rises parabolically to a final depth of about 0.090 in. The stressed regions of the U-bend test specimens, when mounted in an upright orientation, are $1/16$ in. above the bottom of the autoclaves and become wetted by the accumulated water within the first hour after the autoclaves reach the saturation temperature. The analysis revealed that little moisture and very little of the chloride contaminant reside in the saturated steam above the water level. Although the water at the

5. J. P. Hammond, *Fuels and Materials Development Program Quart. Progr. Rep.* March 31, 1972, ORNL-TM-3797, pp. 129-37.

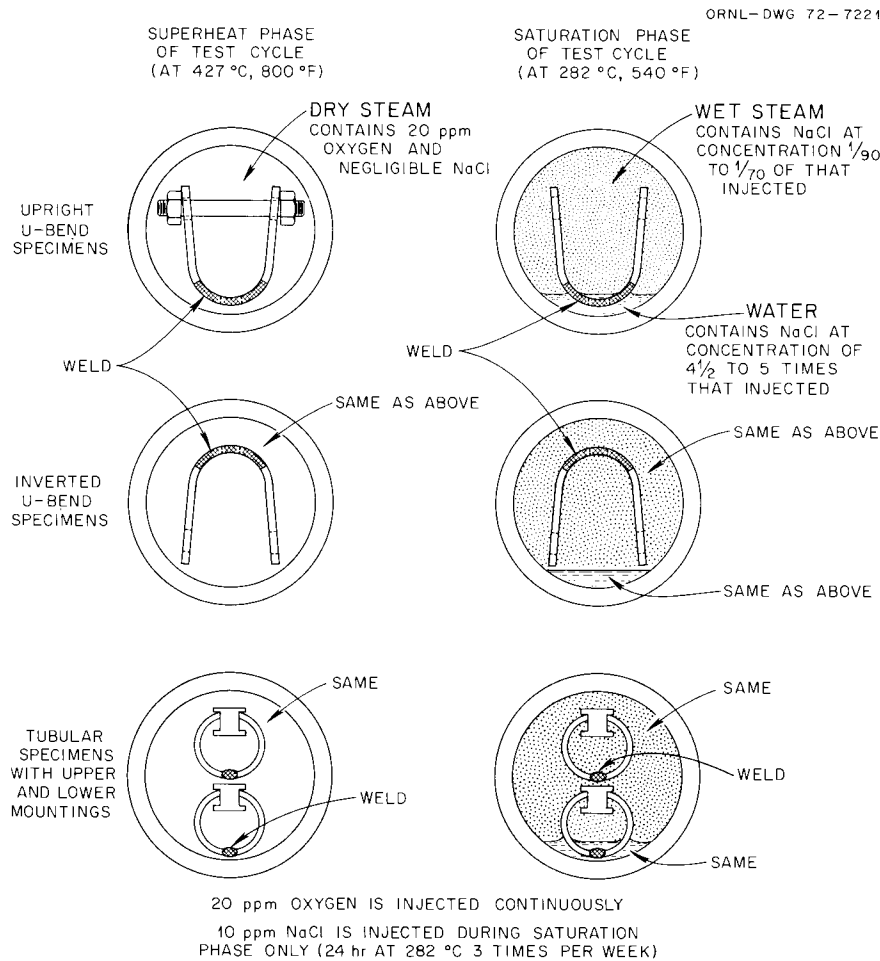


Fig. 13.5. Test specimens and environmental conditions for cyclic stress-corrosion tests. The loop operates at 900 psi.

bottom of the autoclaves contained 44 to 50 ppm NaCl, the saturated steam above contained only 0.11 to 0.14 ppm NaCl. Negligible NaCl was found in the superheated steam.

Figure 13.5 shows schematically the environmental conditions found in the autoclaves during test and illustrates the type of specimens being used and their orientations within the autoclaves. The tubular specimens are stressed by springing the slitted pieces outward while mounting them on an I-shaped rail; thus their stressed region (at the weld) is diametrically opposite from the mounting rail.

The time dependence of the moisture concentration was very similar for the upper and lower autoclaves.⁵ From this we conclude that specimens see similar environments whether exposed in different autoclaves or in different axial positions in the same autoclave.

Corrosion test results. Test results on samples examined in runs 6 through 8 as U-bend specimens in the upright position (see Fig. 13.5) are summarized in Table 13.1. Of the three specimen surface conditions examined (ground, annealed, and pickled), grinding on a 100-mesh belt gave greatest susceptibility to cracking. Incoloy 800 welded with Inconel 82, although not as susceptible as type 304 stainless steel welded with type 308, was definitely susceptible to cracking, as were a host of other stainless steel and high-nickel alloys. However, the Incoloy 800 weldment was only moderately susceptible. Inconel 625 joined with itself and Inconel 601 base metal along with a group of non-welded ferritic materials displayed a seeming immunity to cracking. Of the ferritic materials, 26 Cr-1 Mo steel was an unexpected exception to nonsusceptibility.

Table 13.1. Chloride stress-corrosion results on stainless steels, high-nickel alloys, and ferritic alloy steels^a

Base metal	Filler metal	Failure frequency ^b			Crack size	Location ^c
		G	A	P		
Type 304 SS	Type 308 SS	3 of 3	3 of 3	3 of 3	Large	B into W
18-18-2 SS	18-18-2 SS	3 of 3	3 of 3		Large	B and W
Hastelloy X	Hastelloy X	6 of 6	1 of 6	0 of 3	Large	B through W
Hastelloy N	Hastelloy N	2 of 2	2 of 2		Large	B and W
IN 102	IN 102	6 of 6	3 of 6		Medium	B into W
Incoloy 800	Inconel 82	6 of 6	4 of 6	1 of 6	Medium	B into FL
Inconel 600	Inconel 82	3 of 6	0 of 6	0 of 3	Medium	B into FL
Inconel 625	Inconel 625	0 of 6	0 of 6	0 of 3		
Inconel 601	No weld	0 of 6	0 of 6			
Hastelloy C	No weld	0 of 3	0 of 3			
Hastelloy G	No weld	0 of 3	0 of 3			
2 1/4 Cr-1 Mo steel	No weld	0 of 3	0 of 3			
2 1/4 Cr-1 Mo, Ni, Nb (HT 8 x 6) steel	No weld	0 of 3	0 of 3			
5 Cr-1/2 Mo steel	No weld	0 of 3	0 of 3			
9 Cr-1 Mo steel	No weld	0 of 3	0 of 3			
12 Cr steel	No weld	0 of 3	0 of 3			
12 Cr steel	12 Cr steel	0 of 6	0 of 6	0 of 3		
12 Cr-1 Mo, Ni, W, V (HT-9) steel	No weld	0 of 3	0 of 3			
26 Cr-1 Mo steel	No weld	3 of 3	3 of 3		Large	B

^aWelds were prepared by the gas tungsten-arc process; the duration of test was 12 to 16 weeks.

^bFor surface conditions indicated by G, ground on 100-mesh belt; A, ground and annealed; P, ground, annealed, and pickled.

^cW = weld deposit, B = base metal, FL = fusion line.

Figure 13.6 illustrates failed U-bend specimens in Incoloy 800 welded with Inconel 82 and the microstructural characteristics of the cracks that formed. The cracks in this weldment and various of the other failed weldments of Table 13.1 were usually intergranular; generally they initiated alongside the root pass and progressed along the heat-affected zone. Occasionally cracks propagated into the weld deposits, but never to any appreciable extent in the case of the Incoloy 800 weldment made with Inconel 82.

The testing of materials as inverted U-bend and tubular specimens (Fig. 13.5) is presently under way. Preliminary indications are that for some materials,

type 304 stainless steel welded with type 308 and Hastelloy N welded with itself included, the test environment above the water level may be more severe than that below. It should be noted that while the amount of chloride present here was exceedingly low, specimens tested many cycles may be subject to significantly higher concentrations as a result of chloride accumulation.

Caustic. Southern Nuclear Engineering, Inc., recently completed fabrication of an Inconel 625 corrosion loop for investigating stress corrosion in steam with caustic as the contaminant. Tests in this loop are scheduled to begin in October 1972.

Y-113974

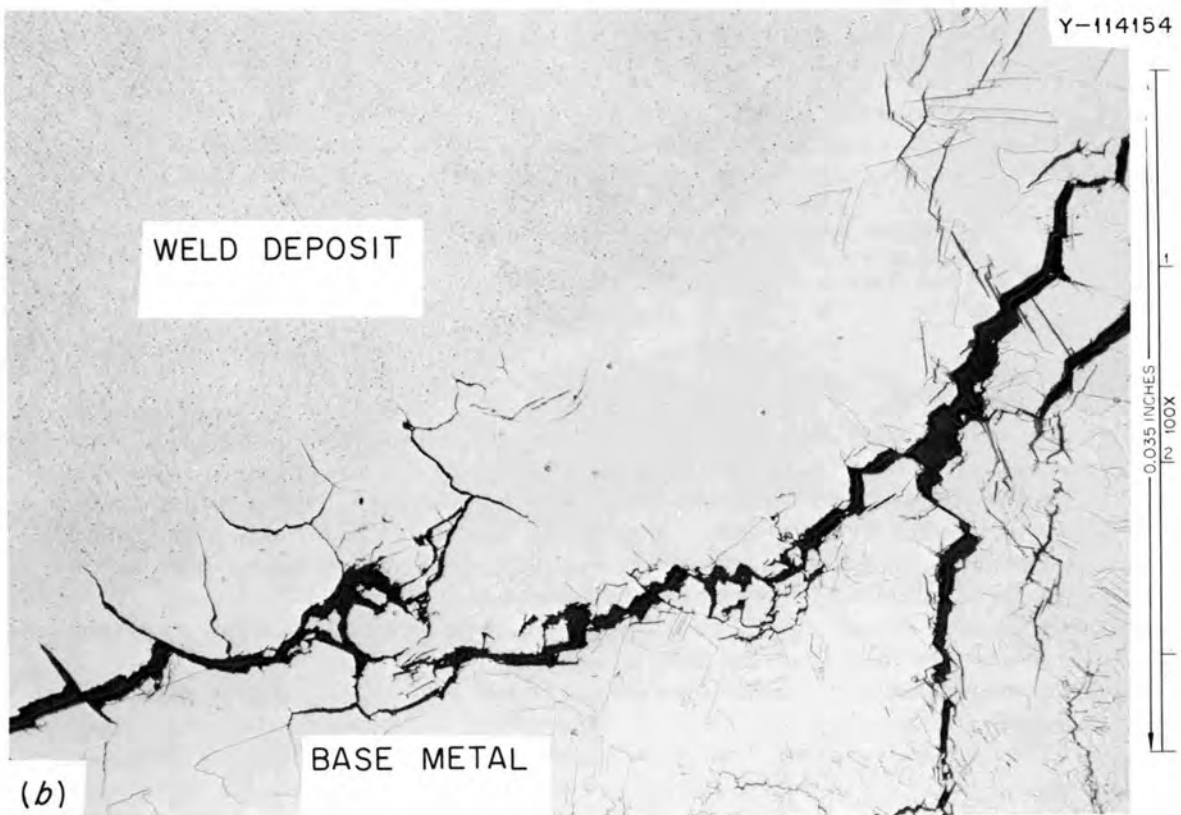
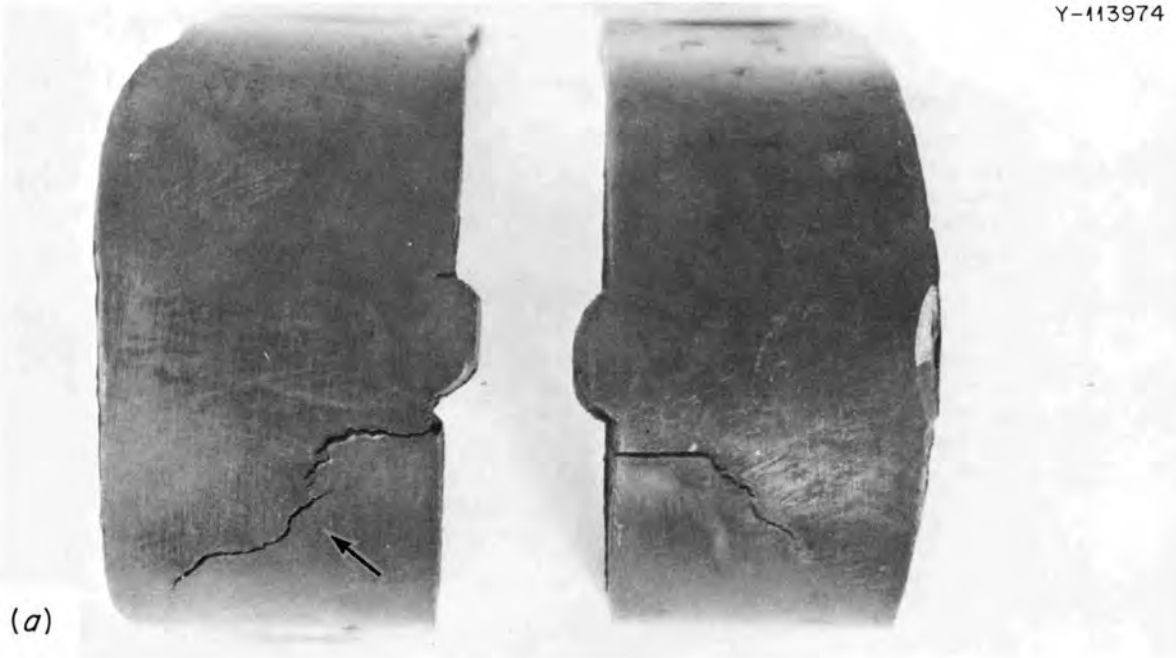


Fig. 13.6. Characteristics of chloride stress corrosion in Incoloy 800 welded with Inconel 82. (a) U-bend specimens after failure. (b) Microstructural features of cracks at arrow on *a*. Etched with H_2O_2 -HCl mixture. Cracks here tend to be intergranular when in the heat-affected zone, but transgranular in the fine-grained material beyond.

14. Development of FBR Neutron-Absorber Materials

R. G. Donnelly W. R. Martin

Boron carbide is planned for control and shim rods for the FTR and demonstration LMFBR. Tantalum is also considered for the demonstration reactor. However, more data are required on the fast-reactor-irradiation behavior of these materials to assure safe and reliable performance for the desired service time. The solid swelling, gas release, and compatibility of boron carbide during irradiation are three of the principal problems. Principal problems with tantalum alloys are lower reactivity worth, solid swelling, compatibility, high after-heat, and stability of mechanical properties during irradiation. Some borides and rare-earth oxides have more reactivity worth per unit volume than tantalum but lack sufficient characterization and irradiation experience to warrant consideration at this time.

The purposes of this program are (1) to determine the irradiation performance of boron carbide and tantalum under expected operating conditions in the FTR and demonstration LMFBR and determine how materials and operating variations affect this performance, (2) to develop vent materials so that helium generated during irradiation of boron carbide may be safely and reliably released to the coolant, and (3) to investigate alternate materials that have possible advantages over boron carbide and tantalum for fast-reactor service and to provide sufficient pertinent data for an evaluation of their performance in service.

IRRADIATION BEHAVIOR OF BORON CARBIDE

Microstructure of Boron Carbide after Fast-Neutron Irradiation¹

A. Jostsons² C. K. H. DuBose

Transmission electron microscopy has been used to investigate the nature of defect clusters produced in boron carbide by fast-neutron irradiation. Ion milling

was used to prepare specimens from pellets of Argonne National Laboratory "higher worth" control rod irradiated in row 5 of EBR-II at an estimated temperature of 500°C to a burnup of 1.7% of ¹⁰B (5470 MWd).

The defect clusters, shown imaged in diffraction contrast in Fig. 14.1a, superficially resembled the vacancy and interstitial dislocation loops formed in neutron-irradiated metals at temperatures below about 0.3 of their absolute melting temperatures. The defect clusters in boron carbide were not prismatic dislocation loops because the size of their images did not change on reversing the sign of the diffraction vector. Under absorption contrast conditions the defects appeared as narrow bright bands surrounded by dark Fresnel fringes in the under-focus condition (Fig. 14.1b) and as dark bands surrounded by light Fresnel fringes in the over-focus condition (Fig. 14.1c). This demonstrates unambiguously, according to the image calculations of Rühle,³ that the defects are small cavities. The lobes of dark contrast in the diffraction image indicated that the lattice surrounding the defects is highly strained, but image overlap prevented determination of the sign of the strain. For this irradiation condition the cavities were present in a concentration of about 10¹⁶/cm³. They were ribbon-like, with the largest face most frequently parallel to the trace of the (111) plane and less frequently to traces of {100} and {110}, indexed on the rhombohedral unit cell. The largest dimension of the cavities ranged between 30 and 200 Å.

The lattice strains around the cavities were eliminated by annealing at or above 1450°C. Annealing also reduced the concentration of cavities but increased their average size.

These cavities are in sharp contrast to the voids found in irradiated metals, which shrink and disappear on annealing and have no noticeable strain fields around them. We conclude that in boron carbide irradiated near

1. Summary of a paper accepted for publication in *Journal of Nuclear Materials*.

2. On attachment from the Australian Atomic Energy Commission, Research Establishment, Lucas Heights, N.S.W.

3. M. R. Rühle, "Transmission Electron Microscopy of Radiation-Induced Defects," p. 255 in *Radiation-Induced Voids in Metals*, ed. by James W. Corbett and L. C. Ianniello, USAEC Office of Information Services, Oak Ridge (1972).

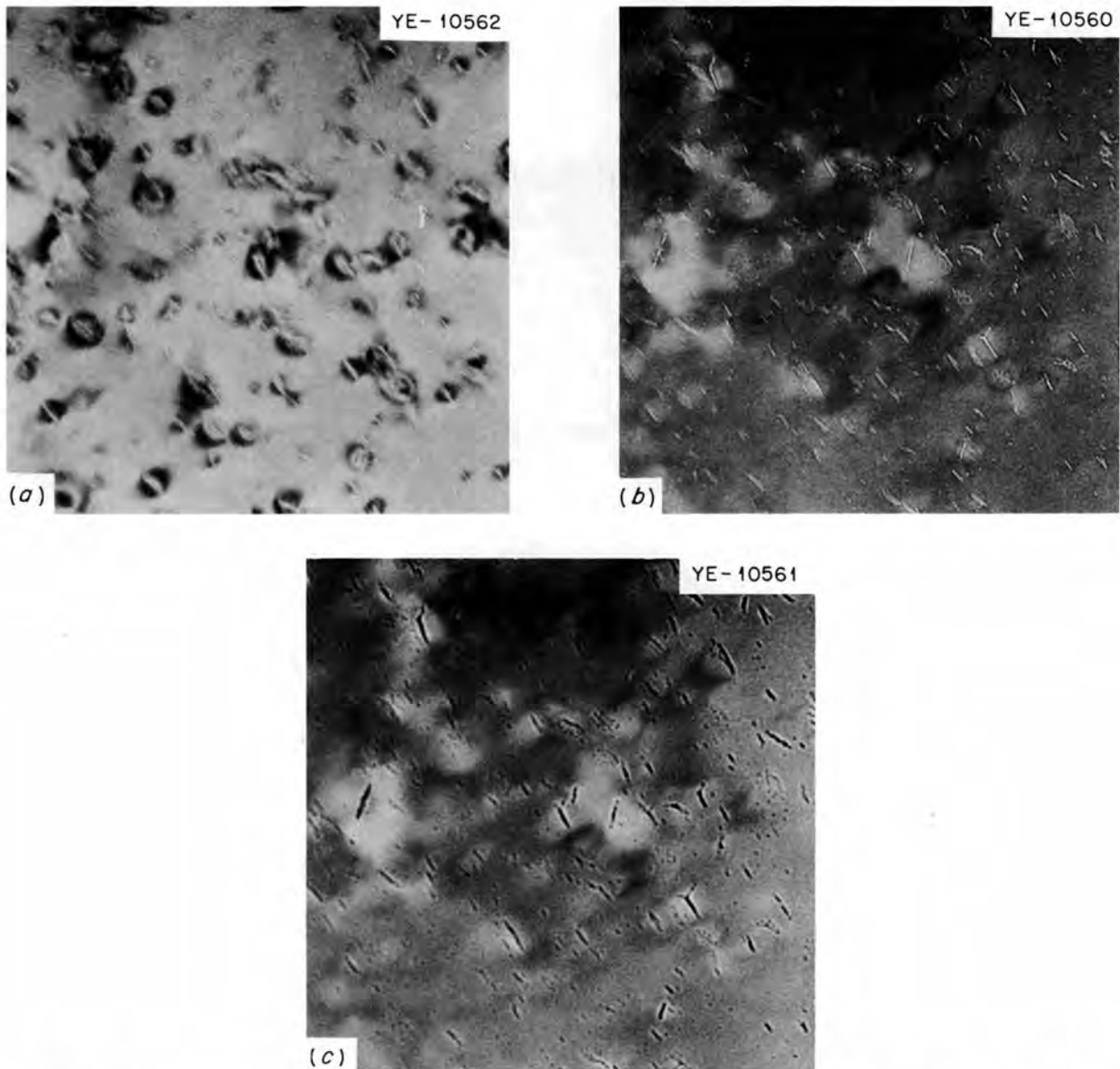


Fig. 14.1. Transmission electron micrographs illustrating the defect structure in neutron-irradiated boron carbide. (a) Bright-field two-beam condition. Bright field absorption contrast with (b) under-focused and (c) over-focused. This specimen had been annealed 1 hr at 1150°C. Similar but smaller defects were present as irradiated. 100,000X.

500°C the cavities probably contain helium at a pressure too high to balance the surface tension restraint. This is the source of the lattice strain. Upon annealing, the cavities grow into equilibrium bubbles, thereby eliminating the strain. According to Speight⁴

4. M. V. Speight, *Met. Sci. J.* 2, 73 (1968).

such behavior is possible under conditions of high gas content if the diffusion coefficient of the gas atoms is much higher than the vacancy diffusion coefficient.

These observations indicate that the helium atoms do not remain dissolved in the open boron carbide lattice and that gas release will be limited by trapping of helium in the cavities.

Evaluation of Fast-Reactor-Irradiated Boron Carbide Powders⁵

G. L. Copeland H. L. Yakel
C. K. H. DuBose

Boron carbide powders were irradiated by Hanford Engineering Development Laboratory in EBR-II to burnups of 3.7 and 4.8% of ^{10}B (7.7 and 10×10^{20} $n, \alpha/\text{cm}^3$) at 730 and 650°C , respectively. We examined the powders by transmission electron microscopy and x-ray diffraction as irradiated and after annealing for 1 hr at temperatures from 700 to 1900°C . As-irradiated powders contained platelike or ribbon-like cavities accompanied by complex strain fields. Previously examined powders irradiated in a thermal-spectrum reactor showed uniform black-spot damage resulting from defects too small for resolution.⁶ The unit cell volume had decreased about 0.4% by a decrease in the rhombohedral a parameter with only a small change in the angle α . After annealing at 1450°C for 1 hr, the lattice parameters had returned essentially to the unirradiated values. The cavities had grown to slab-shaped bubbles, and the strain fields had essentially disappeared. At higher annealing temperatures the bubbles became more equiaxed.

Evaluation of Boron Carbide Pellets from EBR-II Higher Worth Control Rod

G. L. Copeland H. L. Yakel

We have examined capsules G and H from the EBR-II Higher Worth Control Rod. These capsules contained natural boron carbide pellets hot pressed to an average 95% of theoretical density. Each capsule contained 14 pellets about 0.54 in. in diameter by about 1 in. long. The assembly was irradiated at 500°C for 5468 MWd in row 5 of EBR-II, resulting in burnup ranging from about 1 to 1.7% ^{10}B depletion (2.1 to 3.6×10^{20} $n, \alpha/\text{cm}^3$). Plenum gas analysis of capsule H indicated that less than 2% of the helium generated had been released to the plenum during irradiation. Visually the pellets appeared to be in excellent condition. Average volume swelling (determined by dimensional measurements) of the pellets during irradiation was 0.28 and 0.38% for capsules G and H, respectively. Metallography revealed some microcracking, primarily in the

interface between graphite inclusions and the boron carbide and along adjacent grain boundaries.

The lattice parameters as determined by x-ray diffraction after irradiation showed a unit cell volume increase of about 0.3% through an increase in the rhombohedral a parameter and a slight decrease in the angle α . This is in contrast to the powders described above, which decreased in the unit cell volume. After annealing, the lattice parameters behaved similarly. With increasing annealing temperature, a first increased and then decreased to the unirradiated value, whereas α first decreased and then increased to the unirradiated value. The unit cell volume decreased uniformly and returned to the unirradiated value after annealing at about 1300°C .

Transmission electron microscopy revealed bubbles within the grains similar to those in the powders but smaller. A denuded zone free of bubbles was observed adjacent to grain boundaries. Bubbles on the grain boundaries were so few and small that they were found only after grain boundary bubbles had been observed in the X-099 pellets described below. After annealing at 1400°C or greater, the bubbles became very apparent and coalesced similarly to those in the X-099 pellets. In addition, during annealing, bubbles grew within the grains similarly to those in the powders. This results in overall swelling of the material. Pellets annealed 1 hr at 1025 , 1475 , and 1900°C swelled 0.45, 1.23, and 10.8% in volume, respectively. During the 1475°C anneal 29% of the retained helium was released.

Evaluation of Boron Carbide Pellets from ORNL EBR-II Experiment X-099

G. L. Copeland A. Jostsons²

We are examining six pins containing natural boron carbide pellets that had been irradiated for 9700 MWd in row 7 of EBR-II. The results to date on swelling and gas release measurements are shown in Table 14.1. The swelling is higher than anticipated in the O-5 pins and lower than expected in the O-9 and O-10 pins. The gas release is higher than expected for the low-temperature pins and relatively insensitive to temperature (if the pins operated near their design temperatures). The denser pellets released more gas in each case. The most significant result is the severe cracking and lamellar fragmentation observed in pellets in O-9T and O-10T (higher density, higher temperature). Both high- and low-density pellets in O-10 showed radial cracking also. Weakening and separation of the grain boundaries due to gas bubble precipitation and coalescence are thought

5. Modified abstract from ORNL-TM-3729 (May 1972).

6. G. L. Copeland, C. K. H. DuBose, and D. N. Braski, *Metals and Ceramics Div. Annu. Progr. Rep. June 30, 1971*, ORNL-4770, p. 103.

Table 14.1. Summary of data from boron carbide EBR-II test X-099 (as of June 12, 1972)

Pin	Boron-to-carbon ratio	Pellet density (% of theoretical)	Calculated irradiation temperature ^a (°C)	Volume change ^b (%)	Helium released during irradiation ^c (% of total)	Burnup based on total helium		Comments
						Percent ¹⁰ B	$n, \alpha/\text{cm}^3$	
							$\times 10^{20}$	
O-5T	3.8	99	430	2.64	49.3	2.71	5.68	No cracks
O-5B	3.8	90	430	3.29	31.4	3.10	6.50	No cracks
O-9T	3.8	99	750	0.53	40.8	2.75	5.78	No cracks in 6, 7, 8; extensive lamellar cracks in 1-5; no radial cracks
O-9B	3.8	90	750	0.15	34.3	3.01	6.32	No cracks
O-10T	4.2	99	750	1.71	55.4	2.78	5.89	Lamellar and radial cracks; extensive in 1-5
O-10B	4.2	90	750	0.76	49.2	3.06	6.48	Radial cracks; no lamellar

^aBased on gamma heating values for EBR-II as of about March 1972.

^bAverage of eight pellets except for O-9T (pellets 6, 7, 8) and O-10T (pellets 5, 6, 7, 8). Sum of twice the percentage diameter change and the length change.

^cBased on plenum puncture plus vacuum fusion for retained helium.

to be responsible for the cracking. This same mechanism is operating in the lower temperature, lower density pellets and would probably lead to cracking in these pellets at higher burnups.

The high concentrations of bubbles on the grain boundaries are revealed by transmission electron microscopy. These bubbles coalesce, leaving regions of the grain boundaries completely separated. Within the grains, the bubbles have the flat anisotropic shapes with strain fields similar to previous observations. Figure 14.2 shows bubble coalescence at a grain boundary triple point where two of the boundaries are at an angle to the foil. The third boundary is perpendicular to the foil and appears to be almost completely separated. The top grain has contrast to show the strain fields, the contrast shows the bubbles in the right grain, and both are out of contrast in the lower grain. The denuded zone is about 0.2 μm wide, compared to the about 0.15 μm in the EBR-II Higher Worth Control Rod pellets. The bubbles are also strongly attracted to dislocations and stacking faults. If the preferred growth direction of the bubbles lines up with the dislocation or stacking fault direction, these bubbles line up to form extended cracks.

Scanning electron microscopy of surfaces fractured after vacuum annealing at 1600°C for 1 hr reveals a precipitate that was not observed as irradiated and may be a lithium compound, as indicated in Chap. 37 of this

report. Nuclear magnetic resonance studies of as-irradiated boron carbide have given tentative evidence that the lithium is present as ions randomly distributed on interstitial sites. The lithium may precipitate during the anneal and then form compounds when exposed to the atmosphere on the fracture surface.

PERFORMANCE MODELING OF NEUTRON ABSORBERS⁷

F. J. Homan

A computer code to predict the performance of fast-reactor control rods was developed and used to analyze the integrated behavior of a FTR-type control rod in row 2 of EBR-II. In particular, the influence of the ¹⁰B enrichment and solid reaction product swelling have been considered. Control rod claddings are predicted to begin rapid plastic strain very shortly after the fabricated gap between the absorber pellets and the cladding has closed. This strain is due to high contact pressure, which develops with continued pellet swelling. Models for helium gas bubble swelling and release are presented; they suggest minimum swelling from this source at about 1000°C.

7. Abstract of paper presented at the American Nuclear Society Meeting, Richland, Wash., April 24-27, 1972.

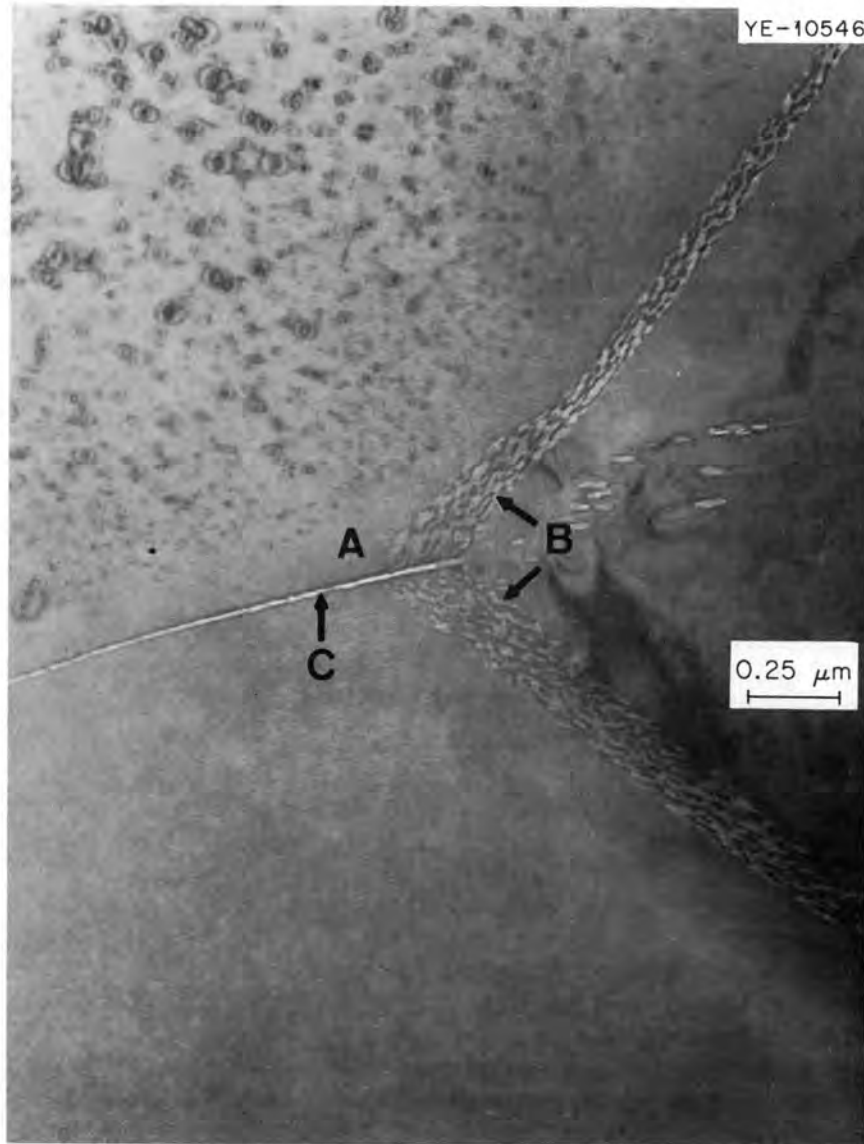


Fig. 14.2. Transmission electron micrograph of irradiated boron carbide showing (A) area adjacent to grain boundary, which is free of bubbles (denuded zone); (B) helium bubble coalescence on grain boundaries; and (C) edge view of grain boundary, indicating virtual separation of the grains. 50,000 \times .

DEVELOPMENT OF VENTS

J. I. Federer

Control rods for the Fast Test Reactor (FTR) consist of boron carbide pellets sealed in a stainless steel container. These rods are limited in life by helium generated from the $^{10}\text{B}(n,\alpha)^7\text{Li}$ reaction. The pressure of helium generated would eventually cause swelling of the stainless steel container, forcing removal of the rods from the reactor before the ^{10}B has been used most efficiently. The purpose of this task is to develop a

venting device to release helium from such absorber elements into the sodium coolant. The basic requirements of helium vents in this application are: (1) a helium leak rate approximately equal to the release rate from boron carbide so as to minimize differential pressure across the vent, (2) compatibility with sodium at about 600°C, (3) no intrusion of sodium into the element due to hydraulic or capillary forces. Important elements of this task include fabrication of porous disks, bonding disks to holders, and characterization of vent assemblies.

Stainless steel and molybdenum disks have been cold pressed and sintered. After sintering, helium leak rates are determined with a calibrated helium leak detector. We are striving to obtain helium leak rates of 10^{-4} to 10^{-3} std cm^3/sec , a range that brackets recent data on helium release from boron carbide. However, vents having larger leak rates than 10^{-3} std cm^3/sec might also be used.

Sintered disks evidently have more porosity around the edges than elsewhere since a slight reduction in the diameter by machining substantially decreases the leak rate in most cases. We are attempting to minimize edge porosity by using a special die punch that densifies the edges of pressed disks about 10% more than the central region. We have also observed that the porosity is unevenly distributed. Flow generally occurs over about one-third of the total area of a disk face. This behavior is attributed to the difficulty in leveling the powder in the die before pressing.

Porous disks having the desired leak rates in the sintered condition must be bonded to a holder such as a tube to form a vent assembly. Bonding by electron-beam welding, brazing, and swaging has been tried. Welding is preferred to brazing, since the latter method introduces materials that may be less resistant to sodium corrosion than the disk and holder. The welded and brazed joints are qualitatively tested by observing the location of helium bubbles in alcohol placed on one side of the disk.

For type 316 stainless steel disks, sintering at 1200°C for 8 hr produced helium leak rates in the range 10^{-4} to 10^{-3} std cm^3/sec with a differential pressure of 1 atm across the disk. Mechanical sealing of these disks in stainless steel tubes to form vent assemblies has been unsuccessful and electron-beam welding only moderately successful. However, brazing with Nicrobraz 50 alloy at 1025°C has consistently produced leak-tight joints.

Molybdenum disks require sintering at 1600°C for 4 hr. However, attempts to braze these disks to type 304 stainless steel tubes with a variety of alloys were unsuccessful. This difficulty was overcome by substituting type 430 stainless steel, which has a coefficient of thermal expansion more closely matching that of the molybdenum.

Our plans include testing of vent assemblies in sodium, fabrication and characterization of vent assemblies with ceramic porous disks, and chemical vapor deposition of porous materials.

THE EFFECT OF TEMPERATURE ON THE MICROSTRUCTURE OF NEUTRON-IRRADIATED TANTALUM⁸

F. W. Wiffen

Fully recrystallized unalloyed tantalum irradiated in EBR-II to 2.5 to 4.4×10^{22} neutrons/ cm^2 (>0.1 MeV) at 425 , 585 , 790 , and 950 to 1050°C was examined by transmission electron microscopy to characterize the damage microstructure. The microstructure produced by irradiation at 425°C contained primarily a very high density of small "black spots," which could not be identified but were likely dislocation loops. There was no tendency for these loops to cluster, and no voids were identified in the sample. The damage was similar to that found at 450°C at one-eighth the fluence.⁹ The samples irradiated at the higher temperatures all contained voids. Void concentrations were determined from sample thicknesses measured stereographically, and void sizes were measured on a particle size analyzer. The void parameters given in Table 14.2 show that trends established in other metals are also seen in tantalum. Within the temperature range of void formation the void concentration decreased and the average void size increased with increasing temperature. Void-denuded zones adjacent to grain boundaries were quite narrow in the specimens, only a few hundred angstroms in width. These narrow denuded zones were usually bordered by zones with higher than average void concentrations. The data in Table 14.2 show that the

8. Revised from summary of talk published in *Trans. Amer. Nucl. Soc.* **14**, 603 (1971).

9. G. L. Kulcinski and B. Mastel, "Microstructure of High-Temperature Neutron-Irradiated Tantalum and Molybdenum," *J. Appl. Phys.* **41**, 4752 (1970).

Table 14.2. Void parameters for neutron-irradiated tantalum

Irradiation temperature ($^\circ\text{C}$)	Fluence ^a (neutrons/ cm^2)	Void parameters		
		Concentration (voids/ cm^3)	Average diameter (A)	Volume fraction (%)
	$\times 10^{22}$	$\times 10^{15}$		
425	2.5	0		
585	2.5	190	61	2.4
790	2.5	6.1	117	0.65
950-1050	4.4	$\leq 0.3^b$	130	$\leq 0.03^b$

^a >0.1 MeV.

^bVoid concentration locally variable. These are upper limits.

temperature range for maximum swelling of irradiated tantalum falls somewhere between 450 and 750°C and can be expected to be in the range 500 to 650°C. These results also show that the lower temperature limit for void formation is between 450 and 550°C and suggest that the upper temperature limit, at the fluence reported here, is probably not very much above 1000°C. These limits on the "temperature window" in which voids form are in close agreement with the limits 500 to 1000°C for void formation calculated by the Bullough-Perrin model,¹⁰ using an activation energy of self-diffusion of 4.78 eV and a vacancy migration energy of 1.25 eV.

The voids in the sample irradiated at 585°C were partially ordered on a bcc superlattice, which was parallel to the bcc metal lattice and had a superlattice parameter of 205 Å. Voids occupied 80% of the superlattice points. The voids in the 790 and 1000°C specimens were not ordered, but they tended to be clustered in the specimen irradiated at 790°C.

The dislocation and loop structures in all samples were partially obscured by deformation during thinning and handling and have not yet been analyzed in detail.

ALTERNATE ABSORBER MATERIALS

M. M. Martin

Our objective is to characterize promising materials other than boron carbide and tantalum alloys for which there are now insufficient data to permit consideration of their use in fast-reactor control systems. Work was concentrated on the tantalum borides but recently has been expanded to include europium sesquioxide. Factors considered are reactivity worth, fabricability, irradiation performance, and compatibility with cladding and coolant.

We have fabricated and characterized pellets of three tantalum borides for irradiation at 500°C in EBR-II. One is a multiphase Ta-TaB_x cermet containing 3.6 wt % B in which the boron is enriched to 40 at. % ¹⁰B. The others are hexagonal TaB₂ of both stoichiometric (2.00) and hypostoichiometric (1.75) compositions. All of these materials have a reactivity worth slightly better than B₄C containing natural boron.

REACTOR EXPERIMENT DESIGN AND FABRICATION

T. N. Washburn E. J. Manthos
J. W. Woods D. A. Dyslin¹¹

The capsules for irradiation testing in EBR-II are listed in Table 14.3. Test series 1, subassembly X-099A, is scheduled to begin irradiation in August 1972 and contains three capsules (O-6, O-7, and O-8) previously irradiated in this subassembly, two capsules (O-12 and O-13) designed and fabricated this year, and two capsules (BTA-7 and -8) fabricated at HEDL. These latter two capsules had end fittings that are no longer standard at EBR-II, and a standard subassembly was modified to accept these two capsules.

The seven capsules for test series 2α were designed and fabricated during FY 1972, and irradiation in EBR-II is scheduled to begin in late August. Capsule O-27 contains test specimens from HEDL capsule B-58, which was disassembled at ORNL to modify the specimen holders to use our standard spacer hardware. These changes were made to reduce the level of uncertainty in calculating specimen temperature.

We began design and fabrication of the seven capsules for test series 2β. Capsule O-23 is funded by NASA and is a high-temperature (1200°C) test of the performance of boron carbide.

10. R. Bullough, personal communication, June 1971.

11. General Engineering Division.

Table 14.3. Neutron absorber irradiation experiments

Test series	Subassembly	Capsule	Control material ^a	Design temperature (°C)
1	X-099A	O-6	B _{4.5} C and B _{4.5} C	430
		O-7	B _{4.5} C and B _{4.5} C	430
		O-8	B _{3.8} C and B _{3.8} C	430
		O-12	Ta alloys	400–900
		O-13	Ta alloys	400–750
		BTA-7 ^b	Ta	700–1250
		BTA-8 ^b	Ta	700–1250
2 α	X-164	O-14	B _{4.0} C + B and B _{4.5} C	430
		O-15	B _{6.5} C and B _{4.0} C	430
		O-16	B _{6.5} C and B _{4.0} C	700
		O-17	B _{6.5} C and B _{4.0} C	850
		O-18	TaB ₂ and B _{4.0} C	500–430
		O-20	Ta ₂ *B and TaB ₂	500
		O-27 ^c	Ta alloys	400–900
2 β	X-1yy	O-19 ^d	B ₄ C+Na and irradiated B _{3.8} C	430
		O-21	*B _{6.5} C and *B ₄ C	700
		O-22	*B _{6.5} C and *B ₄ C + compatibility	700
		O-23	*B _{6.5} C and *B ₄ C	1200
		O-24	*B _{6.5} C and *B ₄ C	700
		O-25	*B _{6.5} C and *B ₄ C + compatibility	700
		O-26 ^d	B _{3.8} C and B _{4.2} C (irradiated)	430 and 750

^aAsterisk indicates that isotopic content of boron differs from naturally occurring content of 19.8% ¹⁰B.

^bCapsules supplied by HEDL.

^cO-27 is reencapsulation of HEDL's B-58.

^dO-26 and O-19B are reconstitution of pellets from X-099 after irradiation.

15. Development of FBR Oxide Fuels

A. L. Lotts F. J. Homan

The oxide fuels development program was a five-year program conducted to advance the technology of (U,Pu)O₂ as an LMFBR fuel. Funding for this program was terminated on June 30, 1972. The program emphasized determination of the properties and performance of sol-gel-derived oxide fuels fabricated by the Sphere-Pac and pelletizing techniques. The performance of these fuels was compared with that of other fuels, such as pellets from mechanically blended or coprecipitated oxide. The main objectives of the oxide fuels development program were:

1. to establish the performance characteristics and limitations of (U,Pu)O₂ fuels fabricated by different processes,
2. to obtain a fundamental understanding of the mechanisms involved in the irradiation behavior of fuel elements incorporating these fuels,
3. to develop fabrication techniques that provide both economy and a product with optimized performance, and
4. to develop analytical models sufficiently accurate to optimize experimental design and to predict fuel element response to LMFBR conditions.

These objectives were met through a program that included fabrication of fuel with different structures, characterization of these structures by out-of-reactor methods, and irradiation under a variety of conditions. The program emphasized irradiation testing, postirradiation examination of the various fuel structures, and evaluation of the results in terms of performance models.

Since a number of irradiation tests were still in progress when the program was terminated, responsibility for these tests was turned over to other USAEC contractors. Accordingly, all documentation, quality assurance work, and archive specimens have been transferred.

DEVELOPMENT OF FABRICATION PROCESSES

J. D. Sease R. A. Bradley

The objective of our (U,Pu)O₂ fabrication program was to develop processes by which mixed oxide fuel of controlled density and stoichiometry can be fabricated for irradiation tests. A large portion of this work has been the development of Sphere-Pac and sol-gel pellet fabrication techniques. The Sphere-Pac process, which uses low-energy vibration to infiltrate a close-packed bed of coarse microspheres (420 to 600 μm) with fine microspheres (<44 μm), has been used to load a number of fuel pins for irradiation tests to smear densities 82 to 84% of theoretical.¹ During the past year we prepared the fuel and loaded the fuel pins for two instrumented ETR capsules and for two irradiation experiments on the Gas-Cooled Fast Breeder Reactor program.

We fabricated the fuel pins for two instrumented capsules (ORNL 43-125 and 43-126) for in situ measurement of fission gas release. The irradiation experiment is described in more detail later. Each fuel pin contains approximately 20 in. of mixed oxide fuel. One contains U_{0.75}Pu_{0.25}O_{1.97} pellets fabricated by WADCO from mechanically mixed powders. The other was loaded by the Sphere-Pac process with U_{0.73}Pu_{0.27}O_{1.97} coarse microspheres and UO₂ fine microspheres to yield a nominal fuel bed of composition U_{0.80}Pu_{0.20}O_{1.98}. The smear densities of both the Sphere-Pac and the pellet pins are 83.5 ± 1.0% of theoretical.

Five replacement fuel pins were fabricated for the GCFBR F-1 irradiation experiment described in Chap. 25 of this report. These fuel pins contained both solid and annular (U,Pu)O₂ pellets with densities 87 and 92%

1. R. A. Bradley, W. J. Lackey, and J. D. Sease, *Metals and Ceramics Div. Annu. Progr. Rep. June 30, 1971*, ORNL-4770, pp. 38-39.

of theoretical and oxygen-to-metal ratios of 1.94 and 1.98. The preparation of the sol-gel powder² and the fabrication of the pellets³ have been described previously.

Fuel for the GCFBR GB-10 capsule, also described in Chap. 25, was fabricated and loaded into the fuel pin. It contains 8.8 in. of nominally 87.5%-dense dished-end $U_{0.88}Pu_{0.12}O_{1.97}$ pellets, with the uranium containing 9% ^{235}U .

IRRADIATION BEHAVIOR

F. J. Homan T. N. Washburn

The irradiation testing portion of the FBR Oxide Fuels Program has been directed at determining the in-reactor properties and performance of (U,Pu) O_2 fuel pins as functions of fabrication form, porosity distribution, stoichiometry, and irradiation conditions. The program included both fast and thermal flux irradiations and steady-state, cyclic, and transient power conditions. Our irradiation program has shown that Sphere-Pac fuels exhibit better cladding-fuel compatibility and thermal conductance than pellet fuels. In all other respects, pellet and Sphere-Pac fuels perform similarly.

Fast Flux Irradiation Tests

A. R. Olsen

The ORNL oxide fuels irradiation in the EBR-II consisted of two series of tests. The five encapsulated Series I pins⁴ all contained Sphere-Pac (^{235}U -20% Pu) O_2 . Series II included 53 unencapsulated pins.⁵ We fabricated 19 of the pins inserted in the first 37-pin subassembly and one replacement pin. The Babcock and Wilcox Company (B&W) fabricated 33 pins, 18 for the initial subassembly loading and 15 replacements. The ORNL pins contained Sphere-Pac and pellet fuels all derived from a sol-gel process. The B&W pins contain sol-gel-derived Sphere-Pac fuels or pellets and Vi-Pac

shards processed from coprecipitated powders. These tests emphasized the effects of fuel form and void distribution on the release of fission gas, fission product redistribution, and mechanical and chemical interactions of fuel and cladding. Linear heat rates were 14 to 16 kW/ft, peak cladding temperatures from 550 to 650°C, and burnup levels up to 13% fissions per initial actinide metal atom (FIMA).

Two pins from the Series I group were examined after a peak burnup of 6% FIMA. The results have been discussed previously,^{6,7} and a final report is in preparation.⁸ The remaining three pins were irradiated for an additional 5200 MWd of EBR-II operation to a peak calculated burnup level of 8.1% FIMA. The nondestructive interim examination of the pins indicated no abnormal behavior, and they are being inserted for continued irradiation.

The unencapsulated Series II pins were irradiated in subassembly XI12 for 10,600 MWd of EBR-II operation. The lead pin peak burnup is approximately 3.8% FIMA. Argonne National Laboratory will assume responsibility for these experiments on July 1, 1972. All replacement pins and the necessary quality assurance documentation have been shipped to the EBR-II project.

Uninstrumented Thermal Flux Irradiations

A. R. Olsen

We have irradiated 11 capsules in this series, six to provide preliminary performance data on sol-gel Sphere-Pac fuels and five, two of which are still under irradiation, to provide short-cooled irradiated fuel for reprocessing studies. The detailed description, purpose, scope, conditions of irradiation, and some results have been reported previously.⁹ The results of the tests irradiated for performance analysis have been presented,¹⁰ and a topical report is in preparation.

2. R. A. Bradley and J. D. Sease, *Gas-Cooled Reactor Program Semiannual Progr. Rep. Sept. 30, 1970*, ORNL-4637, p. 49.

3. J. D. Sease and R. A. Bradley, *Fuels and Materials Development Program Quart. Progr. Rep. Sept. 30, 1971*, ORNL-TM-3550, pp. 4-6.

4. A. R. Olsen, *Experiment Description and Hazards Evaluation for the Series I ORNL Oxide Fuels Irradiation in EBR-II*, ORNL-TM-2635 (April 1970).

5. A. R. Olsen et al., *Preirradiation Data for ORNL Series II and B&W Oxide Fuel Tests in EBR-II*, ORNL-TM-3446 (November 1971).

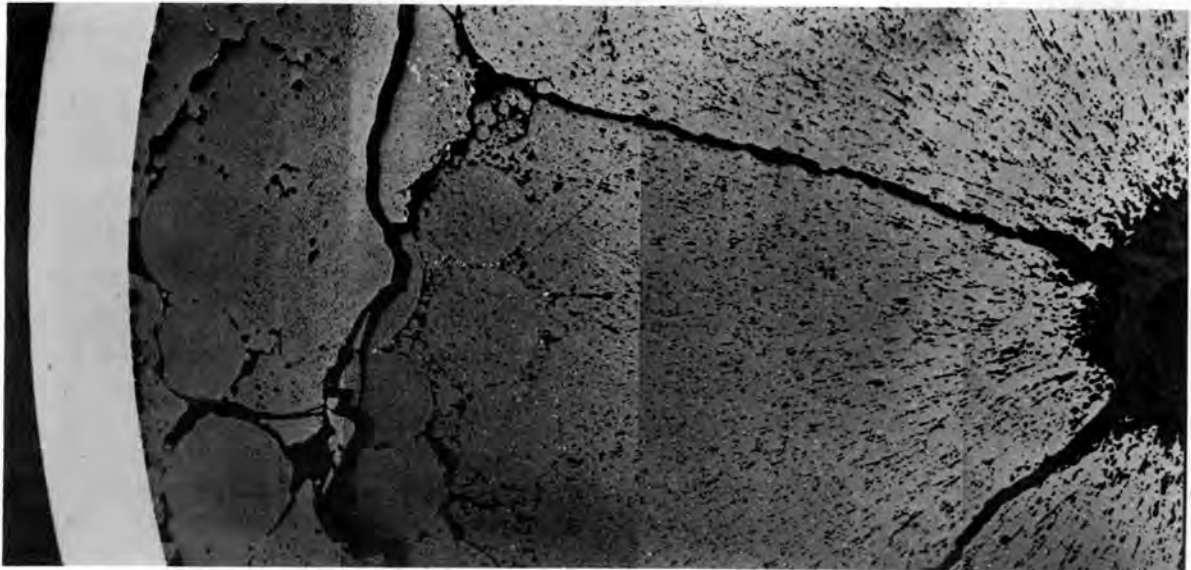
6. A. R. Olsen, *Metals and Ceramics Div. Annu. Progr. Rep. June 30, 1971*, ORNL-4770, pp. 45-47.

7. A. R. Olsen, "Sol-Gel Sphere-Pac (U,Pu) O_2 Fuel Performance in EBR II Irradiation Tests," *Trans. Amer. Nucl. Soc.* 14(2), 596-97 (October 1971).

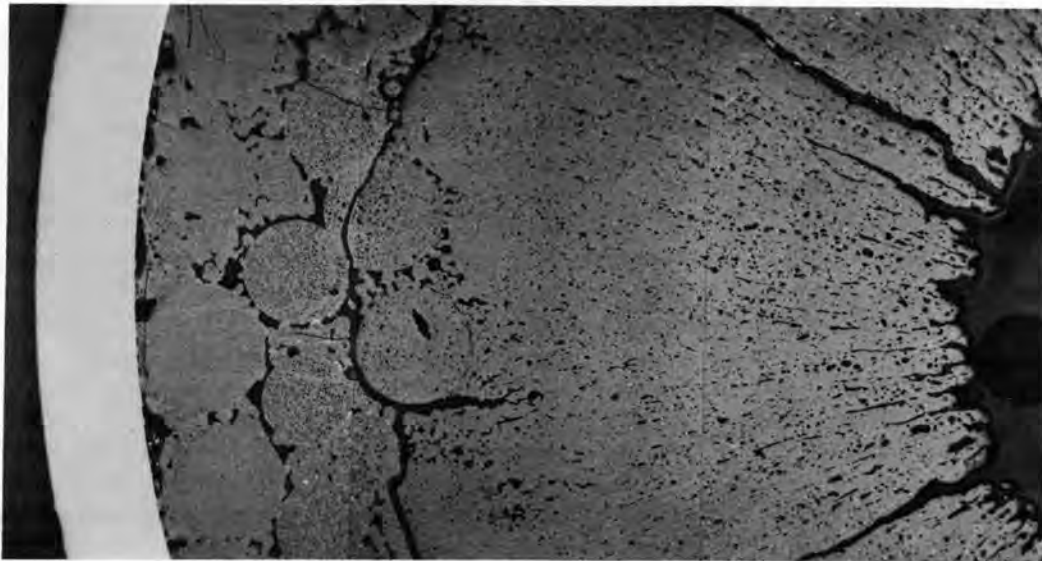
8. A. R. Olsen, *Sol-Gel Sphere-Pac (U,Pu) O_2 Fuel Performance to Intermediate Burnup Levels in a Fast Flux Environment*, report in preparation.

9. A. R. Olsen and D. R. Cuneo, *Metals and Ceramics Div. Annu. Progr. Rep. June 30, 1970*, ORNL-4570, pp. 53-55.

10. A. R. Olsen, C. M. Cox, and R. B. Fitts, *Trans. Amer. Nucl. Soc.* 12, 605-6 (1969); A. R. Olsen, *ibid.* 13, 32-33 (1970), and 15, 181-82 (1972).



43-113-1, 8.8 kW/ft, 8.6% FIMA



43-113-4, 9.6 kW/ft, 9.7% FIMA

↑
0.04 in.
↓

Fig. 15.1. Comparative microstructures of $U_{0.85}Pu_{0.15}O_{1.98}$ fuel pins. As polished.

The examination of the last performance data capsule was completed. The peak burnup achieved in a $^{238}U_{0.85}Pu_{0.15}O_{1.97}$ fuel pin was 11.3% FIMA while the comparison 20%-enriched UO_2 pin reached 13.8% FIMA. This difference reflects the difference in initial percentages of fissionable isotopes (15 vs 20%). The linear heat rate in each pin decreased with fissile

depletion, with the maximum rate of change occurring in the $(U,Pu)O_2$ fuel pin with the highest heat rate and highest burnup; the initial heat rate of 14.7 kW/ft fell to approximately 6 kW/ft at the end of life even though the capsule was moved to a higher flux position in the reactor during its irradiation. The pin with the highest initial maximum heat rate had the lowest integrated

fission gas release (61%). The rationalization of this behavior involves the extended operation at low linear heat rate because of rapid fissile depletion.

The metallographic examination of these pins confirmed the data on restructuring derived from the early lower burnup tests.¹¹ The extent of columnar grain growth was defined by the peak linear heat rates early in life and did not change, although the radius of the more or less solid core of fuel increased significantly by the more time-dependent sintering processes. This can be seen in Fig. 15.1 where the sintering is defined by the circumferential cracks.

The third reprocessing capsule (43-118) was discharged from the reactor late in May, and the last capsule (43-123) was inserted in the same location. The processing studies on the first two capsules in this series have been reported elsewhere.¹²

ETR Instrumented Tests

A. R. Olsen R. A. Buhl

The ETR instrumented tests are designed to determine the performance of mixed oxide fuel under simulated LMFBR design operating conditions. The first two capsules (43-120 and 43-121) were irradiated to investigate fuel swelling and fuel-cladding chemical interactions of Sphere-Pac and pellet (U,Pu)O₂ fuels. Each capsule contains four fuel pins, with two thermocouples at the axial midplane of each pin.

Both capsules have completed their irradiation. Capsule 43-121 was discharged in January and 43-120 in May, both with a calculated burnup of approximately 8% FIMA. Details of the irradiation have been reported elsewhere.¹³ Capsule 43-121 has been examined incompletely, and capsule 43-120 is in storage in the ETR pool pending a decision on where it is to be examined.

The second set of tests in this series consists of three instrumented capsules, each designed to measure fission gas pressure during testing and each containing one fuel pin with a 20-in.-long column of fuel. One capsule

contains FTR-type pellets of the highest permissible density (94% of theoretical), the second contains FTR pellets of the lowest permissible density (88% of theoretical), and the third contains a packed bed of Sphere-Pac U-Fines fuel. In the latter fuel, all the plutonium is contained in the coarse fraction (approx 400 μm diam), and a fine fraction (<44 μm diam) of depleted UO₂ is infiltrated into the coarse bed. These capsules have been partially assembled.

Fuel-Cladding Mechanical Interaction Tests

B. Fleischer R. L. Senn¹⁴
R. B. Fitts

The MINT-1 capsule was fabricated and put into operation. The purpose of this test was to measure fuel column and cladding length changes and fission gas release under prototype FTR power and temperature conditions. It operated from in November 1971 to June 1972, including 32 power cycles, six of which were less than 10 kW/ft during startup. The fuel element operated for 15,800 kWhr, achieving an estimated burnup of 1.7% FIMA. A typical power cycle above 10 kW/ft consisted of a slow heatup (≈ 1.5 to 3 hr) to operating power, hold at power overnight or over the weekend, then rapid cooldown (less than 2 min) by continuous retraction of the capsule to the minimum power position.

The most significant outcome of the experiment is the gas release behavior. The gas release was continuous with increasing burnup at power and not significantly changed by power transients. This behavior, shown graphically in Fig. 15.2, contrasts with that observed by other investigators,^{15,16} who found very little gas release at power and significant gas release during power cycling. The reason for the disparity between these results is not evident. Our gas release measurements have shown a total gas release of approximately 56% over the life of the test. This quantity is within the range expected for 1.7% FIMA in the operating level of 13 to 17 kW/ft based on ANL data.¹⁷

11. A. R. Olsen, R. B. Fitts, and W. J. Lackey, "In-Reactor Restructuring Temperatures and Kinetics for (U,Pu)O₂," pp. 579-602 in *Proc. Conf. Fast Reactor Fuel Element Technology*, ed. by Ruth Farmakes, American Nuclear Society, Hinsdale, Ill., 1971.

12. J. H. Goode, *Chem. Technol. Div. Annu. Progr. Rep. Mar. 31, 1972*, ORNL-4794, pp. 27-29.

13. A. R. Olsen and R. A. Buhl, *Fuels and Materials Development Program Quart. Progr. Rep. Sept. 30, 1971*, ORNL-TM-3550, pp. 15-17; *ibid.*, Dec. 31, 1971, ORNL-TM-3703, pp. 10-11; *ibid.*, Mar. 31, 1972, ORNL-TM-3797, pp. 8-17.

14. Reactor Division.

15. T. B. Burley and M. D. Freshly, *Trans. Amer. Nucl. Soc.* 11(1), 106-7 (1968).

16. M. J. Motley, R. DesHaies, and J. R. MacEwan, *Trans. Amer. Nucl. Soc.* 8(2), 424-25 (1965).

17. J. D. B. Lambert et al., "Performance of Mixed-Oxide Fuel Elements - ANL Experience," pp. 517-53 in *Proc. Conf. Fast Reactor Fuel Element Technology*, ed. by Ruth Farmakes, American Nuclear Society, Hinsdale, Ill., 1971.

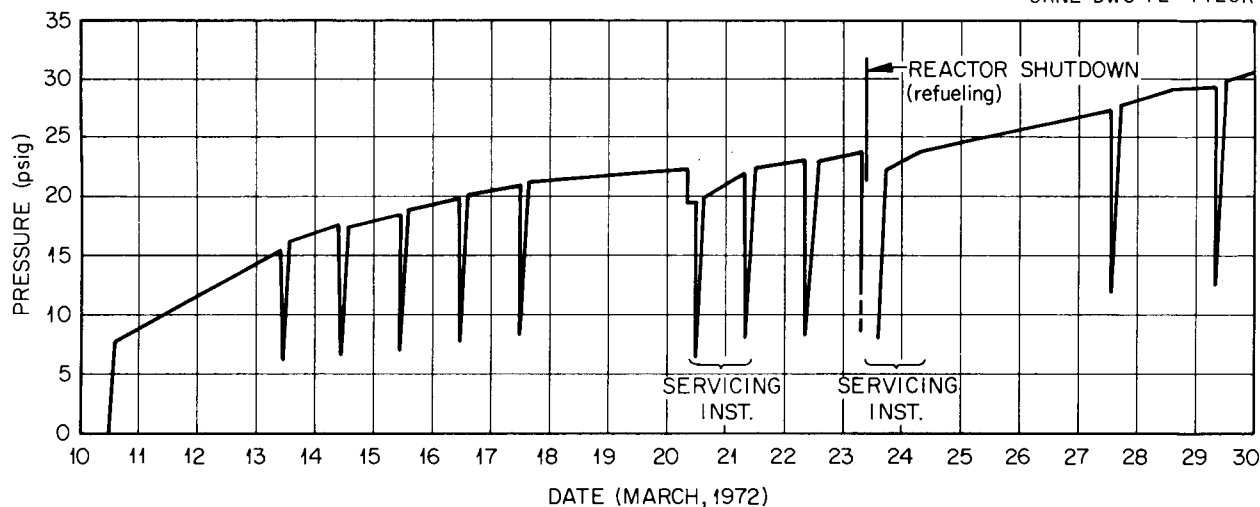


Fig. 15.2. MINT-1 fuel element internal pressure.

Fuel column length change measurements using the motion transducer are shown in Fig. 15.3. These measurements indicate that (1) the fuel column grew as a result of thermal expansion during heatup, (2) shortened during early constant power operation, probably because of creep or restructuring, and (3) expanded slowly as expected from fission product swelling.

Cladding Chemical Reactions

A. R. Olsen J. M. Leitnaker
R. A. Buhl

Chemical interactions between oxide fuels, fission products, and cladding materials¹⁸ have been recognized as a potential limiting factor to the operating conditions and attainable burnup. The fact that oxidation of the cladding is the primary reaction has also been established.^{19,20} Two types of oxidation have been seen:

1. a general or matrix oxidation, with the buildup of a significant surface oxide layer and a more or less uniform reduction in wall thickness, and

18. R. B. Fitts, A. R. Olsen, C. M. Cox, and E. L. Long, Jr., *Metals and Ceramics Div. Annu. Progr. Rep. June 30, 1971*, ORNL-4770, pp. 57-59.

19. R. B. Fitts, E. L. Long, Jr., and J. M. Leitnaker, "Observations of Fuel-Cladding Chemical Interactions as Applied to GCBR Fuel Rods," pp. 431-58 in *Proc. Conf. Fast Reactor Fuel Element Technology*, ed. by Ruth Farmakes, American Nuclear Society, Hinsdale, Ill., 1971.

20. J. M. Leitnaker, J. P. DeLuca, and R. B. Fitts, "Influence of Burnup on Reactivity of Oxide Fuel with Cladding," *Trans. Amer. Nucl. Soc.* **14**, 177 (1971).

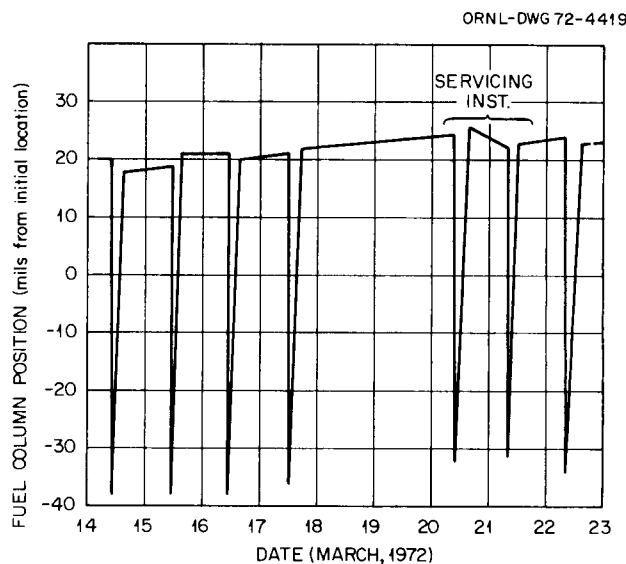


Fig. 15.3. MINT-1 fuel column behavior.

2. an intergranular attack, which is often only in localized areas but which proceeds to significant depths, sometimes greater than 50% of the 0.016-in. tube wall thickness.

The intergranular attack, which usually shows some fission products such as cesium in the grain boundaries, is the source of greatest concern.

In a series of experiments, solution-treated type 316 stainless steel tubing was exposed to flowing Ar-4% H₂ with controlled moisture contents of 4000 or 40 ppm of H₂O to control the oxidation potential. A temperature gradient was maintained along each 10-in.-long

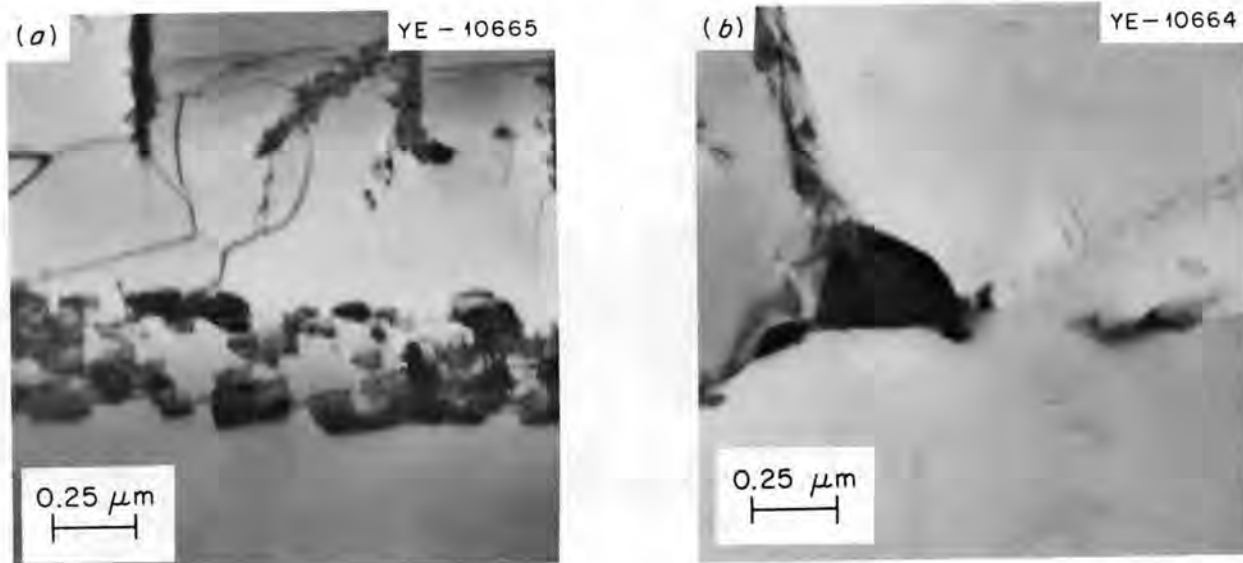


Fig. 15.4. Morphology of precipitates in stainless steel tubing heated in Ar-4% H₂-4000 ppm H₂O for 500 hr. (a) 615°C region; (b) 650°C region.

tube. Two gradients were used: 450 to 650°C or 500 to 710°C. In all, nine tubes have been tested in three groups of three tubes each. The entire length of each tube was nondestructively inspected for wall thickness with an eddy-current technique.²¹ Two tests were conducted for 500 hr each and one for 1000 hr. All nine tubes showed an apparent wall thickness reduction, which was localized in the 560 to 650°C range with the maximum change at 585 to 605°C. In the 1000-hr test with the higher oxygen potential a second and greater change in wall thickness was indicated above 660°C. Standard metallographic examinations of the two 500-hr tests show no significant change in the geometric wall thickness. Although there are other metallographic differences, the most pronounced observation is the distinct increased sensitivity to etching (glyceria regia at room temperature) of all six sections cut from the 600°C region. The grain boundaries are most rapidly attacked; this effect is less on sections from higher or lower temperature regions.

Thinned sections from one tube in the 500-hr test with 4000 ppm H₂O have been examined by transmission electron microscopy. These samples, one from the 650°C region and one from the 615°C region, showed only M₂₃C₆ precipitates in the structure.

However, the morphology of these precipitates is distinctly different, as shown in Fig. 15.4, with thin sheetlike precipitate covering most of the grain boundary in the lower temperature section and thicker, separated, agglomerated precipitate in the higher temperature section. This observation is in excellent agreement with the findings of Stickler and Vinckier.²² These same authors report a maximum in intergranular embrittlement after exposure to Strauss solution for samples heat treated in the range 565 to 650°C. In another experiment in a dry environment, Pickering, Beck, and Fontana²³ report on corrosion tests in the range 93 to 760°C with NaCl with and without the presence of oxygen. Oxygen was required for both matrix and intergranular attack. Also, the reaction occurred most rapidly with M₂₃C₆ compounds. The salt led to the production of Na₂CrO₄ instead of a protective chromic oxide. Matrix attack producing of large amounts of surface scale occurred only at 704 to 760°C, whereas intergranular attack was very pronounced at 593°C.

22. R. Stickler and A. Vinckier, "Morphology of Grain-Boundary Carbides and Its Influence on Intergranular Corrosion of 304 Stainless Steel," *Trans. Amer. Soc. Metals* **54**, 362-80 (1961).

23. H. W. Pickering, F. H. Beck, and M. G. Fontana, "Rapid Intergranular Oxidation of 18-8 Stainless Steels by Oxygen and Dry Sodium Chloride at Elevated Temperatures," *Trans. Amer. Soc. Metals* **53**, 793-803 (1961).

21. C. V. Dodd and W. A. Simpson, Jr., *Thickness Measurements Using Eddy-Current Techniques*, ORNL-TM-3712 (March 1972).

Thus the work of others on intergranular corrosion may help explain our nondestructive test results in stainless steel heat treated in a pure oxidizing atmosphere. The postulated reaction for the apparent wall thickness reduction measured by the eddy-current technique is the formation of thin intergranular oxide layers where the thin interconnected sheets of $M_{23}C_6$ are formed near 600°C . Agglomerated carbide at higher temperatures does not provide a continuous path, so less penetration occurs until the matrix oxidation rate increases and a thicker continuous carbide precipitate is formed at the highest temperatures of our tests. The intergranular oxides would electrically insulate the grains and increase the resistivity, thus causing an apparent reduction in wall thickness.

The presence of fission product cesium in the grain boundaries of intergranularly attacked cladding on irradiated oxide fuel pins may also be the result of the formation of Cs, Cr, and O_2 compounds by removal of carbon from the $M_{23}C_6$ precipitate as CO. This would yield a surface area relatively free of carbide, as we have noted in some of our high-temperature tensile tests of previously heat treated type 316 stainless steel.²⁴ The postulated reactions require additional experimental proof. The known effects of neutron irradiation on carbide precipitation kinetics^{25,26} may lower the temperature range.

ANALYSIS OF FUEL ELEMENT PERFORMANCE

F. J. Homan

The data derived from irradiation testing of oxide fuels from both the ORNL program and experimental programs at other sites have been used to develop analytical models for predicting and evaluating the performance of LMFBR fuel pins. The models are both theoretical and empirical and have emphasized the thermal, chemical, and mechanical performance of the fuel elements, particularly during startups, power cycles, and transients. This work includes direct support of the irradiation testing program in terms of optimizing experimental designs, interpreting results, and extrapolating these results to LMFBR conditions.

24. J. M. Leitnaker and H. Mateer, *Fuels and Materials Development Program Quart. Progr. Rep. Mar. 31, 1972*, ORNL-TM-3797, pp. 92-96.

25. T. T. Claudson, R. W. Barker, and R. L. Fish, "The Effects of Fast Flux Irradiation on the Mechanical Properties and Dimensional Stability of Stainless Steel," *Nucl. Appl. Technol.* 9, 10-23 (1970).

26. P. J. Barton, *Some Observations on the Structure and Tensile Properties of AISI Type 316 Steel as a Function of Fast Reactor Irradiation Temperature*, AERE-R-6435 (June 1970).

Performance Model Development

F. J. Homan

Development of the FMODEL code²⁷ during this reporting period was limited primarily to updating the individual models included in the code to reflect recent experimental data and the incorporation of a sophisticated gap conductance model.²⁸⁻³⁰ The newly incorporated gap conductance model replaces the model used formerly, where the code user had to specify the gap conductance for each time period of interest. This model considers conductance across an open gap and across a gap that has closed so that the fuel contacts the cladding. It also considers the burnup-dependent changes in the composition and thermal conductivity of the gas phase due to the introduction of fission gases into the plenum. Accommodation theory is also applied where the size of the gap is of the same order of magnitude as the mean free path of the gas species.

The major modeling effort during this reporting period has been in the area of sensitivity analysis. The sensitivity of predicted fuel pin performance to uncertainties in physical and mechanical properties of the fuel and cladding were investigated in detail. In addition, the influence of the manner of employment of individual phenomenological models within the integrated fuel performance model was analyzed. The purpose of the sensitivity work is to gain understanding of the influence of individual material properties on the overall performance of fuel pins. In particular, it is desirable to know where uncertainty associated with a given property is sufficiently large to cause concern for the fuel pin performance. One of the objectives of the modeling work is to identify areas in which experimental study needs intensification.

The influence of uncertainties in thermal expansion of both fuel and cladding on pins with small fabricated gaps was considered using the FMODEL code.³¹ Uncertainty was defined by comparing property measurements published for nominally similar materials and

27. F. J. Homan, *Metals and Ceramics Div. Annu. Progr. Rep. June 30, 1971*, ORNL-4770, pp. 52-54.

28. C. M. Cox and R. L. Diamond, *LMFBR Fuel Cycle Studies Progr. Rep. July 1971, No. 29*, ORNL-TM-3534, p. 55 (limited distribution).

29. C. M. Cox, F. J. Homan, and R. L. Diamond, *LMFBR Fuel Cycle Studies Progr. Rep. August 1971, No. 30*, ORNL-TM-3571, pp. 38-39.

30. C. M. Cox, F. J. Homan, and R. L. Diamond, *LMFBR Fuel Cycle Studies Progr. Rep. February 1972, No. 36*, ORNL-TM-3759, pp. 42-53 (limited distribution).

31. F. J. Homan, *A Parametric Analysis of Fuel-Cladding Mechanical Interactions*, ORNL-TM-3508 (August 1971).

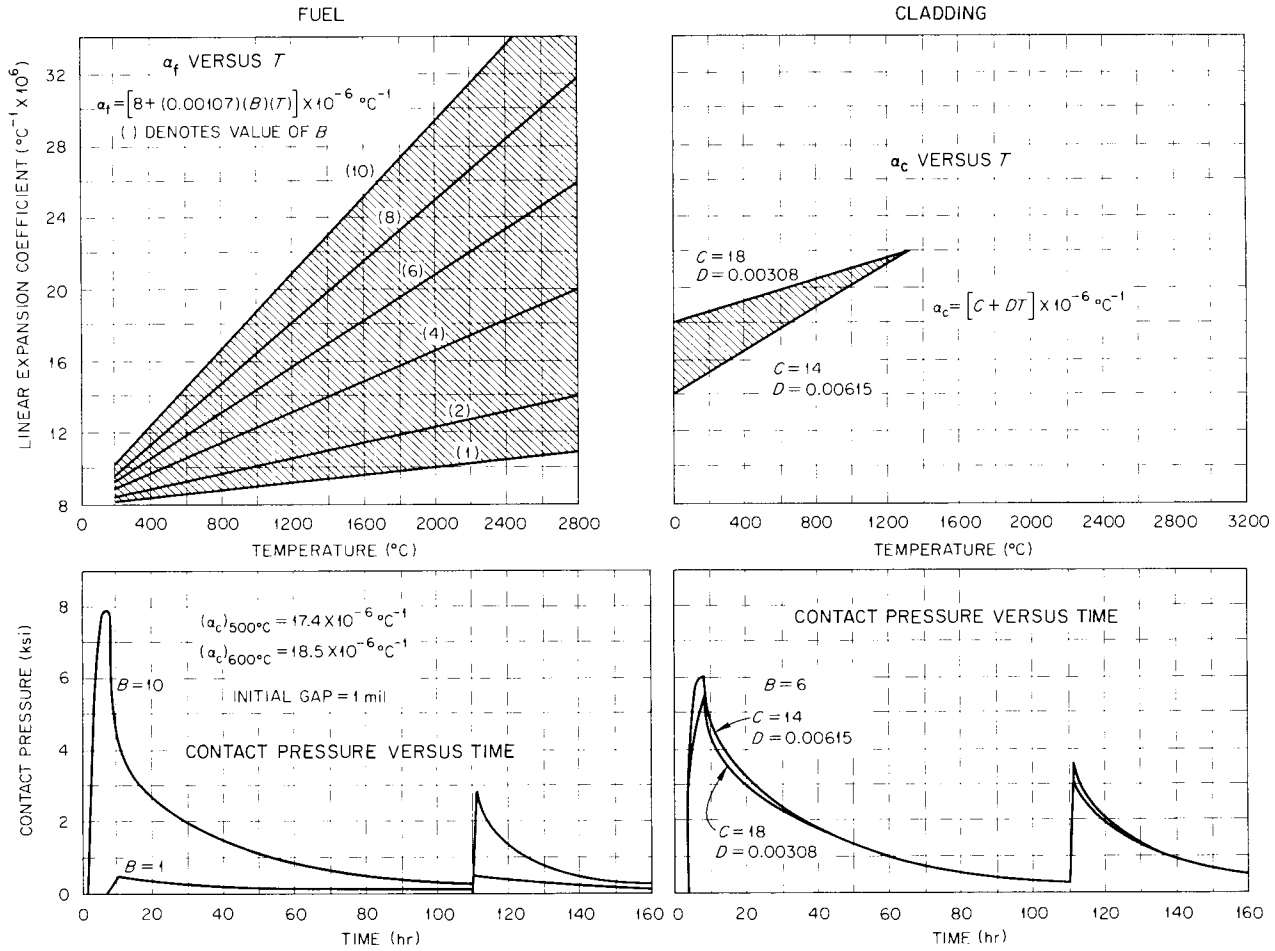


Fig. 15.5. Influence of uncertainty in fuel and cladding thermal expansion characteristics on mechanical interaction.

using the range of values as a measure of uncertainty. Then, using property data from the outer boundaries of the envelope of values so defined, performance was predicted with FMODEL, and the spread in predicted behavior used as a measure of the influence of uncertainty for that particular property. Using this technique we demonstrated that the uncertainty in cladding thermal expansion values was of little consequence; however, the uncertainty in fuel thermal expansion was of considerable importance in predicting the amount of mechanical interaction that would occur during the startup of a fuel pin with a small initial fuel-cladding gap.³¹ This comparison is shown in Fig. 15.5. Also, the magnitude of this influence diminishes with increasing fabricated gap size.³¹ From this analysis we concluded that additional experimental work is necessary to adequately characterize the thermal expansion characteristics of mixed oxide fuel, especially

over the range of stoichiometries and compositions of interest for LMFBR.

The sensitivity of predicted performance to uncertainty in fuel thermal conductivity properties was also analyzed.³² Thermal conductivity of mixed oxide fuels is influenced by a number of variables, including stoichiometry, density, temperature, burnup, plutonium content, and the shape and distribution of fabricated porosity. This last variable, the shape and distribution of fabricated porosity, is very influential as shown in Fig. 15.6, so the uncertainty related to this variable alone was investigated.³² The study revealed a substantial impact on both the heat rate to melting and the mechanical interaction between fuel and cladding during startup of a small-gap, LMFBR-type fuel pin.

32. F. J. Homan, *LMFBR Fuel Cycle Studies Progr. Rep. September 1971, No. 31*, ORNL-TM-3614, pp. 42-46.

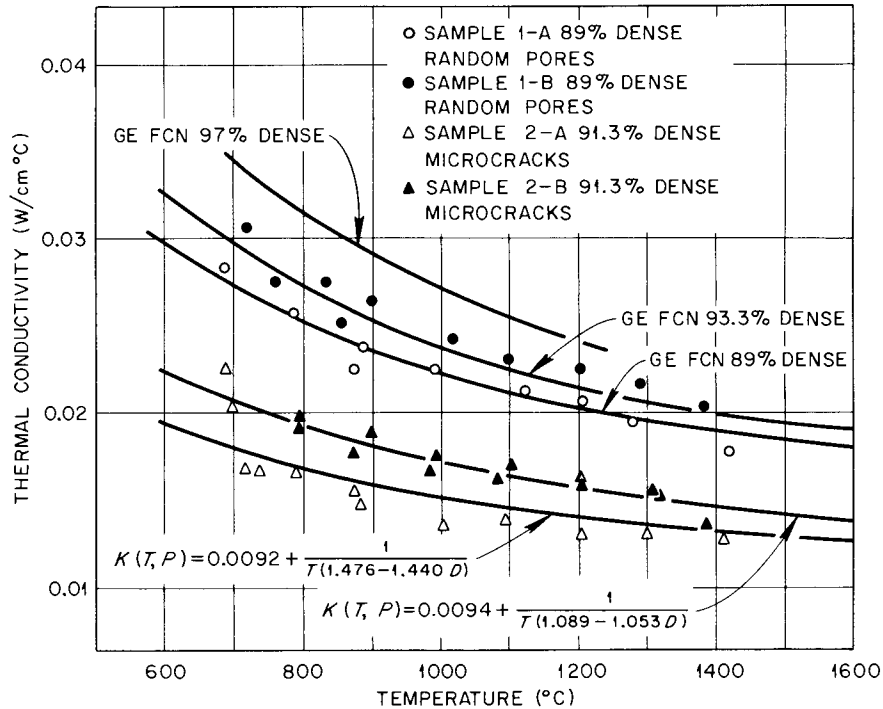


Fig. 15.6. Effects of pore morphology on thermal conductivity of $\text{UO}_2-25\% \text{PuO}_2$ pellets sintered to about 90% of theoretical density.

This influence is shown in Fig. 15.7. The conclusions drawn in this case are somewhat different from those in the thermal expansion case, for a substantial body of information exists pertaining to thermal conductivity properties of mixed oxide fuels. However, it is important that the thermal conductivity properties of a given batch of fuel be carefully related to its microstructure and composition and that changes in these characteristics during irradiation be carefully taken into account³³ when the behavior of this fuel is modeled.

Studies of the influence of uncertainty in a given material property are fairly straightforward. Similar techniques can be employed to investigate effects that are postulated but not yet understood quantitatively. For example, the currently available equations to describe cladding swelling indicate a dependence on temperature and fast-neutron fluence. However, a stress effect has been postulated for some time^{34,35} because of the differences noted between diametral expansion of the cladding, postirradiation immersion density measurements, and predicted behavior for a number of experimental pins using the temperature-fluence swelling correlations. Understanding the stress influence on void swelling in cladding materials is obviously needed to predict accurately how a fuel pin will behave in reactor.

As indicated earlier, the existing cladding swelling correlations describe swelling as a function of fast-neutron fluence and temperature. Given the fact that neutron fluence is relatively constant but a substantial temperature gradient exists across the cladding thickness, the question arises as to how to employ the swelling correlations. Should they be applied at one cladding node to represent the average cladding temperature, and thus the average volume change, or should they be applied at several nodes through the cladding to bring in the influence of differential swelling due to the temperature gradient? The predicted mechanical behavior of the cladding depends strongly on which alternative is selected, as can be seen in Fig. 15.8. In this figure the curve labeled "normal swelling" was calculated by applying the temperature-fluence cladding

33. W. J. Lackey, F. J. Homan, and A. R. Olsen, *Porosity and Actinide Redistribution during Irradiation of (U,Pu)O₂*, ORNL-TM-3762 (June 1971).

34. A. Boltax, T. P. Soffa, and A. Biancheria, *Trans. Amer. Nucl. Soc.* 14, 631 (1971).

35. F. A. Garner et al., "The Effect of Stress on Radiation-Induced Void Growth," p. 841 in *Radiation-Induced Voids in Metals* (Proc. Intern. Conf., Albany, New York, June 9-11, 1971), ed. by J. W. Corbett and L. C. Ianiello, USAEC Office of Information Service, Oak Ridge, Tenn., 1972.

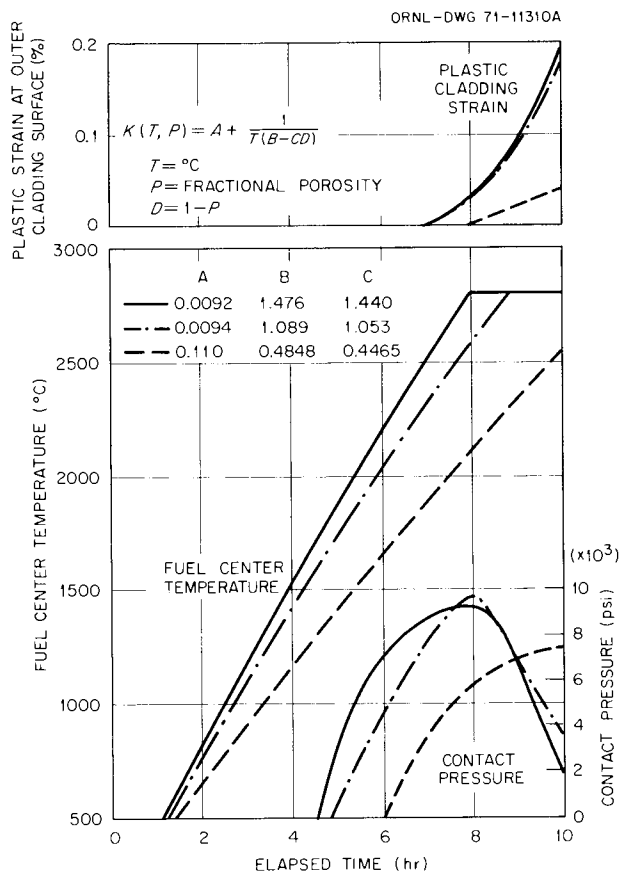


Fig. 15.7. Influence of fuel thermal conductivity on fuel pin performance during startup.

swelling correlation to each of six radial nodes spaced through the cladding wall. The curve labeled "constant swelling" was calculated by applying the correlation at only one node and assuming that cladding swelling is constant through the wall. The "no swelling" curve was calculated by assuming that the cladding does not swell because of irradiation and is shown merely for comparison. It is easily seen that the calculated cladding stresses and strains are strongly influenced by which cladding swelling assumptions are used in the calculations, indicating the need for more complete understanding of this phenomenon to achieve reliable performance predictions.

If swelling is calculated at several radial nodes throughout the cladding wall a swelling gradient is produced and causes stresses analogous to thermal stresses. Depending upon the location of the cladding temperatures with respect to the peak swelling temperatures, these stresses may either add to or subtract from the stresses due to internal pressurization. As with the

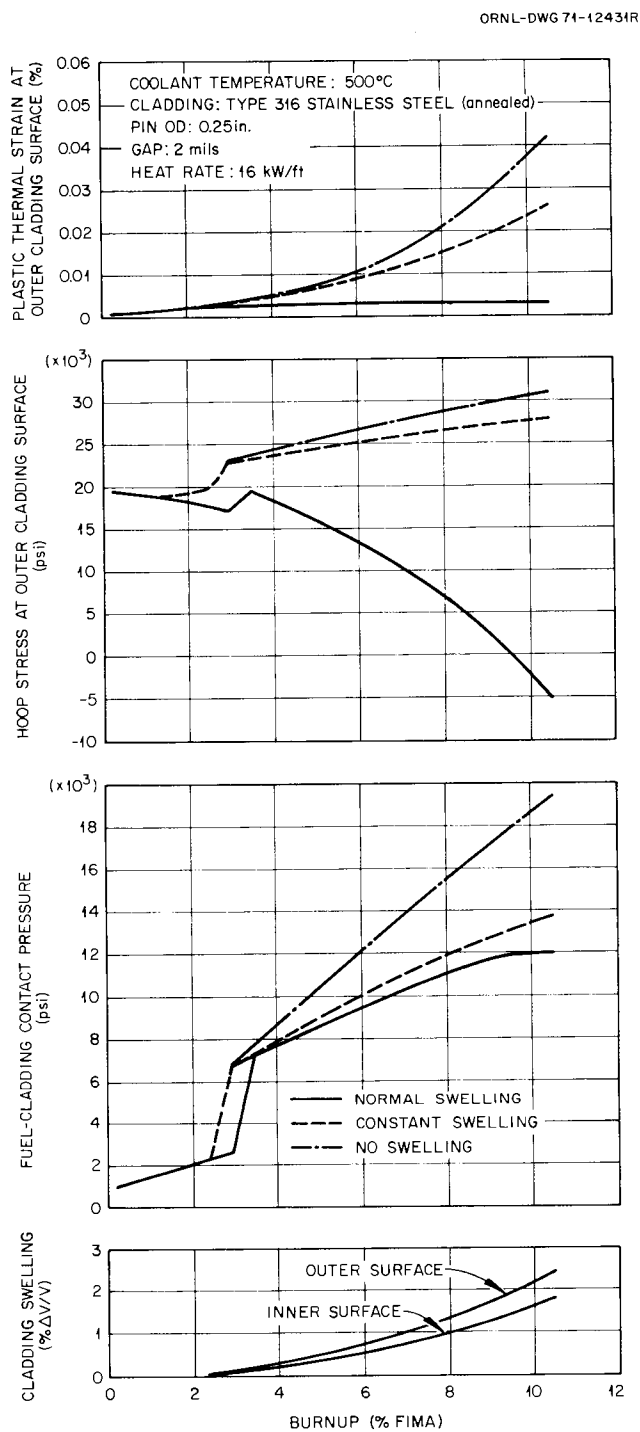


Fig. 15.8. Influence of method of application of cladding swelling equation on predicted mechanical behavior of cladding.

thermal stresses, the stresses due to differential swelling across the cladding wall are relaxed with creep, but at high neutron exposures, where the temperature-fluence correlations predict very high cladding swelling rates,

very high stresses are calculated. The temperature-fluence correlations do not include stress effects, however, and if one side of the cladding is swelling more rapidly than the other, this side will be placed into compression and the other side into tension. It is intuitively appealing that cladding placed in tension will swell faster at the same temperature and neutron exposure than unstressed cladding, and theoretical calculations support this intuition.^{3,2} The net effect is to reduce the swelling gradient and therefore the stresses caused thereby. If the converse is also true, and compressive stresses retard the swelling rate (also intuitively appealing), then the effect is more pronounced and the stresses due to swelling gradients are further reduced. The need for quantitative understanding of the stress influence on cladding swelling in order to achieve realistic behavior predictions in operating fuel pins is described in detail.^{3,6}

Porosity, Actinide, and Oxygen Redistribution in Irradiated (U,Pu)O₂

W. J. Lackey F. J. Homan
A. R. Olsen

Thermal-gradient-induced redistribution of porosity and fuel components during irradiation of (U,Pu)O₂ will sufficiently alter the radial heat-generation profile,^{3,7} fuel conductivity,^{3,8-4,0} melting point,^{4,1,4,2} oxygen activity,^{4,3,4,4} and mechanical properties to significantly influence fuel pin performance. Accord-

ingly, we have measured radial porosity and actinide profiles of irradiated fuel pins. Further, analytical models, which should prove useful in design and analysis of LMFBR fuels, were developed for predicting radial profiles of porosity, Pu:(U + Pu), and oxygen. These models have been incorporated into FMODEL, permitting determination of the consequences of fuel component redistribution on the thermal and mechanical performance of (U,Pu)O₂ fuel pins.

The interrelated porosity and actinide redistribution models are kinetic and based on the evaporation-condensation mechanism. An axial segment of the fuel pin of unit length is divided into 30 radial increments. After calculation of the radial temperature profile, it and the overall oxygen-to-metal ratio of the fuel are used to calculate the oxygen-to-metal distribution according to a previously proposed irreversible thermodynamic approach.^{4,5} Next, the porosity of each of the radial increments at the end of a short time period is determined from knowledge of the initial porosity and calculation^{4,6} of the movement of pores (or equivalently material) into and out of each radial increment. Similarly, since the initial Pu:(U + Pu) ratio for each radial increment and the amount of fuel transported into and out of each increment are known, the Pu:(U + Pu) ratio of each increment at the end of the time period can be calculated if the composition of the transported vapor is known. This composition was calculated^{4,7} by equilibrium thermodynamics as a function of the temperature, oxygen-to-metal ratio, and Pu:(U + Pu) ratio of the solid fuel. Repeating the calculations for a series of time periods spanning the irradiation time can give the porosity, actinide, and oxygen radial profiles at any desired time.

Experimentally measured porosity and Pu:(U + Pu) radial profiles for a U_{0.85}Pu_{0.15}O_{2.00} fuel pin clad with 1/4-in.-OD stainless steel are shown to compare favorably with predicted profiles in Fig. 15.9. This Sphere-Pac fuel pin was irradiated in the ETR at a linear heat rate of 13.6 kW/ft to a burnup of 0.7% FIMA. The columnar grain region is considerably more porous than previously generally believed. We have observed the same to be true for pins irradiated in a fast-neutron flux. In the present case, the calculated fuel center

36. F. J. Homan, *LMFBR Fuel Cycle Studies Progr. Rep. October 1971, No. 32*, ORNL-TM-3624, pp. 46-64 (limited distribution).

37. W. T. Sha, P. R. Huebotter, and R. K. Lo, *Trans. Amer. Nucl. Soc.* **14**, 183-84 (1971).

38. R. L. Gibby, *J. Nucl. Mater.* **38**, 163-77 (1971).

39. R. L. Gibby, *The Effect of Oxygen Stoichiometry on the Thermal Diffusivity and Conductivity of U_{0.75},Pu_{0.25}O_{2-x}*, BNWL-727 (January 1969).

40. General Electric Breeder Reactor Development Operation, *Sodium-Cooled Reactors, Fast Ceramic Reactor Development Program*, GEAP-10028-35 (September 1970), pp. 44-49.

41. W. L. Lyon and W. E. Baily, *J. Nucl. Mater.* **22**, 332-39 (1967).

42. E. A. Aitken and S. K. Evans, *A Thermodynamic Data Program Involving Plutonia and Urania at High Temperatures*, *Quart. Rep. No. 4*, GEAP-5672 (1968).

43. J. A. Christensen, "Transport Processes in Oxide Nuclear Fuels," pp. 109-25 in *Ceramic Nuclear Fuels International Symposium, May 3-8, 1969, Washington, D.C.*, American Nuclear Society, Hinsdale, Ill., 1969; also BNWL-1202.

44. E. A. Aitken and S. K. Evans, "Thermodynamic Behavior of Plutonium Oxide Systems in a Temperature Gradient," pp. 772-80 in *Plutonium 1970 and Other Actinides*, *Nucl. Met.* **17**, (Part 2), The Metallurgical Society of AIME, New York, 1970.

45. General Electric Breeder Reactor Development Operation, *Sodium-Cooled Reactors, Fast Ceramic Reactor Development Program*, GEAP-10028-37 (March 1971), pp. 38-40.

46. F. J. Homan, *Fuels and Materials Development Program Quart. Progr. Rep. Dec. 31, 1970*, ORNL-TM-3300, pp. 33-39.

47. W. J. Lackey, A. R. Olsen, and D. K. Bates, *Fuels and Materials Development Program Quart. Progr. Rep. Dec. 31, 1970*, ORNL-TM-3300, pp. 33-39.

temperature was 9.6% (200°C) higher when based on the observed porosity distribution rather than the previously generally assumed three-zone porosity distribution model. This work has been described.^{4,8}

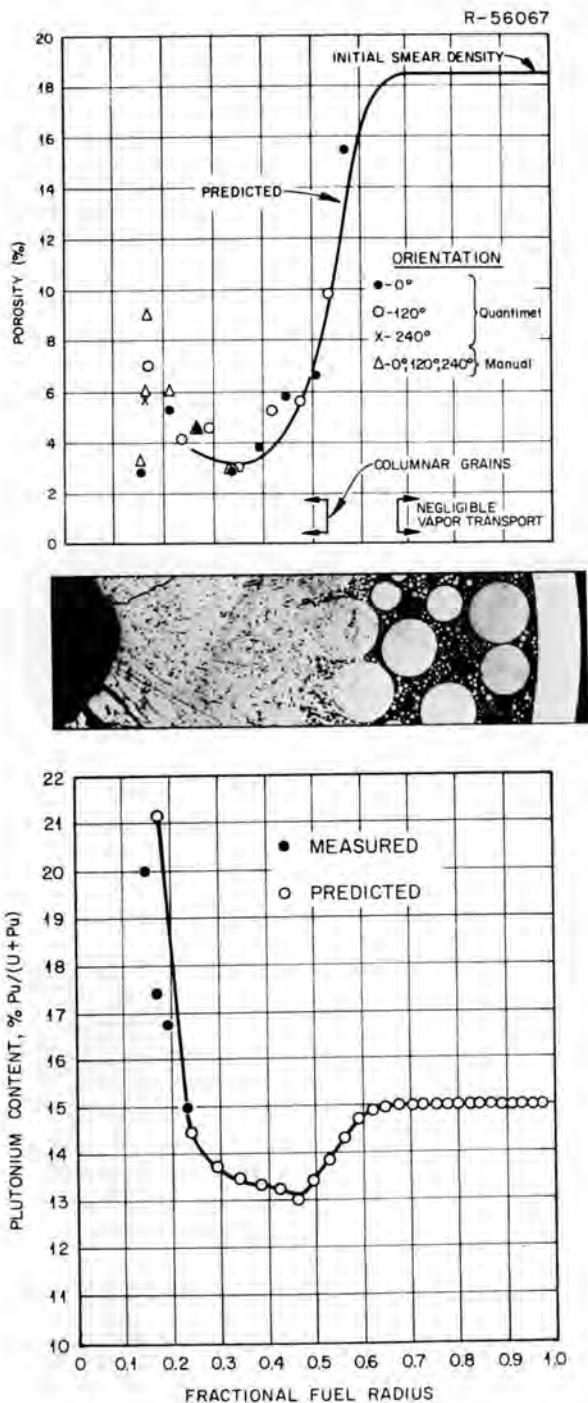


Fig. 15.9. Comparison of measured and predicted porosity and Pu:(U + Pu) profiles.

Analysis of ORR Instrumented Thermal Performance Tests

R. B. Fitts F. L. Miller^{4,9}

Two type 304 stainless-steel-clad (U,Pu)O_{1.99} fuel pins, one containing pellet fuel and the other Sphere-Pac fuel, were irradiated⁵⁰⁻⁵² in the third thermal performance test capsule, SG-3, in the Oak Ridge Research Reactor. In each pin the fuel smear density was 82% of theoretical, and the burnup achieved was about 0.5% FIMA. The goal of this irradiation test was to compare and quantify the relationship between center-line temperatures and average heat generation rates within the two fuel pins. The final detailed analysis of the thermometry data has been carried out and reported during the past year.^{5,3}

Data from the SG-3 capsule were obtained from 12 thermocouples at the midlength of each fuel pin. The fuel and cladding temperatures and the heat flow from the fuel pins were monitored. The method of data analysis consisted of iteration of two steps. First, low-order polynomials were fitted by least squares to functions of the measured temperatures (e.g., center-line temperatures vs the average from the cladding thermocouples). Then deviations or differences from the fitted line were plotted against time, and patterns in these deviations were investigated. The polynomial used to describe the data was finally revised to better represent the data.

The above technique permitted a statistically valid definition of the differences in behavior of the two fuel pins, leading to the following observations.

1. Under the same conditions of steady-state heat generation rate and cladding temperature, the central temperature (°C) in the Sphere-Pac fuel is always cooler than that in the pellet fuel by $11.7 \pm 1.2\%$ at the 99% confidence level (see Fig. 15.10).

48. W. J. Lackey, F. J. Homan, and A. R. Olsen, *Porosity and Actinide Redistribution during Irradiation of (U,Pu)O₂*, ORNL-TM-3762 (June 1971).

49. Mathematics Division.

50. R. B. Fitts et al., *Trans. Amer. Nucl. Soc.* **13**, 549-50 (1970).

51. A. R. Olsen, R. B. Fitts, and W. J. Lackey, "In-Reactor Restructuring Temperatures and Kinetics for (U,Pu)O₂," pp. 579-602 in *Proc. Conf. Fast Reactor Fuel Element Technology*, ed. by Ruth Farmakes, American Nuclear Society, Hinsdale, Ill., 1971.

52. R. B. Fitts, *Metals and Ceramics Div. Annu. Progr. Rep. June 30, 1971*, ORNL-4770, pp. 50-51.

53. R. B. Fitts and F. L. Miller, *Trans. Amer. Nucl. Soc.* **15**(1), 180 (1972).

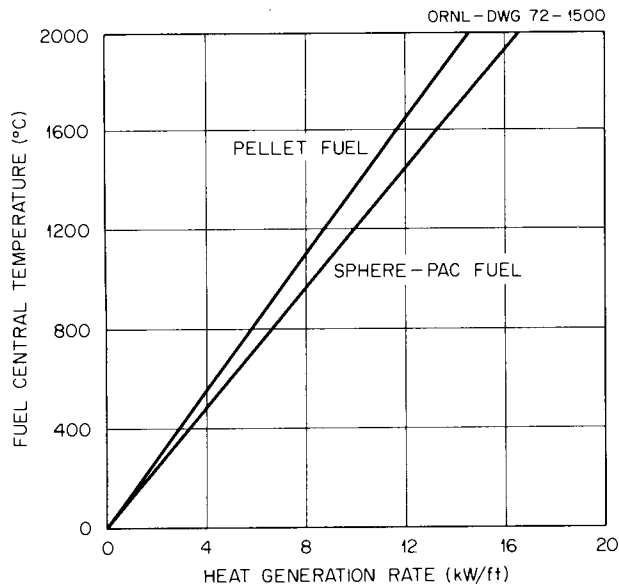


Fig. 15.10. Relationship between central temperature and heat rating for Sphere-Pac and pellet fuel pins in capsule test SG-3. The Sphere-Pac fuel is always $11.7 \pm 1.2\%$ cooler than the pellet fuel at the 99% confidence level.

2. Power cycling significantly affects fuel pin central temperature. In both fuel pins the central temperature at 8 to 16 kW/ft was about 250°C higher upon initial return to power after a reactor shutdown than it was at the same heat rate during steady-state operation. The duration of this fluctuation (several hours) was a function of the operating conditions and fuel form; the pellet fuel required the longer recovery time.

3. The effect of time at temperature on the temperature in the Sphere-Pac fuel pin was not significant, but small decreases in the heat generation rate were required to maintain a given pellet fuel temperature, indicating a slow worsening of heat transfer in the pellet fuel pin.

CASDAR: A Nuclear Data Manipulation Program

J. D. Jenkins⁵⁴ G. W. Cunningham⁴⁹

A computer program, CASDAR⁵⁵ (Cross Sections and Spectra Direct Access Retrieval), has been com-

54. Reactor Division.

55. J. D. Jenkins and G. W. Cunningham, *CASDAR, a Cross Section and Spectrum Direct Access Retrieval System for Nuclear Data Manipulation*, report in preparation.

pleted and conveniently manipulated the large amounts of nuclear data used in fuel depletion and radiation damage calculations. The program contains an extensive library of neutron cross section data culled from a number of sources⁵⁶⁻⁵⁸ and a library of neutron spectra for a number of reactors used as irradiation facilities. In addition, neutron spectrum information for specific experimental configurations as calculated by a number of reactor physics design codes⁵⁹⁻⁶¹ can be conveniently input to the program. These data can be used to provide spectrum-averaged effective cross sections.

The program interfaces with the depletion program ORIGEN,⁶² which is designed to calculate the isotopic history of fuel and cladding materials during and after irradiation. CASDAR will provide on demand a properly spectrum-averaged neutron cross section library for ORIGEN using either one of its precalculated and stored library spectra or an input spectrum for a specific experimental facility.

In addition, the program can provide other types of data needed for the design and interpretation of irradiation experiments. For example, the program will provide on request spectrum-averaged damage cross sections, few-group averaged cross sections, calculated reaction rates for dosimeter evaluation, and plots of neutron cross sections and spectra. All of this information is available from the precalculated and stored data in the CASDAR library. Thus the program provides the materials scientist with convenient access to nuclear data and reactor spectra in a form directly applicable to the design and interpretation of his experiments and relieves him of the onus of calculating this information for himself.

56. H. C. Honeck, *Specifications for an Evaluated Nuclear Data File for Reactor Applications*, BNL-50066 (May 1966), revised by S. Pearlstein, Brookhaven National Laboratory, July 1967.

57. G. D. Joanou and J. S. Dudek, *GAM-II: A B₃ Code for the Calculation of Fast-Neutron Spectra and Associated Multi-group Constants*, GA-4265 (1963).

58. W. E. Alley, R. W. Gell, and R. M. Lessler, *Semiempirical Neutron Induced Reaction Cross Sections*, UCRL-50484 (August 1968).

59. W. W. Engle, Jr., *A User's Manual for ANISN*, K-1693 (March 1967).

60. N. M. Greene and C. W. Craven, Jr., *XSDRN: A Discrete Ordinates Spectral Averaging Code*, ORNL-TM-2500 (July 1969).

61. T. B. Fowler and D. R. Vondy, *Nuclear Reactor Core Analysis Code: CITATION*, ORNL-TM-2496 (July 1969).

62. M. J. Bell, *ORIGEN: The ORNL Isotope Generation and Depletion Code*, ORNL-4628, to be published.

CHEMICAL MODELING OF FUEL-CLADDING ATTACK IN LMFBROXIDE PINS

Our goal in this program has been to understand the chemical attack that occurs between $(U,Pu)O_2$ and stainless steel cladding.

Analysis of Intergranular Attack Data

J. M. Leitnaker F. J. Homan

Since intergranular attack (IGA) seems potentially of greatest concern to LMFBRO cladding, we analyzed much of the available data on this phenomenon. Out-of-reactor IGA of type 316 stainless steel by $Ar-4\% H_2-4000 \text{ ppm } H_2O$ in the range 948 to 1190°K (ref. 63) obeys the rate equation⁶⁴

$$\log_{10} \text{IGA (cm/hr)} = 4816/T(^{\circ}\text{K}) - 1.3129.$$

In comparison, for a well-characterized thermal reactor experiment, GE pin B3C, which contained $(U,Pu)O_2$ with starting oxygen-to-metal ratio (O/M) of 2.00 clad with type 347 stainless steel, available data^{64,65} in the range 821 to 1043°K fit the equation

$$\log_{10} \text{IGA (cm/hr)} = -4666/T(^{\circ}\text{K}) - 1.080.$$

We compare these data in Fig. 15.11. Other in-reactor IGA data of less well-known temperatures and with starting O/M between 1.94 and 2.00 fall suggestively near these parallel lines; these data are shown in Fig. 15.12. Note that the IGA rate appears to drop as the O/M decreases.

In marked contrast to the above results, Sphere-Pac fuels made from sol-gel-derived $(U,Pu)O_2$ with starting O/M of 2.00 show no IGA. These data are shown in Fig. 15.13 as limits of experimental observations, 5×10^{-4} cm on IGA. The data seem to imply that the rate-limiting IGA mechanism is similar in all cases except Sphere-Pac fuel pins, in which a blocking mechanism occurs.

63. R. B. Fitts, E. L. Long, Jr., and J. M. Leitnaker, "Observations of Fuel-Cladding Chemical Interactions as Applied to GCBRO Fuel Rods," pp. 431-58 in *Proc. Conf. Fast Reactor Fuel Element Technology*, ed. by Ruth Farmakes, American Nuclear Society, Hinsdale, Ill., 1971.

64. J. M. Leitnaker and R. E. Adams, *LMFBRO Fuel Cycle Studies Progr. Rep. November 1971, No. 33*, ORNL-TM-3663, pp. 40-47 (limited distribution).

65. K. E. Gregoire, P. E. Novak, and R. E. Murata, *Failed Fuel Performance in Naturally Convecting Liquid Metal Coolant*, GEAP-13620 (June 1970).

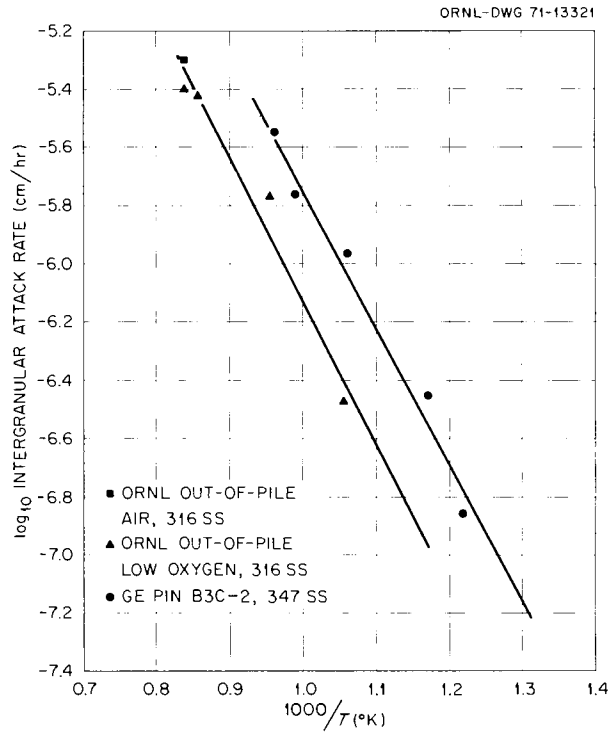


Fig. 15.11. Intergranular attack rates in stainless steel.

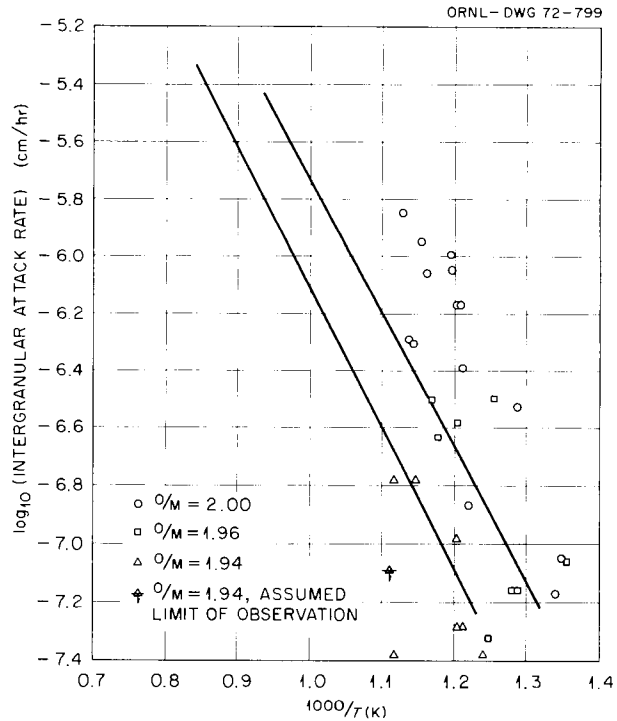


Fig. 15.12. Influence of fuel oxygen-to-metal ratio on cladding intergranular attack rates. Reference lines from Fig. 15.11.

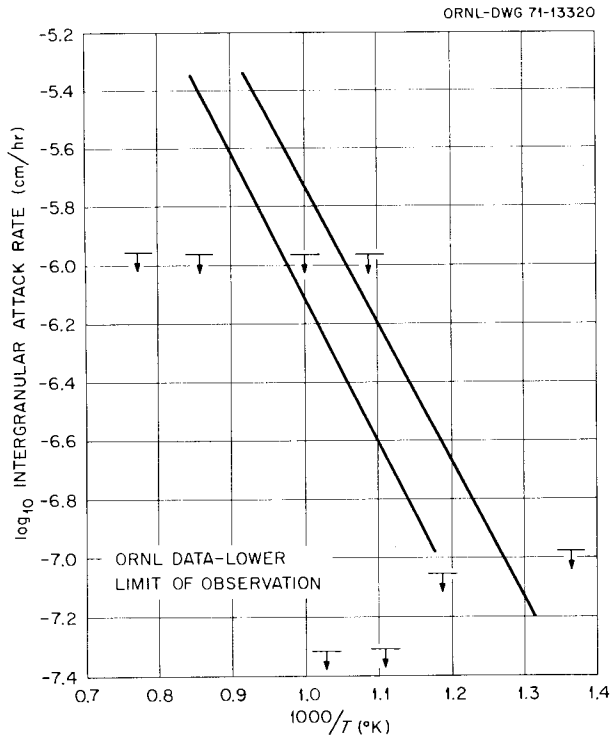


Fig. 15.13. Limit of intergranular attack rate on sol-gel-derived Sphere-Pac mixed oxide fuel. Reference lines from Fig. 15.11.

Elimination of CO₂ and H₂O as Oxygen Transport Species in Mixed Oxide Fuel Pins⁶⁶

J. M. Leitnaker K. E. Spear⁶⁷

Thermodynamic and kinetic calculations show that both CO₂ and H₂O do not transport oxygen in typical near-stoichiometric LMFBR mixed oxide fuel.⁶⁸ Thus, current gas-phase transport theories^{69,70} do not correctly describe the oxygen distribution mechanism in such a pin. A method for measurement of the oxygen potential across an oxide fuel pin involving determination of Mo and MoO₂ concentrations is possible and may serve as a basis to establish the actual mechanism.⁶⁸

66. Submitted to *Journal of Nuclear Materials*; also ORNL-TM-3849 (June 1972).

67. Consultant from Materials Research Laboratory, Pennsylvania State University, University Park, Pa. 16802.

68. J. M. Leitnaker, *Fuels and Materials Development Program Quart. Progr. Rep. Dec. 31, 1971*, ORNL-TM-3703, pp. 13-18.

69. M. H. Rand and L. E. J. Roberts, "Thermodynamics and Nuclear Engineering," pp. 3-31 in *Thermodynamics*, vol. 1, International Atomic Energy Agency, Vienna, 1968.

70. M. H. Rand and T. L. Markin, "Some Thermodynamic Aspects of (U,Pu)O₂ Solid Solutions and Their Use as Nuclear Fuels," pp. 637-50 in *Thermodynamics of Nuclear Materials*, International Atomic Energy Agency, Vienna, 1968.

16. Fabrication Development for Fast Breeder Reactor Cladding

W. R. Martin A. C. Schaffhauser

The goals of this program are consistent with the need for high-quality but economical tubing for the FBR. For this reporting period, our efforts have been directed toward testing the effects of surface defects on the mechanical properties of type 316 stainless steel.

BIAXIAL CREEP-RUPTURE OF STAINLESS STEEL TUBING WITH ELECTRO-DISCHARGE MACHINED NOTCHES

R. T. King K. V. Cook
G. A. Reimann

The biaxial stress-rupture properties of annealed and 20%-cold-worked type 316 stainless steel tubing at 650°C have been investigated by testing internally pressurized tubes. Electro-discharge machined notches were made in the surfaces of 0.635-cm-diam X 0.041-cm-wall-thickness tubes, and they were always located on the thinnest segment of the wall. The effects of nominal notch depths equivalent to 10, 33, and 66% of the wall thickness and notch lengths of 0.076 and 0.635 cm were systematically explored as a function of applied stress. After machining, the notches were about 0.006 cm wide.

The test stresses produced rupture times varying from about 1 to 1000 hr. Under these conditions, all notched tubes that failed in the gage length of the specimen failed at the notch. Metallographic studies consistently showed accelerated deformation and intergranular cracking beneath the notches. This behavior was observed for both annealed and cold-worked tubing, regardless of whether the notches were located on the inside or outside surface of the tube.

The circumferential strains and rupture times of notched tubes and un-notched control specimens were compared. Notched tubes exhibited shorter rupture times and less circumferential strain, and the degradation of properties increased with increasing notch depth. Long notches had significantly greater effect upon the rupture life and circumferential strain than short notches because of the smaller constraint to

deformation under a long notch. Within the limits of experimental error, there was no distinguishable difference between locating a given notch on the inner or outer surface of a tube. Generally, the effects of a given notch geometry were less severe in annealed tubing than in the cold-worked tubing.

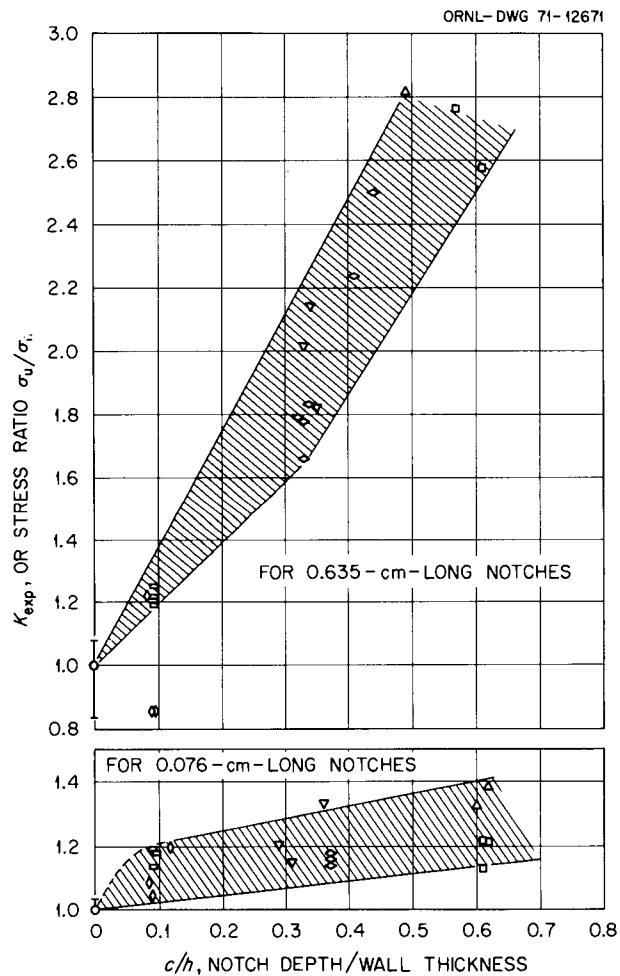


Fig. 16.1. Ratio of control specimen stress (σ_c) to notched specimen stress (σ_n) to cause failure after the same time for cold-worked type 316 stainless steel tubing at 650°C.

The results are not unique to the materials employed in this experiment. An abbreviated series of tests on tubing fabricated from another heat of type 316 stainless steel produced similar results.

There are several theoretical treatments of the stresses present near notches and cracks in elastic materials, but the rupture times for these tests do not correlate well with any such stresses. Such agreement would be fortuitous, in view of the involved time-dependent plastic flow processes under these notches. An interim analysis based on steady-state creep and a strain-limited fracture criterion have been developed and applied to the data to interpret these results. The analysis provides an internally consistent explanation of the observations.

A significant conclusion is that a simple design allowance for defects in cold-worked tubing based on the remaining cross-sectional area beneath the defect is not sufficient. A notch whose depth equals 10% of the wall thickness may require about a 20% reduction in stress to produce rupture in a given time. The ratio of stresses required to cause an un-notched tube (σ_u) and a notched tube (σ_n) to fail in a given time is a measure of the design stress concentration allowance that should be made for various ratios of notch depth to wall thickness. The specific results for 20%-cold-worked tubing are shown in Fig. 16.1.

EFFECTS OF SHARP ARTIFICIAL NOTCHES ON THIN-WALL TYPE 316 STAINLESS STEEL TUBING

R. T. King K. V. Cook
G. A. Reimann

Techniques have been developed for fabricating drawn tubing containing sharp artificial notches (about 0.0001 in. wide) parallel to the tube axis.¹ Sharp notches having 0.0005-, 0.0012-, and 0.0036-cm nominal depths and 0.63-cm lengths have been produced in 20%-cold-drawn type 316 stainless steel tubing. Sets of tubes were then tested in biaxial creep at 650°C over a range of stresses selected to produce rupture times ranging from about 10 to nearly 1000 hr.

The results of these tests show that sharp notches produce effects on tubing rupture life and ductility similar to those produced by electro-discharge machined notches (see above). Because of the stress concentrating effect of the notches, more rapid deformation occurs beneath the notches than elsewhere in the tube (Fig. 16.2). Almost all of the tubes bearing deeper

1. K. V. Cook, G. A. Reimann, and R. W. McClung, *Metals and Ceramics Div. Annu. Progr. Rep. June 30, 1971*, ORNL-4770, p. 80.

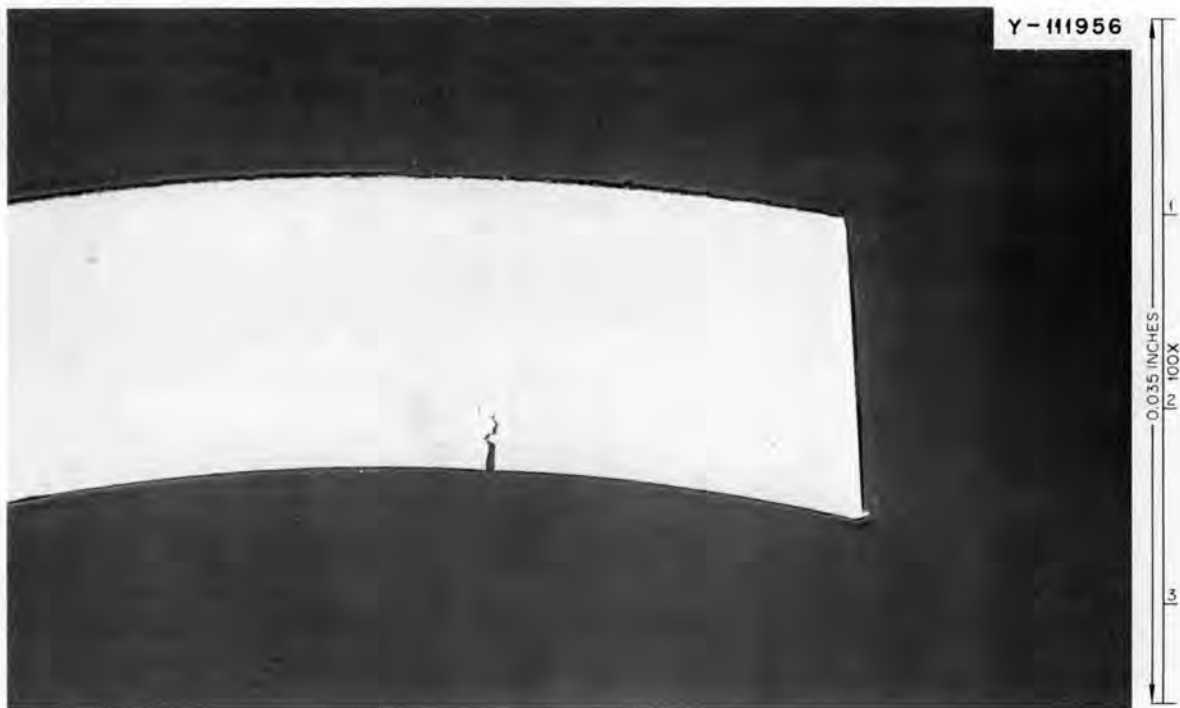


Fig. 16.2. Typical cross section of specimen tested with deep sharp notch. Test interrupted before failure occurred.

notches failed at the notches, whereas several tubes bearing 0.0005-cm-deep notches did not fail at the notches, and the effect of increasing notch depth was to

reduce rupture time and ductility. A report concerning the analysis of the results is being prepared.

17. Joining of Structural Materials

G. M. Slaughter

The LMFBR welding development program is concentrated on three types of materials: austenitic stainless steels, nickel-rich alloys such as Incoloy 800 and Inconel 718, and ferritic steels.

STAINLESS STEELS

G. M. Goodwin N. C. Cole R. G. Berggren

We are studying the effect of chemical composition, welding process, and variables within a process on the behavior of weldments in austenitic stainless steels at 370 to 650°C for application to LMFBR vessels and components. Included in the program are the shielded metal-arc, gas tungsten-arc, submerged-arc, gas metal-arc, and electroslag welding processes. Section sizes range from 1/2 in., typical of LMFBR piping wall thicknesses, to 2 3/8 in., representative of a typical LMFBR vessel wall. The information generated in these programs has pointed out a serious lack of long-term, elevated-temperature ductility in conventional austenitic stainless steel weldments and has been influential in the selection of a "controlled residual element" (CRE) filler metal having superior strength and ductility for use in the Fast Flux Test Facility vessel.¹ Piping welds are currently under intensive study.

Heavy Section Weldment Evaluation

We continued the evaluation of 36 heavy section (≥ 1 in. thick) weldments prepared using the shielded metal-arc, submerged-arc, gas metal-arc, and electroslag welding processes.

The study of the shielded metal-arc process has concentrated on the effects of minor compositional variations of the weld deposit produced by altering the electrode coating composition. We produced 23 welds in 1-in.-thick type 304 stainless steel plate, all conforming to the AWS-ASTM composition specifications

1. G. M. Goodwin, N. C. Binkley, N. C. Cole, and R. G. Berggren, *Metals and Ceramics Div. Annu. Progr. Rep. June 30, 1971*, ORNL-4720, pp. 82-85.

for type 308 stainless steel filler metal. The series was composed of three welds of nominally identical composition made with different type electrode coatings, and 20 welds with intentional variations in the amounts of B, P, Si, S, C, and Ti in the deposit. Approximately 100 specimens from the weldments were creep tested at 650°C for times up to 5000 hr. Based on the single effects of each of the above elements, an optimized composition containing boron, phosphorus, and ferrotitanium was developed. These special "controlled residual element" (CRE) electrodes yield welds with excellent high-temperature strength properties and, as shown in Fig. 17.1, superior high-temperature creep ductility.

Eleven submerged-arc welds were produced in both 1- and 2-in.-thick plates. The object was to study the variability in elevated temperature properties attributable to flux composition and to the energy input used during welding. Only commercially available fluxes were investigated, and for these fluxes other variables,

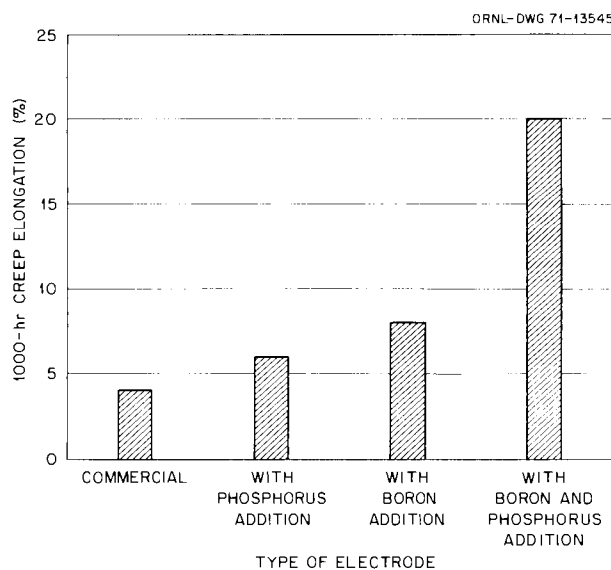


Fig. 17.1. Effect of residual elements on the ductility of type 304 stainless steel shielded metal-arc welds at 650°C.

particularly deposit composition, far outweighed the effect of flux formulation. Increasing heat input had a significant effect of decreasing strength and increasing ductility, but the effect was small by comparison with other variables.

Two electroslag weldments are being studied. Both are in 4-in.-thick material, with one weld joining two type 304 stainless steel plate sections and the other between two type CF8 stainless steel castings. Creep data have been collected for both base materials and the weld deposits. In general, the weld deposits are weaker than either the wrought or cast base material but have comparable ductility. The electroslag welds are slightly weaker but of greater ductility than the submerged-arc welds, presumably at least in part because of the heat input effect mentioned above. Two gas metal-arc welds produced with different shielding gas mixtures are being examined.

We have procured approximately 42 lin ft of weldment in $2\frac{3}{8}$ -in.-thick plate for a detailed study discussed below. The welds are made in plate from two of the five FFTF vessel heats and electrodes from 7 of the 11 batches used to date in fabrication of the vessel.

Properties of Stainless Steel Welds with Controlled Residual Elements

R. T. King G. M. Goodwin J. O. Stiegler

We are investigating the structure and properties of CRE double-U-joint test weldments similar to those in the FFTF vessel to obtain design data and an understanding of properties. The test weldments join $2\frac{3}{8}$ -in.-thick sections of type 304 stainless steel plate. Tensile and creep specimens have been prepared from different depths within the weld. Specimens oriented parallel to the welding direction (longitudinal), perpendicular to the welding direction (transverse), and perpendicular to the plate surfaces have been prepared with a 0.25-in.-diam \times 1.25-in.-long gage section.

The CRE weld metal specimens from near the surface of the test weldments are generally weaker and more ductile than those from nearer the center of the weldments in tensile tests from 25 to 649°C. Hardness indentation profiles also showed increasing hardness from the surface to the center of the welds. This variation in short-time mechanical properties may be related to localized variations in the microstructure of the weld with an unknown contribution from chemical segregation effects. Near the surface of the weld, about 10^{10} straight dislocation lines/cm² and a few small loops exist; in the same region, relatively few carbide precipitate particles are found on austenite-ferrite inter-

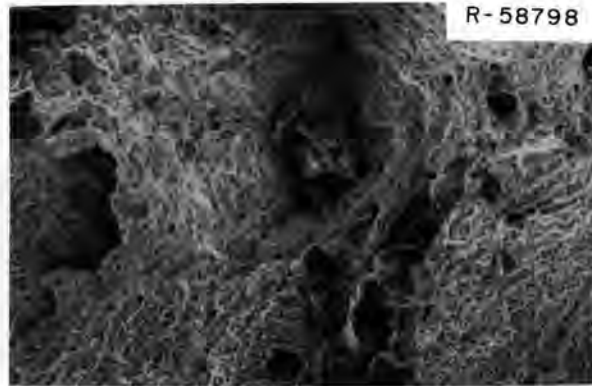


Fig. 17.2. Fracture surface of a controlled residual element weld specimen tested at 565°C. Inclusion particles are embedded in the fracture surface. 130 \times .

faces. Toward the center of the weld, the loop and dislocation line densities increase, and most dislocations are involved in a well-defined cell structure. Also, the austenite-ferrite interfaces are decorated with carbide precipitate particles.

Transverse tensile specimens always fractured in the weld metal rather than in the base metal or heat-affected zones. Anisotropic deformation occurred in both longitudinal and transverse specimens, and the directions of the principal axis of anisotropy probably coincide with the local substructural orientation, which changes from point to point in the weld cross section.

The creep properties showed similar variations through the weld thickness to those observed in tensile tests. In one series of tests, weld metal from near the surface had a minimum creep rate nearly 1000 times greater than did similar specimens from near the weld center. The fracture surfaces of creep-rupture specimens were covered with shear dimples, which are normally associated with ductile fractures in metals. Figure 17.2 shows the fracture surface of a specimen that failed at 565°C after 2780 hr at 33,000 psi; ductile tearing occurred but is related to the local substructure only in isolated areas. Creep specimens exhibited ductility in excess of 15% for all tests completed to date. Although there is some tendency for the ductility to decrease with increasing rupture time (Fig. 17.3), the ductility of the CRE welds is considerably higher than that reported for conventional type 308 stainless steel weld metal.

Filler Metal Development for Pipe Welding

We are studying the properties of welds in $\frac{1}{2}$ -in.-thick wrought types 304 and 316 stainless steel for application to LMFBR piping systems. In addition to

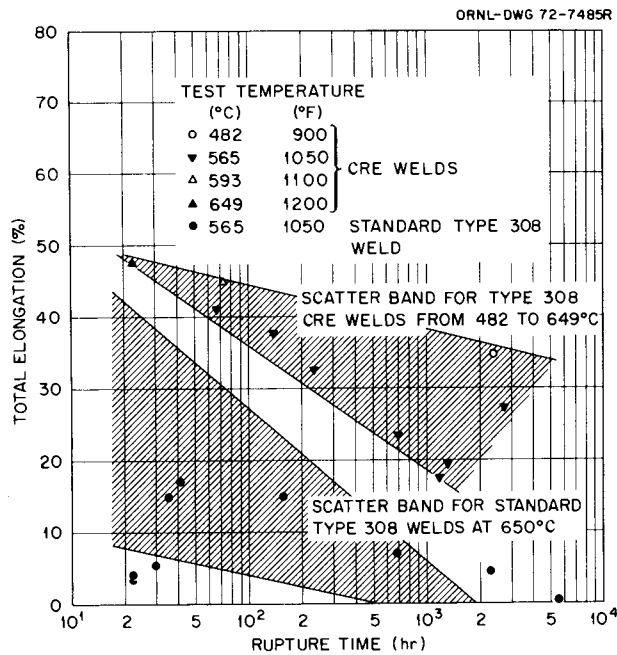


Fig. 17.3. Ductility in creep-rupture tests of type 308 stainless steel welds.

determining the elevated-temperature mechanical properties of conventional filler metals used with the shielded metal-arc and gas tungsten-arc processes, we are attempting to develop improved filler metals for types 304 and 316 stainless steel using essentially the same approach as was outlined in the heavy-section weldment study described above. Automated orbital welding equipment will be used to apply the information obtained to the production and evaluation of actual pipe welds in typical LMFBR piping up to and including 28 in. in diameter.

To date, 34 weldments, each approximately 10 in. long, have been produced in 1/2-in.-thick wrought types 304 and 316 stainless steel. Welds were made with the gas tungsten-arc and shielded metal-arc processes and conventional types 308, 316, and 16 Cr-8 Ni-2 Mo stainless steel filler metals, in addition to ten experimental tungsten-arc filler wires and 16 experimental batches of shielded metal-arc electrodes. As anticipated, the type 316 stainless steel weldments (including type 16 Cr-8 Ni-2 Mo stainless steel filler metal) exhibit greater strength than any of the type 308 stainless steel welds, but the ductility values obtained to date indicate a reduction in long-term creep ductility similar to that noted for type 304 stainless steel heavy section weldments. Our present plans emphasize the development of "controlled residual element" compositions for type 316 stainless steel weldments for direct application to the FFTF hot-leg piping.

NICKEL-RICH ALLOYS

D. A. Canonico

Inconel 718

We have assisted Aerojet Nuclear Corporation in preparing a program plan for the study of Inconel 718, an age-hardenable high nickel alloy. Our interest is associated with the effect of welding on the mechanical properties, in particular ductility, of postweld-heat-treated components. The aim of this program is to obtain ASME Code approval for Inconel 718.

Incoloy 800

Incoloy 800, an Fe-Ni-Cr alloy, is being considered for the construction of LMFBR steam generators. The weldability of this alloy without filler-metal additions is marginal, and current practices usually require the use of Inconel 82 filler metal. Inconel 82 is a Ni-Cr-Fe alloy whose physical and mechanical properties are quite unlike those of Incoloy 800. The study of the effect of various minor elements on the weldability of Incoloy 800 has provided an insight into their effect on cracking sensitivity.

We have continued² our studies on several experimental Incoloy 800 (Fe-32.5% Ni-21% Cr) compositions prepared in the Melting and Fabrication Laboratory at ORNL. Hot-ductility studies have shown that 0.08% C in the presence of 0.38% Ti slightly impairs the recovery of ductility after a thermal excursion simulating that experienced in the heat-affected zone of a weld. Adding nominally 0.015% S to an experimental alloy of a similar composition caused a distinct loss in the alloy's ability to recover ductility. This is in contrast to the ductility recovery observed when similar sulfur and titanium levels, without carbon, were investigated. Apparently, the carbon combines with the titanium, thereby negating its ability to immunize the Incoloy 800 against the deleterious effects of sulfur.

The use of experimental Incoloy 800 alloys as filler metals has provided additional information regarding the effect of the minor elements on weldability. A filler metal with high titanium ($\approx 0.60\%$), medium carbon ($\approx 0.04\%$), low sulfur ($< 0.010\%$), and medium phosphorus ($\approx 0.015\%$) produced a weld metal with the least fissuring propensity. Furthermore, our studies have shown that the weld metal fissures were intergranular.

2. D. A. Canonico, *Metals and Ceramics Div. Annu. Progr. Rep. June 30, 1971*, ORNL-4770, pp. 128-29.

Welds made with the commercial 82T filler metal and the experimental Incoloy 800 filler metals showed a dramatic difference in microstructure.

The 82T welds exhibited a cellular microstructure, whereas the experimental Incoloy 800 filler metal welds contained large columnar grains epitaxially growing from the base metal. Reducing the grain size of the heat-affected zone at the fusion line did not affect the weld metal microstructure. Much of the cracking sensitivity exhibited by the Incoloy 800-type filler metals is attributed to the solidification morphology of the experimental weld metal. Thus our efforts to eliminate the cracking problems with Incoloy 800 weld metal have been somewhat successful. We have produced weld microstructures similar to those seen in welds made with Inconel 82 filler metal. A slight propensity toward cracking prevails, however, and our alloy development studies will continue on a limited basis.

FERRITIC STEELS

D. A. Canonico

Stabilized Grades

The investigation of the stabilized ferritic steels has concentrated on the niobium-stabilized $2\frac{1}{4}$ Cr–1 Mo– $\frac{1}{2}$ Ni low-alloy grade. The effort is directed toward the determination of the basic weldability of this alloy. Our previous³ studies showed that it is prone to hot cracking when welded under highly restrained conditions. The cracks can be sealed by backfilling with a eutectic of Fe_2Nb and δ -iron.

We made a number of gas tungsten-arc welds in $\frac{1}{4}$ - and $\frac{1}{2}$ -in.-thick plates from two heats of niobium-stabilized steel. The filler metal employed was prepared from the base metals, and the welds were fully restrained. The niobium-to-carbon ratios for the two

heats were 11 and 13. Table 17.1 contains the chemical composition of the heats studied. All weldments satisfactorily passed room-temperature bend tests around a $2T$ radius mandrel (T = base-metal thickness). Metallographic studies of the welds showed the boundaries of the large austenite grains in the heat-affected zone to be outlined with the eutectic phase. Further, islands of the eutectic are visible in the heat-affected zone when viewed at a magnification of 500X.

Tensile tests in the as-welded condition showed the welds to have excellent strength and ductility, both at room temperature and 565°C (1050°F). Table 17.2 contains the results of the tensile tests. Charpy V-notch properties of the welds in both the as-welded and postweld heat-treated conditions were obtained at $+40^\circ\text{F}$. The postweld heat treatment did not improve the weld metal toughness, but it did tend to normalize the impact properties at about 55 ft-lb. The as-welded values ranged from 42 to 111 ft-lb.

A metallographic study of the initiation site for fracture (at the root of the machined notch) showed considerable plastic deformation. The grain boundary film seen in the heat-affected zone of the base metal and in the weld metal, which was previously identified as a eutectic between Fe_2Nb and δ -iron, was not brittle. Indeed, it is capable of a great degree of deformation and has proven to be tough.

In summary, the niobium-stabilized $2\frac{1}{4}$ Cr–1 Mo– $\frac{1}{2}$ Ni low-alloy steel has a sensitivity toward microfissuring during welding due to the formation of a liquid phase at 1370°C (2500°F). However, the completed weld does not exhibit a degradation of toughness at room temperature.

Low-Carbon Grades

The study of the low-carbon $2\frac{1}{4}$ Cr–1 Mo steels is directed toward the assessment of the effect of carbon content on the mechanical properties of weldments. These properties will serve as a guide in the selection of the optimum carbon level to be used in the fabrication of steam generators for demonstration plants.

3. D. A. Canonico and N. C. Binkley, *Metals and Ceramics Div. Annu. Progr. Rep. June 30, 1971, ORNL-4770*, pp. 85–88.

Table 17.1. Chemical compositions of niobium-stabilized steel plate used in this study

Heat	Composition (wt %) ^a								
	C	Si	Mn	P	S	Cr	Ni	Mo	Nb
403150	0.09	0.27	0.48	0.017	0.004	2.36	0.60	0.97	0.98
450543	0.08	0.35	0.46	0.011	0.005	2.18	0.54	0.94	1.08

^aBalance, Fe.

Table 17.2. Results of tensile tests on welds in the niobium-stabilized
2¼ Cr-1 Mo-½ Ni steel

Heat (base metal and filler metal)	Test thickness (in.)	Test temperature (°C)	Strength (psi)		Ductility (%)	
			Yield (0.2% offset)	Ultimate	Elongation	Reduction in area
403150	0.25	Room	61,700	85,700	13	77
403150	0.5	Room	64,400	80,000	18	76
450543	0.25	Room	65,400	86,200	15	75.5
450543	0.5	Room	57,100	74,100	15.6	76.1
403150	0.25	565	45,200	51,000	12.2	76
403150	0.5	565	41,800	44,600	14.2	80.7
450543	0.25	565	44,100	50,400	10	80
450543	0.5	565	35,400	40,100	16.8	80.0

Table 17.3. Results of hardness traverses on welds with varying carbon contents

Carbon content (%)	Condition	Diamond pyramid hardness number				Base metal
		Heat-affected zone		Weld metal		
		Last pass	Early pass	Last pass	Early pass	
0.003	As welded	166-239	165-177	242-266	152-180	129-135
0.035	As welded	163-225	180-210	291-307	205-275	127-145
	Stress relieved	135-176	126-142	203-211	164-196	115-117
0.11	As welded	238-264	234-312	361-394	256-361	177-194
	Stress relieved	205-228	190-218	223-234	199-228	180-192

Welds have been made with parameters identical to those previously reported.⁴ These were made in ½-in.-thick plates that had been normalized at 930°C for 1 hr and tempered at 705°C for 1 hr. These weldments were sectioned to provide transverse specimens for the mechanical property studies.

Hardness traverses through the weld metal, heat-affected zone, and base metal were conducted on weldments of all three carbon levels. These data are presented for the as-welded and welded-and-stress-relieved conditions in Table 17.3. In the as-welded condition, the base metal is evidently the softest zone regardless of carbon content. This is also true after a 705°C postweld heat treatment for welds made with the medium (0.035%) and high (0.11%) carbon materials. Insufficient material was available to obtain postweld heat treatment data for the low-carbon welds.

This investigation has been handicapped by a lack of commercial steel. However, we received in late June

1972 a commercial heat of low-carbon (0.027% C) 2¼ Cr-1 Mo steel. This material will be used in future weldability and mechanical properties studies.

Tube-to-Tube-Sheet Welding Studies

D. A. Canonico

The adequate evaluation of the mechanical properties of tube-to-tube-sheet welds is handicapped by the geometric configuration of the weld. In an effort to overcome this problem, we have developed a simulated bore-side tube weld using flat plates. This technique permits the machining of flat specimens for mechanical property testing and nondestructive test development. We have also developed a double-torch technique that will allow the simulation across an entire weldment of that area that may be most critical in a tube-to-tube-sheet weld, namely the weld overlap region. Figure 17.4 is a sketch showing the simulated specimen configuration for the tube-to-tube-sheet weld.

4. D. A. Canonico and N. C. Binkley, *Metals and Ceramics Div. Annu. Progr. Rep. June 30, 1971*, ORNL-4770, p. 86.

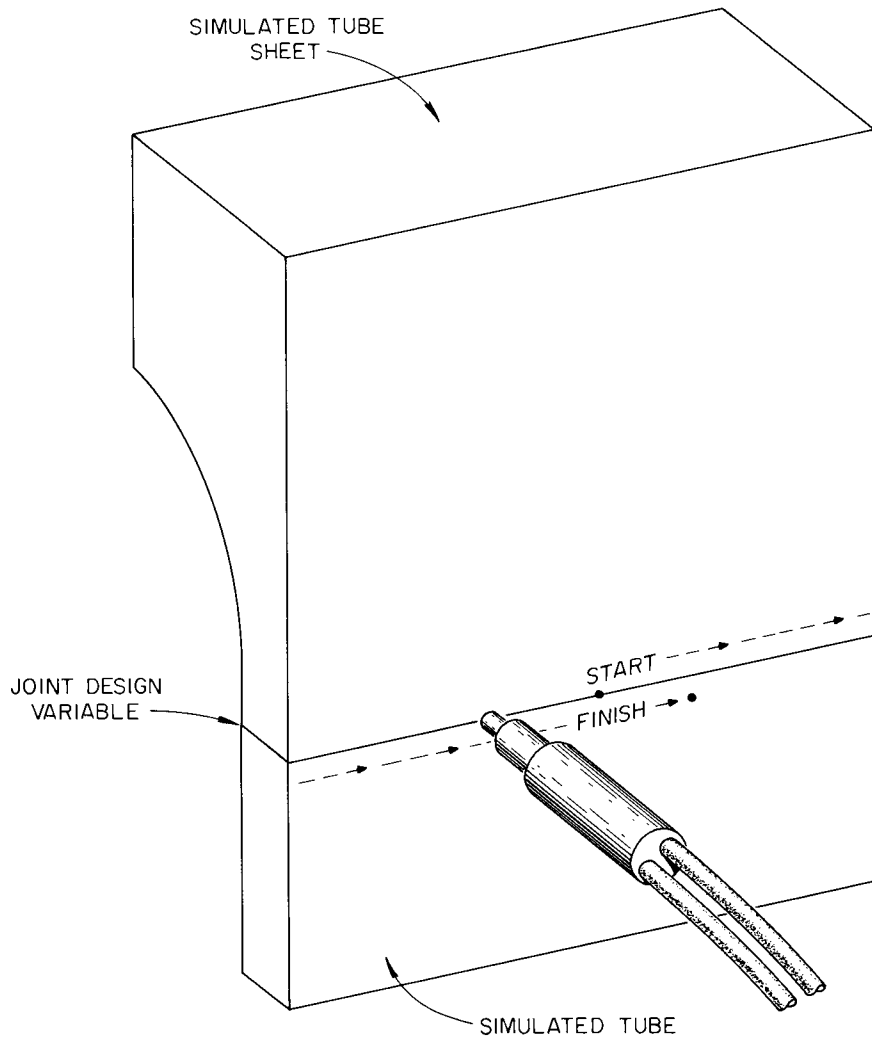


Fig. 17.4. Specimen configuration to simulate bore-side welds.

18. Mechanical Properties of Alloys in Reactor Environments

W. R. Martin H. E. McCoy, Jr.

Type 316 stainless steel will be used for fuel element cladding and fuel subassembly ducts in the FTR and possibly in future liquid metal fast breeder reactors. In these applications the alloy will operate in the range 350 to 750°C for times of several thousand hours. This alloy is unstable, and such thermal exposure will cause the precipitation of carbides (primarily $M_{23}C_6$) and intermetallic phases such as sigma, chi, and eta or Laves. In addition, voids and a dislocation structure will be formed by the precipitation of irradiation-produced vacancies and interstitials at temperatures in the range 350 to 650°C, and helium bubbles will be formed at higher irradiation temperatures. To reduce the swelling caused by the void-dislocation structure, the alloy will probably be used in the cold-worked condition, but a cold-worked structure will significantly alter the kinetics of the carbide and sigma precipitation reactions, in general by shifting the time-temperature-precipitation curves to shorter times and lower temperatures. In addition, irradiation may alter the precipitation kinetics and phase stability. The purpose of this program is to relate these complex microstructural changes to the deformation and fracture characteristics of the irradiated alloy and thus predict behavior under service conditions. Additional work is directed towards the development of alloys, such as the titanium-modified type 316 stainless steel, that exhibit improved resistance to radiation damage, particularly embrittlement.

SWELLING OF AUSTENITIC STAINLESS STEEL

J. O. Stiegler E. E. Bloom

Our studies of irradiation-induced defect structures in annealed specimens of type 304 stainless steel were extended into the fluence range above 10^{23} neutrons/cm² (>0.1 MeV) through examination of control and safety rod thimbles removed from EBR-II. Although void concentrations were observed to saturate, no limitation to void growth was found, and volume changes as high as 11% were measured for irradiation to a fluence of 1.7×10^{23} neutrons/cm² at 420°C. Our

first experimental subassemblies containing type 316 stainless steel were returned from EBR-II. Specimens irradiated in the annealed and several cold-worked states were examined along with some modified by the addition of 0.23% Ti. Significant observations of defect structures and swelling in these steels are summarized below; mechanical properties measured on the same or equivalent specimens are reported in the following section.

Annealed Type 304 Stainless Steel

Work¹ during the past year established that void concentrations reach limiting or saturation values but that the concentration at saturation and the fluence at which saturation occurs are temperature dependent. For example, at 370°C, voids were first observed at a fluence of about 10^{21} neutrons/cm². The concentration increased with increasing fluence until it reached a limiting value of 1.5×10^{16} voids/cm³ at a fluence of 1×10^{23} neutrons/cm². At 590°C, void nucleation occurred only in the narrow fluence interval between about 1.5 and 3×10^{22} neutrons/cm², and the limiting concentration was less than 2×10^{14} voids/cm³. During the time in which voids were nucleated, the mean void diameter increased slowly, as less than the $1/6$ power of fluence. Limited results indicated that after saturation in the void concentration the mean diameter increased more rapidly, so that the rate of swelling changed little, if any. Especially at the higher irradiation temperatures, some heat-to-heat variations were evident in the numbers and sizes of voids, but the swelling was not significantly affected.

From comparison of the observations with predictions derived from models we were able to conclude that homogeneous nucleation and nucleation in displacement spikes, in overlapping spikes, or at pre-existing sites were unlikely to be major sources of the voids

1. E. E. Bloom, J. O. Stiegler, and C. J. McHargue, "Radiation Damage in Annealed Type 304 Stainless Steel," *Radiation Effects* (to be published).

Table 18.1. Comparison of void concentration and size distribution in annealed stainless steel: types 304,^a 316, and 316 + 0.23% Ti

Stainless steel type	Irradiation temperature (°C)	Fluence >0.1 MeV (neutrons/cm ²)	Concentration (voids/cm ³)	Mean void diameter (Å)	Volume swelling (%)
		$\times 10^{22}$			
304	450	1.9	1.3×10^{15}	178	0.54
316	450	1.9	6.9×10^{13}	236	0.06
316 + 0.23% Ti	450	1.9	6.8×10^{14}	172	0.20
304	515	2.3	7.3×10^{14}	218	0.63
316	510	1.5	1.8×10^{13}	337	0.05
316 + 0.23% Ti	515	2.3	1.8×10^{13}	313	0.04
304	580	1.9	1.7×10^{13}	258	0.26
316	580	1.9	1×10^{13}	666	0.21
316 + 0.23% Ti	580	1.9	$\approx 10^{12}$		<0.02

^aValues for type 304 stainless steel were calculated with the empirical equations of Brager et al., *Met. Trans.* 2, 1893 (1971).

in neutron-irradiated stainless steel. Models for nucleation on helium bubbles or in displacement spikes stabilized by helium atoms did not disagree in any way with the experimental observations.

Since the threshold fluence for void formation increased with increasing irradiation temperature, the shape of the swelling vs temperature curve changed with increasing fluence. The temperature of maximum swelling increased with increasing fluence, and the curves extended to higher temperatures. We concluded that data obtained at a low fluence cannot be simply scaled up to predict behavior at higher fluences.

Annealed Type 316 Stainless Steel²

The defect structures found in type 316 stainless steel are qualitatively similar to but quantitatively different from those observed in type 304. Voids were observed for irradiation between 450 and 590°C, with the concentration decreasing and the mean size increasing with increasing irradiation temperature. For fluences of about 2×10^{22} neutrons/cm², void concentrations were less than $1/10$ that in type 304. Sizes were somewhat larger in the type 316, but not enough to overcome the reduced concentration, so that the overall

swelling was significantly less. The difference was greater at the lower irradiation temperatures, as can be seen from the statistics given in Table 18.1. Similar behavior was found for the dislocation structure. However, precipitation reactions appeared to be enhanced in the type 316 material, although there was no obvious change in either type or morphology of precipitate particle. The range of defect structures produced in type 316 stainless steel for irradiation at 590°C is illustrated in Fig. 18.1, where voids, Frank loops, dislocation lines, $M_{23}C_6$ particles, and an unidentified ribbon-like precipitate are all present. The microstructural changes produced by irradiation between 450 and 580°C are described quantitatively.

Cold-Worked Type 316 Stainless Steel²

Prior deformation of 20% by cold working produced significant modifications in the microstructures of type 316 stainless steel irradiated to a fluence of about 2×10^{22} neutrons/cm² at temperatures between 450 and 800°C by suppressing the formation of voids and enhancing and changing the development of precipitate particles. Voids were found only in isolated recovered areas of a specimen irradiated at 580°C. No interstitial loops or structure that could be attributed to the displaced atoms was detected in any of the specimens. Partial recrystallization was observed in specimens irradiated above 680°C, but recrystallization was not complete in a specimen irradiated at a temperature that rose from 735°C at the start of the irradiation to 795°C at the finish. A 10-hr treatment at 750°C was sufficient

2. Summarized from E. E. Bloom and J. O. Stiegler, "Effect of Irradiation on the Microstructure and Creep-Rupture Properties of Type 316 Stainless Steel," paper presented at the 6th International Symposium on the Effects of Radiation on Structural Materials, ASTM Annual Meeting, Los Angeles, June 26-28, 1972 (to be published in the Proceedings).

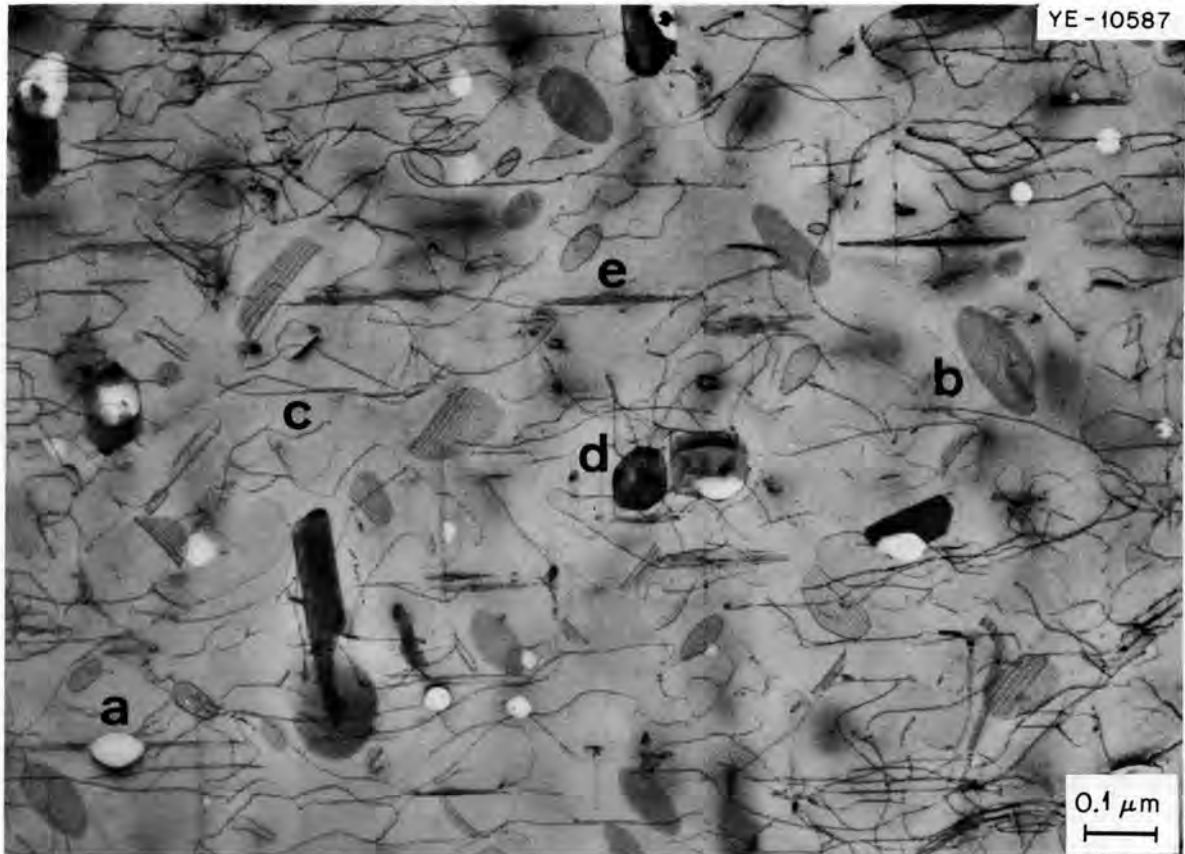


Fig. 18.1. Transmission electron micrograph illustrating the defect structures formed in type 316 stainless steel irradiated in EBR-II to a fluence of 2×10^{22} neutrons/cm² at 580°C. Features indicated are (a) voids, (b) Frank loops, (c) dislocation lines, (d) $M_{23}C_6$ particles, and (e) unidentified ribbon-like precipitate.

to cause complete recrystallization in the laboratory. Helium bubbles were found on grain boundaries of the irradiated specimens and may have inhibited recrystallization. Specimens that recrystallized also developed sigma-phase precipitates, usually at triple grain junctions. At the lower irradiation temperatures, $M_{23}C_6$ and Laves phase particles formed, usually in association with the stacking fault bands.

Void formation was also suppressed in a specimen deformed 10% before irradiation at 590°C to a fluence of 2.3×10^{22} neutrons/cm² and in one deformed 50% before exposure to 1.5×10^{22} neutrons/cm² at 640°C. In the former, small $M_{23}C_6$ and Laves phase precipitates formed, again in association with the stacking fault bands. In the latter, massive precipitate particles, as yet unidentified, were found.

Titanium-Modified Type 316 Stainless Steel

The addition of 0.23% Ti to type 316 stainless steel produced a steel having radiation damage characteristics

different from types 304 and 316 stainless steels.^{3,4} This further illustrates our contention that the damage introduced into stainless steels by fast neutron irradiation is extremely sensitive to composition. When irradiated at a low temperature (450°C) to a fluence of about 2×10^{22} neutrons/cm² the titanium-modified steel showed void concentrations midway between types 304 and 316 (see Table 18.1). At higher temperatures (515°C) it swelled less than either of the other two, and at 580°C it showed no measurable swelling at all, in contrast to 0.26 and 0.21% in types 304 and 316, respectively. These observations suggest that the small addition of titanium changes the temperature dependence of the swelling by decreasing the

3. H. R. Brager et al., *Met. Trans.* **2**, 1893 (1971).

4. E. E. Bloom, "Nucleation and Growth of Voids in Stainless Steels during Fast Neutron Irradiation," pp. 1-29 in *Radiation-Induced Voids in Metals* (Proc. Int. Conf. Albany, N.Y., June 9-11, 1971), ed. by J. W. Corbett and L. C. Ianniello, U.S. Atomic Energy Commission Office of Information Services, Oak Ridge, Tenn., 1972.

temperature of maximum swelling. Alternatively, it may act by increasing the threshold fluence for void formation.

MECHANICAL PROPERTIES OF AUSTENITIC STAINLESS STEELS

E. E. Bloom D. Fahr J. O. Stiegler

To predict the behavior of austenitic stainless steels under LMFBR service conditions the relationships between microstructure and properties must be known. In initial studies, annealed and cold-worked type 316 stainless steel were irradiated at temperatures of interest to LMFBR's to a maximum fluence of 2.7×10^{22} neutrons/cm² (>0.1 MeV). The postirradiation tensile and creep-rupture properties were related to the irradiation-produced microstructure. Future irradiations will extend the fluence to about 2×10^{23} neutrons/cm², near the peak fluence for LMFBR components.

Type 316 Stainless Steel²

The most pronounced effect of neutron irradiation was a significant reduction in rupture life and ductility. For irradiation in the annealed condition, the rupture life was decreased by a factor of 3 or less in the range 550 to 700°C. At 750°C the rupture life was reduced 10- to 100-fold, with the effect being greater at the higher stress levels. The creep rates and stress dependency of the creep rate were not significantly affected by irradiation in the range 550 to 700°C. The creep rate was, however, markedly increased at 750°C.

For specimens irradiated in the cold-worked condition, the changes in creep-rupture properties were more complex. The rupture life appeared to increase and creep rates to decrease at 550°C, while at 600°C the opposite trend was observed. At 700 and 750°C the limited data suggested a decreased rupture life and increased creep rate at high stress levels with the effect becoming less and possibly reversing at lower stress levels.

Creep strain at the beginning of tertiary creep and total creep elongation for the unirradiated and irradiated conditions are shown in Fig. 18.2. For irradiation in the annealed condition, the specimens were less ductile at all temperatures in the range 550 to 750°C. For cold-worked material, the ductility after irradiation was reduced at 550 to 650°C but was increased sharply and equaled or exceeded the as-cold-worked values at 700 and 750°C. This latter effect appeared to be related to recovery and recrystallization during irradiation.

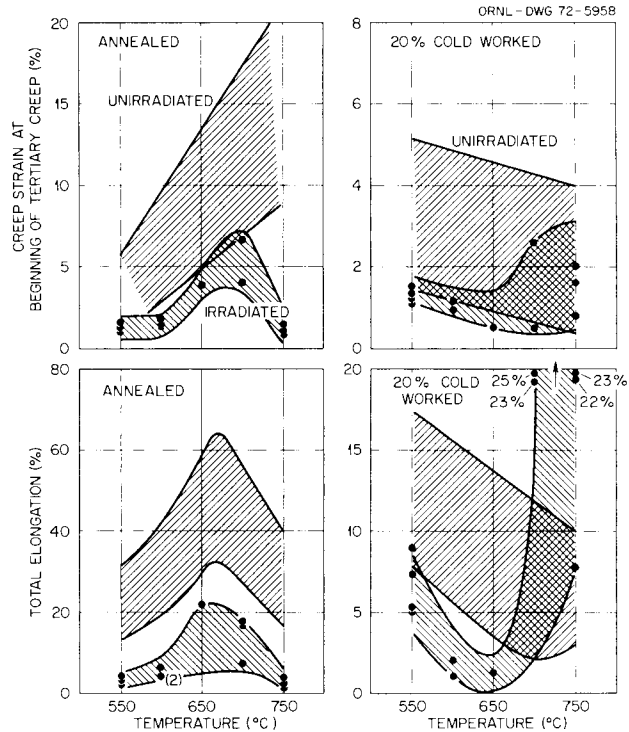


Fig. 18.2. Effect of irradiation on the creep-rupture ductility of type 316 stainless steel.

Longitudinal sections of samples irradiated in the annealed condition and tested to failure at 550, 650, and 750°C are shown in Fig. 18.3. At each temperature, extensive cracking occurred on grain boundaries approximately normal to the applied load. Cracks such as those shown in Fig. 18.3 were not localized to the region of the fracture but were found along the entire gage section. At 550 and 600°C a crack, particularly in a region removed from the fracture, was not wedge shaped but rather had nearly constant width from one triple point to another. Many of those boundaries normal to the applied load contained isolated cavities. Often a string of cavities extended from the tip of a grain boundary crack. At the higher temperature of 650°C, most of the cracks were wedge shaped, but again we observed small cavities on many of the grain boundaries. At the highest temperature, 750°C, the cracks were obviously formed by the linking of grain boundary cavities.

Scanning microscopy showed that at least two types of fracture occurred in the samples irradiated in the annealed condition and tested at 550 and 600°C. A portion of the fracture was completely intergranular, as shown in Fig. 18.4a. Other regions of the fracture consisted of areas of intergranular fracture surrounded

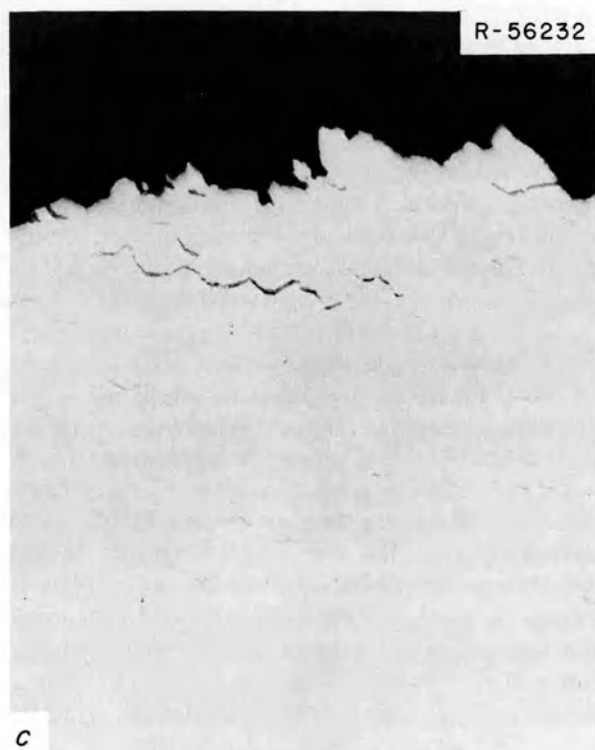
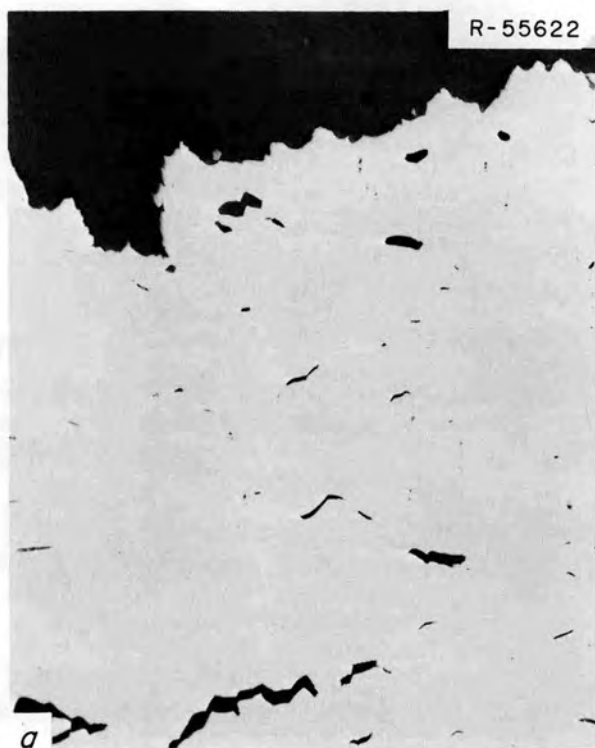


Fig. 18.3. Creep-rupture fractures of type 316 stainless steel irradiated in the annealed condition. 100X. (a) Irradiated at 580°C, 2.7×10^{22} neutrons/cm²; tested at 550°C, 45,000 psi. (b) Irradiated at 630°C, 2.3×10^{22} neutrons/cm²; tested at 650°C, 25,000 psi. (c) Irradiated between 735 and 795°C, 2.7×10^{22} neutrons/cm²; tested at 750°C, 7500 psi.

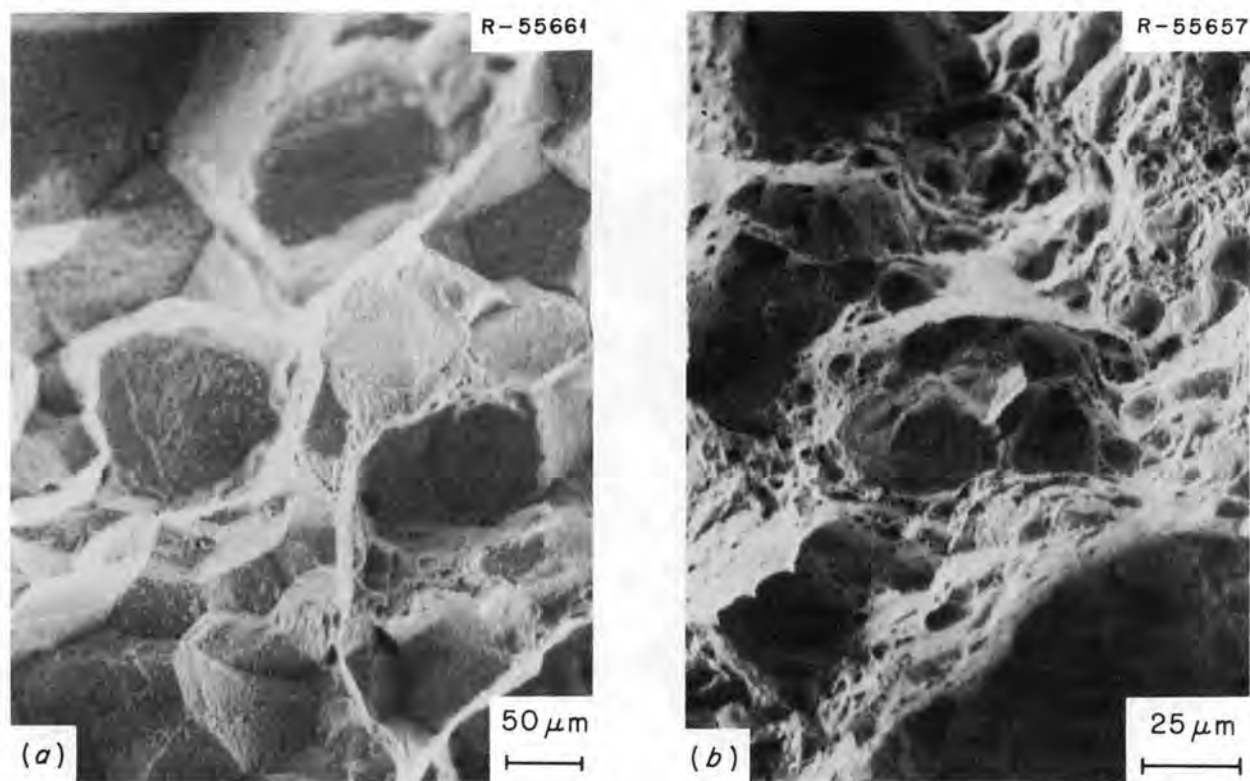


Fig. 18.4. Scanning electron micrographs of fracture in type 316 stainless steel irradiated at 580°C to 1.9×10^{22} neutrons/cm² and tested at 550°C and 45,000 psi. (a) Area of intergranular fracture. (b) Area of inter- and transgranular fracture.

by ductile transgranular fracture Fig. 18.4*b*. The failure was apparently initiated by the formation of grain boundary cracks, which propagated and eventually reduced the effective cross section of the specimen. The final separation then occurred by the linking of these cracks at a higher strain rate with considerable transgranular fracture.

For samples irradiated in the 20%-cold-worked condition and then tested in the range 550 to 650°C, the grain boundary cracks were fewer than in the companion samples irradiated in the annealed condition. The cracks were generally narrower in the cold-worked specimens than in the annealed specimens, and the percentage of intergranular fracture was much larger. Such observations suggest strongly that the strength of the matrix is important in crack initiation, propagation, or both. At 750°C, extensive sigma-phase precipitation was apparent, and cavities were usually associated with the sigma particles. The sigma phase particles were never fractured; the cavities and cracks were located at the particle-matrix interface.

These results suggest that at all temperatures, grain boundary cracks formed by the stress-induced growth and linking of grain boundary cavities. We believe that helium bubbles serve as cavity nuclei and stress-induced growth occurs by the vacancy-diffusion mechanism proposed by Speight and Harris.⁵ Propagation of these cracks depended upon the flow stress of the matrix. At the lower irradiation temperatures, which resulted in high flow stresses, cracks were narrow and extended large distances (often across several triple grain junctions), possibly as a result of increased cavity growth rates near the leading edge of a crack due to stress concentration at the crack tip. At slightly higher temperatures, this stress concentration was apparently reduced by plastic deformation, and the crack propagation was sufficiently reduced to allow grain boundary sliding and matrix deformation. At the highest temperatures, cavity growth rates were sufficiently rapid to reduce the rupture life a factor of about 100.

5. M. V. Speight and J. E. Harris, *Metal Sci. J.* 1, 83 (1967).

Table 18.2. Postirradiation tensile properties of annealed type 316 + 0.23% Ti stainless steel

Irradiation temperature (°C)	Fluence >0.1 MeV (neutrons/cm ²)	Test temperature (°C)	Stress (psi)		Total elongation (%)	Reduction in area (%)
			Yield	Ultimate tensile		
	$\times 10^{22}$					
465	1.2	450	44,400	82,200	35.4	30.3
510	0	500	21,200	84,500	47.8	58.8
	1.5	500	35,100	78,300	31.9	50.6
630	0	600	19,700	80,400	34.7	42.8
	1.2	600	31,200	56,600	29.8	56.7

Table 18.3. Postirradiation creep-rupture properties of annealed type 316 + 0.23% Ti stainless steel

Irradiation temperature (°C)	Fluence >0.1 MeV (neutrons/cm ²)	Test temperature (°C)	Stress (psi)	Rupture life (hr)	Creep rate (%/hr)	Total elongation (%)
	$\times 10^{22}$					
580	2.3	550	55,000	252.9	0.031	17.1
580	2.7	550	45,000	1930.0	0.0036	19.9
580	2.7	550	45,000	(452.4) ^a	(0.0026) ^a	(3.6) ^a
580	1.5	600	50,000	184.7	0.01	10.1
580	2.3	600	40,000	535.8	0.01	18.1
580	1.9	600	40,000	(199.4)	(0.008)	(3.4)
610	1.9	650	35,000	55.8		35.6
630	2.3	650	25,000	1590.3	0.01	28.2
630	2.3	650	25,000	(346.6)	(0.03)	(21.6)
870	2.7	750	7,500	>3600		>6.5
835	4.4	750	7,500	642.0	0.02	25.8
825	4.4	(750)	7,500	(105.3)	(0.018)	(3.3)

^aValues in parentheses are typical results for type 316 stainless steel irradiated and tested at the same conditions as the titanium-modified alloy.

Titanium-Modified Type 316 Stainless Steel⁶

Thermal reactor irradiation experiments on four heats of vacuum-melted type 316 stainless steel containing 0.23, 0.33, 0.46, and 0.60% Ti demonstrated that 0.2 to 0.3% Ti resulted in maximum ductility for irradiation and test conditions that produced helium embrittlement. Specimens of the heat containing 0.23% Ti were irradiated in the EBR-II at temperatures in the range 450 to 850°C to maximum fast neutron fluences

of 2.7×10^{22} neutrons/cm² (>0.1 MeV). Postirradiation examination included tensile and creep-rupture tests, which are summarized in Tables 18.2 and 18.3. The increase in tensile yield strength was a result of the void-dislocation-precipitate structure produced during irradiation. The decrease in ultimate tensile strength at the higher irradiation temperatures appears to result from the precipitation of carbon and is a result of thermal history rather than irradiation per se. The postirradiation creep properties compared favorably with those of standard type 316 stainless steel irradiated in the same experiment. Postirradiation ductilities were significantly higher than those of the standard alloy.

6. Summarized from E. E. Bloom and J. O. Stiegler, "Effect of Irradiation on Titanium-Modified Type 316 Stainless Steel," presented at the Annual Meeting of the American Nuclear Society, Las Vegas, Nev., June 18-22, 1972.

19. Mechanical Properties of Structural Alloys

W. R. Martin H. E. McCoy, Jr.

The use of structural materials in nuclear reactors at progressively higher temperatures requires that we improve design methods to ensure dependable and safe operation of such systems. The design methods program involves the procurement of mechanical property data under various possible service conditions and the development of analytical methods for using these materials properties to design complex structures. ORNL is currently active in both of these areas, but we will be concerned here with only the mechanical properties information.

Although many of the methods that will be developed will be universally applicable for high-temperature design, the current work is concerned primarily with LMFBR's. The materials being studied include types 304 and 316 stainless steel and Croloys.

EXPLORATORY TESTS ON TYPE 304 STAINLESS STEEL IN SUPPORT OF THE HIGH-TEMPERATURE STRUCTURAL DESIGN METHODS FOR LMFBR COMPONENTS PROGRAM

R. W. Swindeman

We have been creep testing two heats of type 304 stainless steel over the range 538 to 649°C and for times extending to 5000 hr. The purpose is to collect basic data for use in the interpretation of the mechanical response of stainless steel under more complicated loading conditions, such as would be experienced by an LMFBR high-temperature component during its service life.

After a graphical analysis of our creep curves, we conclude that none of the more popular strain-time formulations perfectly model the mechanical behavior of either heat. However, the Garofalo¹ expression for metals appears to be a fair approximation to the observed behavior. This equation may be written:

$$\epsilon = \epsilon_e + \epsilon_p + \epsilon_t(1 - e^{-rt}) + \dot{\epsilon}_{min}t,$$

where ϵ is the total strain, t is time, ϵ_e is the elastic component, ϵ_p is the plastic component, $\dot{\epsilon}_{min}$ is the minimum or linear creep rate after transient creep has been exhausted, ϵ_t is the final transient creep component, and r describes the rate of approach to ϵ_t . One of the problems with this equation at stresses and temperatures typical of conditions where type 304 stainless steel is commonly used is that ϵ_t , r , and $\dot{\epsilon}_{min}$ are difficult to obtain, because the time required to exhaust primary creep extends beyond our available test data. Some typical data are shown in Fig. 19.1.

We have begun testing under more complicated loading conditions. For example, a number of step load tests were performed under conditions where primary creep prevailed. Most tests were run for 300- to 500-hr intervals between load changes. The results for both heats were similar and revealed several interesting features. For example, when measurable creep occurred, the plastic yield stress was increased. The creep rate at the higher stress, however, generally correlated with the constant-load creep rate compared on the basis of creep strain rather than the total strain or time under stress. Our results tended to validate the strain-hardening rule for cumulative creep. Decreases in loads did not result in any appreciable creep recovery. Hence, it appears that the microstructures developed during creep at temperatures in the range 538 to 649°C must be fairly stable, at least for materials that are initially fully annealed.

Included in our test matrix are relaxation, compressive creep, cyclic creep, and superimposed creep and cyclic plasticity tests. Our available results are too preliminary to allow complete validation of any general laws or constitutive equations governing material behavior.

1. F. Garofalo et al., "Strain-Time, Rate-Stress, and Rate-Temperature Relations during Large Deformations in Creep," pp. 1-31 in *Joint International Conference on Creep*, The Institute of Mechanical Engineers, London, 1963.

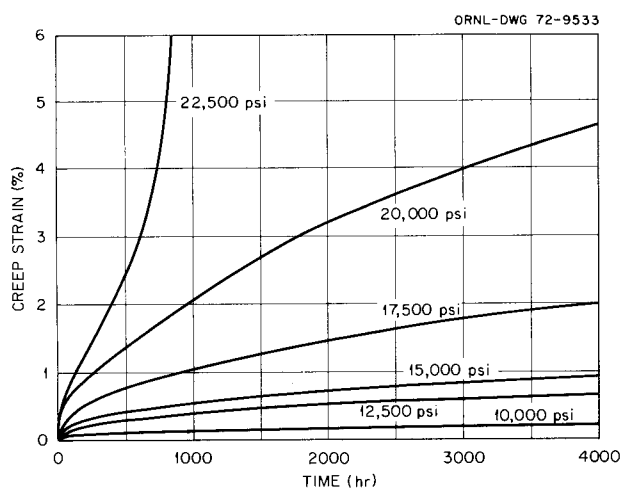


Fig. 19.1. Creep curves at 593°C for type 304 stainless steel. These curves show the long times during which primary creep dominates. Heat 9T2796 reannealed at 1093°C.

HEAT-TO-HEAT VARIATIONS IN THE MECHANICAL PROPERTIES OF TYPE 304 STAINLESS STEEL

R. D. Waddell, Jr.

A study of the heat-to-heat variation of the mechanical properties of austenitic stainless steels began this year and now involves 17 heats of type 304 stainless steel. The heats selected for study encompass a fairly wide range of compositions and have been involved in some five or six additional programs.²

Tensile properties for several heats of type 304 stainless steel at room temperature, 427, 593, and 649°C, in both the as-received and reannealed conditions, have been determined.² We are also collecting creep and stress-rupture data at 538, 593, and 649°C. Figure 19.2 shows the wide range of variation in creep behavior for ten heats of type 304 stainless steel at 649°C and 25,000 psi stress. Similar curves for tests at 593°C and 30,000 and 35,000 psi have been reported.²

Figure 19.3 shows how nine heats in the as-received condition and heat 9T2796 (plate) in the reannealed condition compare with an isochronous stress-strain curve as taken from ASME code case 1331-5. The nine heats in the as-received condition compare favorably with the 1331-5 curve, but the reference heat, 9T2796 in the reannealed condition, falls considerably below

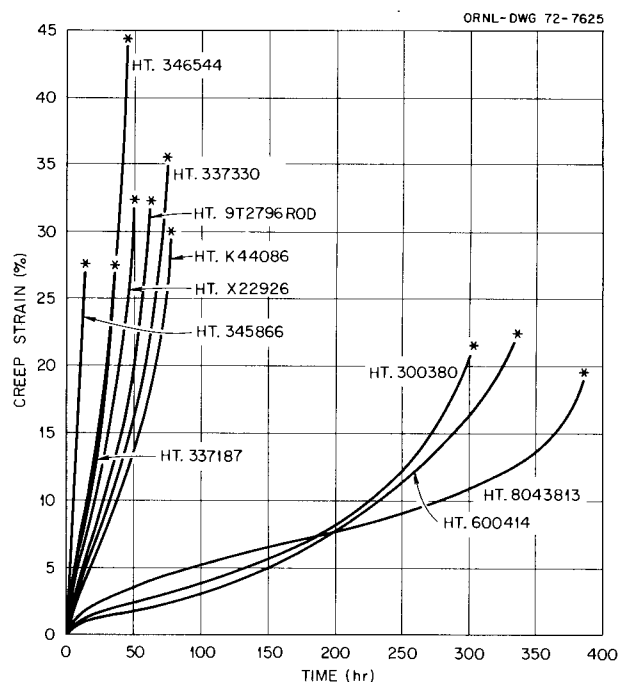


Fig. 19.2. Comparison of creep curves at 649°C and 25,000 psi for ten heats of type 304 stainless steel.

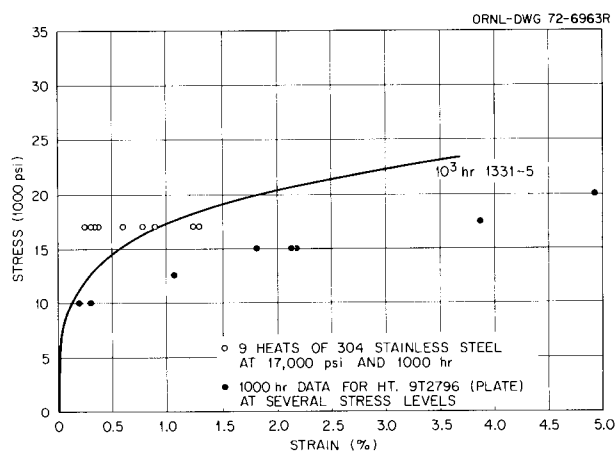


Fig. 19.3. Comparison of creep results with an isochronous stress-strain curve per code case 1331-5 at 1100°F for several heats of type 304 stainless steel.

the 1000-hr curve. We are also conducting a series of ten tests on one heat (X22926) in the reannealed condition at 593°C and 35,000 psi to ascertain what variation one might expect to find within one heat due to test methods, etc. The results of these tests to date indicate these variations to be small compared to the variation between heats.

2. R. W. Swindeman and R. D. Waddell, Jr., *Fuels and Materials Development Program Quart. Progr. Rep. Mar. 31, 1972*, ORNL-TM-3797, pp. 185-203.

MECHANICAL PROPERTIES OF STRUCTURAL MATERIALS FOR STEAM GENERATORS

R. L. Klueh

The steam generator for the LMFBR demonstration plant will probably be constructed of a ferritic steel or Incoloy 800. The mechanical properties program on steam generator materials comprises a determination of the important properties of welds and base metals as required by RDT and ASME elevated-temperature design requirements. Properties are to be measured for base metal and weld metal of 2¼% Cr-1% Mo steel (Croloy) and Incoloy 800 and to a limited extent on stabilized 2¼% Cr-1% Mo steel and high-chromium ferritic stainless steels. During the reporting period, all of the mechanical property effort was on the unstabilized 2¼% Cr-1% Mo steels.

A potential problem with the use of standard 2¼% Cr-1% Mo steel, which is allowed a maximum of 0.15% C (it usually contains about 0.1%), is the transfer of carbon by flowing sodium from the ferritic steel to the austenitic stainless steel of the intermediate heat exchanger. Such a transfer could lower the strength of the Croloy and embrittle the stainless steel. One possible remedy is to decrease the carbon level of the Croloy to near the solid solubility limit.

We are studying the mechanical properties of base metal and welds from laboratory heats of 2¼% Cr-1% Mo with three carbon levels, designated low, medium, and high (the high-carbon material is typical of a 2¼% Cr-1% Mo steel, ASTM A213-T-22 and ASTM A387 grade D). Weld metal and transverse weldment specimens were made from ½-in. plates (0.003, 0.035, and 0.110% C) that had been normalized 1 hr at 927°C and tempered for 1 hr at 704°C before welding. Base metal properties for normalized and tempered material (1 hr at 927°C, 1 hr at 704°C) were determined from specimens taken from ⅞-in. rods (0.009, 0.030, and 0.120% C). A 1-in. plate of commercial Croloy (0.135% C) is also being factored into the program.

Weldments

The tensile properties of all weld metal and transverse weld specimens were determined at room temperature and 565°C. For the weld metal the yield and tensile stresses increased with increasing carbon content and decreased after tempering for 1 hr at 704°C (the largest effect of tempering was in the high-carbon alloy). The uniform strain values range from 3 to 12% and the total strains from 8 to 20%, with little systematic variation; reductions of area are quite large, indicating low uniform elongation but high local strains at fracture.

The tensile properties of the transverse weld specimens also show increasing strength with increasing carbon content, although the difference is small at 565°C; strength values decrease and ductility values increase with tempering. Although the strength values are all below those for the weld metal, there is little difference in the ductility parameters. Fractures occurred in the base metal.

We collected creep-rupture data for weld metal and transverse welds of the modified carbon steels at 565°C and have begun tests at 510°C. Creep-rupture curves and minimum creep rates at 565°C are given in Figs. 19.4 and 19.5 for tempered weld metal and transverse welds, respectively. Examination of Fig. 19.5a shows little difference in the stress-rupture properties for the low- and medium-carbon steels for the transverse welds (only one curve is given for both materials). There appear to be separate curves for the three weld metals (Fig. 19.4a), although the difference for the low- and medium-carbon steels is small (Fig. 19.4b). A stress-rupture curve for annealed weld metal, taken from Smith's compilation of elevated-temperature properties for standard Croloy,³ is also shown. The weld metal data for the high-carbon alloy seem to lie on this curve.

In all cases, the weld metal curves of Fig. 19.4 fall above those for the transverse welds of Fig. 19.5. Examination of the failures of the transverse welds by light microscopy and comparison of the failed specimens with macroetched specimens of similarly welded materials indicated that the failures occurred in the base metal that was unaffected by welding. Limited data on base metal taken from the plates on which the welds were made verified this conclusion.

Base Metal

Specimens from the ⅞-in.-diam rod with variable carbon content and the 1-in. plate of standard Croloy were tensile tested in the range 25 to 565°C. The data have been compared with a scatter band from Smith's compilation.³ The results for the high-carbon rod and the standard Croloy plate — both comparable to the materials in Smith's compilation — fall at the top of Smith's scatter band for yield and tensile strength and just below the elongation band. The low- and medium-carbon steels have similar properties that fall just below the scatter band for yield and tensile strength and at the upper end of the scatter band for elongation.

Creep-rupture data for the three steels (⅞-in. rod) with different carbon contents and the 1-in. plate of commercial Croloy were determined at 565°C, and tests at 510°C began. Creep-rupture curves for 565°C are given in Fig. 19.6a along with a curve for normalized

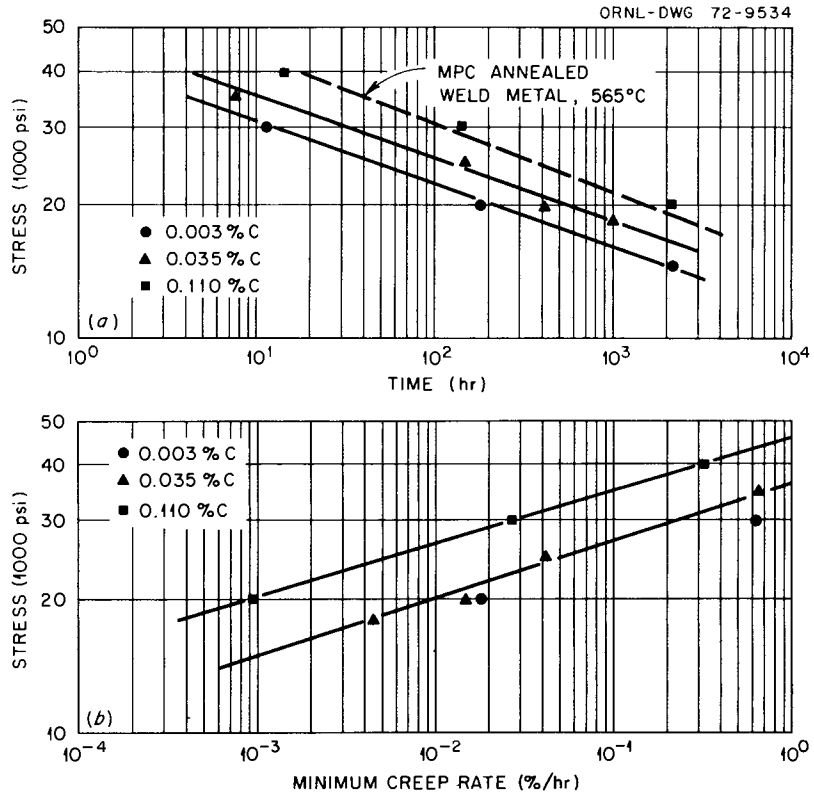


Fig. 19.4. Creep-rupture properties of tempered $2\frac{1}{4}\%$ Cr-1% Mo weld metal at 565°C. (a) Rupture life. (b) Minimum creep rate.

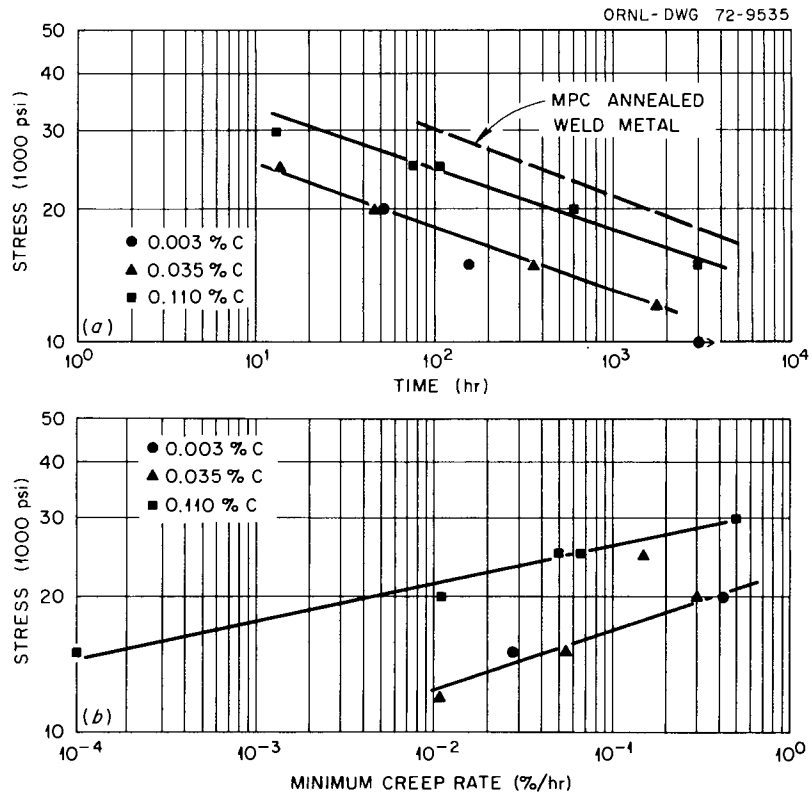


Fig. 19.5. Creep-rupture properties of tempered (after welding) $2\frac{1}{4}\%$ Cr-1% Mo transverse welds at 565°C. (a) Rupture life. (b) Minimum creep rate.

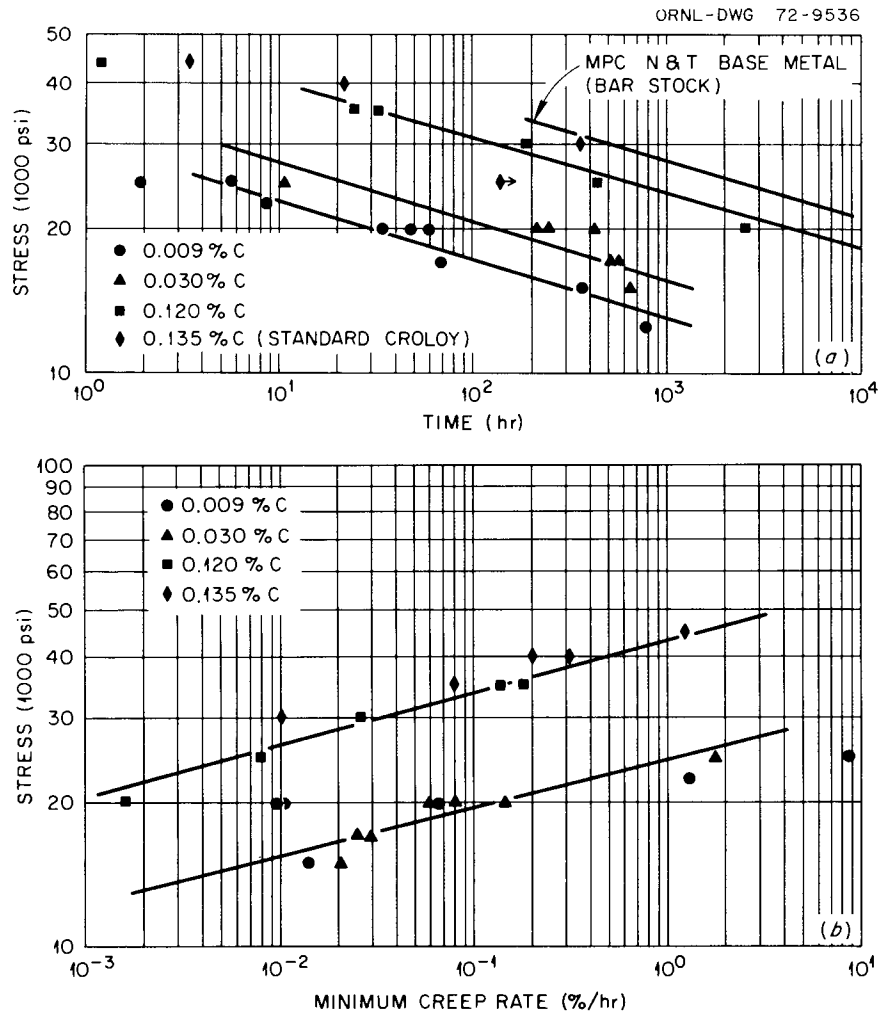


Fig. 19.6. Creep-rupture properties of normalized and tempered $2\frac{1}{4}\%$ Cr-1% Mo steel at 565°C . (a) Rupture life. (b) Minimum creep rate.

and tempered bar taken from Smith.³ Figure 19.6b gives minimum creep rates as a function of stress at 565°C (Smith has only two minimum creep rate data

3. G. V. Smith, *An Evaluation of the Elevated Temperature Tensile and Creep-Rupture Properties of $2\frac{1}{4}\%$ Cr-1% Mo Steel*, to be published by the American Society for Testing and Materials, Philadelphia.

points at 565°C , both in agreement with the data for the high-carbon rod and standard Croloy plate).

In general, the strength increases with increasing carbon, although the low- and medium-carbon steels again show similar properties, especially the rate data in Fig. 19.6b. Likewise, the high-carbon rod and 1-in. plate have similar properties at 565°C .

20. Nondestructive Test Development

R. W. McClung

This program is designed to develop new and improved methods of examining materials and components for the Liquid Metal Fast Breeder Reactor (LMFBR). To achieve this, we study the pertinent physical phenomena, develop instrumentation and other equipment, devise application techniques, and design and fabricate reference standards. Among the methods being studied are electromagnetic induction, ultrasonics, and penetrating radiation. Special emphasis is being given to developing techniques for inspection problems related to steam generators.

NONDESTRUCTIVE TEST DEVELOPMENT FOR STEAM GENERATORS

R. W. McClung

We began a development program to solve specific problems of nondestructive testing of steam generators for LMFBR. The inspection of bore-side tube-to-tube-sheet joints is emphasized, although other problems such as in-place inspection of tubing will also receive attention.

Radiography

B. E. Foster R. W. McClung

We began an investigation of the availability and capability of radiographic equipment (x-ray tubes, isotopic sources) for inspection of the bore-side weld. In conjunction with other European travel, Roentgen Technische Dienst in Rotterdam, Holland, was visited to see and discuss the small-diameter, long-rod-anode x-ray tube developed there.¹

We borrowed a small-rod-anode x-ray tube and generator from the Los Alamos Scientific Laboratory (LASL). Measuring the focal spot of the x-ray tube, we demonstrated that the beam was out of focus and the focal spot was much larger than desired. Extensive

1. R. W. McClung and B. E. Foster, *Fuels and Materials Development Program Quart. Progr. Rep. Dec. 31, 1971*, ORNL-TM-3703, pp. 177-78.

effort was devoted to developing techniques to achieve and assure proper alignment and focusing.²

For initial evaluation of this rod-anode tube, a preliminary standard was fabricated from a stainless steel tube 0.625 in. OD with 0.100 in. wall. We used the Electro-Discharge Machining (EDM) technique to put flat-bottom holes (0.002 in. diam \times 0.002 in. deep, 0.005 in. diam \times 0.005 in. deep, and 0.010 in. diam \times 0.005 in. deep) in the inner surface of the wall.

Penetrators are being fabricated from stainless steel with thicknesses from 0.001 to 0.010 in., each with 0.005, 0.010, and 0.020-in.-diam holes. These penetrators can be placed on the outer and inner wall of the tubing for radiography and system evaluation.

We are also fabricating a film loading-and-clamp mechanism to support the film around the tubing and facilitate loading and unloading the film. Appropriate radioisotopic sources are being acquired.

Liquid Penetrants

K. V. Cook B. E. Foster

We are developing techniques for liquid-penetrant inspection of the tube-to-tube-sheet weld joints. We have developed preliminary hardware for penetrant application and removal, for scanning tubing bores, and for coupling closed-circuit television to the borescope.³ Because of limited illumination⁴ with fluorescent penetrants, we have selected a red-dye visible penetrant. This improved the lighting problem, but slightly brighter illumination than that from our available borescope is desirable. We are investigating new, commercially available borescope systems.

2. B. E. Foster and R. W. McClung, *Fuels and Materials Development Program Quart. Progr. Rep. Mar. 31, 1972*, ORNL-TM-3797, pp. 180-81.

3. K. V. Cook and B. E. Foster, *Fuels and Materials Development Program Quart. Progr. Rep. Dec. 31, 1971*, ORNL-TM-3703, pp. 178-79.

4. K. V. Cook and B. E. Foster, *Fuels and Materials Development Program Quart. Progr. Rep. Mar. 31, 1972*, ORNL-TM-3797, p. 181.

Eddy Currents

C. V. Dodd W. A. Simpson

We are continuing our investigations into the design of an eddy-current system for the detection of defects in tubular sections.^{5,6} This is the first stage of studies for the inspection of tube-to-tube-sheet joints and the in-place inspection of tubing. In the initial phase we considered two approaches. The first employed a dual encircling-coil bridge system, which was designed to be operated in an unbalanced mode. This configuration provides maximum rejection of diametral and conductivity variations, but it has the inherent disadvantage of low sensitivity to surface defects. The second design used a reflection-type encircling coil. This system is similar to a balanced bridge configuration in its rejection of diametral changes, but it has slightly greater sensitivity than the dual encircling-coil system to deep defects, vastly greater sensitivity to surface defects, and less sensitivity to drifts in the driving circuit elements. A prototype coil of this design was ordered and tested. It exhibited good sensitivity to defects, but the response to diametral changes was somewhat higher than we had hoped. This was not unexpected, since the rejection of diametral changes is achieved in this design merely by placing the pickup coils close together, thereby minimizing the response to changes that occur over distances larger than the coil separation.

To improve the rejection of diametral changes, we have begun the study of a reflection-type encircling coil whose pickups are operated in an unbalanced mode. This configuration will have additional diametral rejection, and we hope that it will retain the advantages of the reflection-type coil system.

Ultrasonics

K. V. Cook H. L. Whaley

Ultrasonic methods also offer a strong potential for the examination of the tube-to-tube-sheet weldments. The first work is being conducted on flat weld specimens that simulate typical joint configurations to determine optimum test parameters. Methods of introducing calibration notches have been established⁷ and used to develop preliminary scanning techniques.

An x - y - z plan view recording system, which permits continuous, simultaneous, quantitative recording of the analog amplitude of discontinuities as well as their coordinates within the specimen, has been completed and is operational.

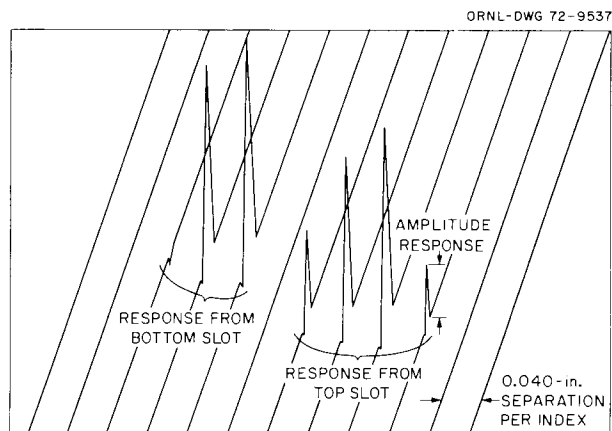


Fig. 20.1. Plan view recording of the ultrasonic response from two circular slots in Croloy $2\frac{1}{2}$ Cr-1% Mo. The specimen is scanned parallel to the slots at 0.040-in. intervals. The recorder is so operated that the traces are diagonal to prevent overlap of the peaks in successive traces.

Figure 20.1 is a plan view recording made on a $\frac{1}{8}$ -in.-thick flat plate (Croloy, $2\frac{1}{4}$ Cr-1 Mo) that contains two circular slots. The depths of the slots (0.026 and 0.039 in.) are greater than will be required for weld inspection but were made large to facilitate equipment development. This recording was made to illustrate the capabilities of the x - y - z recording system that we have assembled. The scan direction, parallel to the notches, produces a skewed y axis trace. After each index along the x axis (each index is perpendicular to the weld), another parallel scan line is produced. If a flaw or notch is detected by the ultrasonic instrumentation, a sudden pen deflection along the y axis is produced that is proportional to the size of the discontinuity detected. Since this analog response appears to produce a third direction, we refer to it as a y' or z response. Displays such as this should be very beneficial in our weld inspection development work and reduce the number of recordings required.

5. C. V. Dodd and W. A. Simpson, *Fuels and Materials Development Program Quart. Progr. Rep. Dec. 31, 1971*, ORNL-TM-3703, pp. 179-80.

6. C. V. Dodd and W. A. Simpson, *Fuels and Materials Development Program Quart. Progr. Rep. Mar. 31, 1972*, ORNL-TM-3797, pp. 181-83.

7. K. V. Cook and H. L. Whaley, *Fuels and Materials Development Program Quart. Progr. Rep. Mar. 31, 1972*, ORNL-TM-3797, pp. 182-84.

ELECTROMAGNETIC INSPECTION METHODS

C. V. Dodd W. A. Simpson C. C. Cheng⁸
W. E. Deeds⁸ J. H. Smith⁹ C. W. Nestor¹⁰

We continued both theoretical and experimental research and development of electromagnetic inspection methods. We are preparing a report;¹¹ the abstract follows.

This report contains the theoretical analysis and computer programs for reflection-type coils above multiple layered conductors. The performance of the coils when connected to phase-sensitive eddy-current instrumentation can be evaluated. The programs calculate the effects of defects or variations in either conductivity or thickness for multiple conductors, all in the presence of lift-off variations. In addition, program options are included that allow the study of the design of the coil, the study of the effects of small variations or drifts of all the coil, conductor, and instrument parameters, and the effect of the instrument transmitting and receiving impedance on the problem. Examples are given of the use of the programs for the design of eddy-current tests with reflection-type coils.

We applied our computer programs to design a series of probes for a wide range of eddy-current problems. These probes have been constructed and tested. We also applied our computer programs to the design of a series of attenuators to match these coils at various frequencies. These attenuators reduce both the system noise and the effects of temperature variations on the coil.

We completed a report on thickness measurements.¹² It discusses the results of recent computer-based and experimental studies related to the design of optimum test conditions for measuring both the thickness of a single conductor and the thickness of one conductor clad on another. The various graphs in the report provide insight on the effects on thickness measurement of such variables as frequency, coil size, specimen conductivity, coil-to-conductor spacing, and coil resistance, allowing simple design of optimum test parameters and prediction of attainable results.

8. Consultant from the University of Tennessee.

9. On assignment from UCN Y-12 Plant, Oak Ridge.

10. Mathematics Division.

11. C. V. Dodd, C. C. Cheng, J. H. Smith, and W. E. Deeds, *The Analysis of Reflection-Type Coils for Eddy-Current Testing*, report in preparation.

12. C. V. Dodd and W. A. Simpson, Jr., *Thickness Measurements Using Eddy-Current Techniques*, ORNL-TM-3712 (March 1972); also presented at the Spring Conference of the American Society for Nondestructive Testing, Los Angeles, March 15, 1972.

We completed the computer design, construction, and testing of a new system for measuring the changes in permeability produced in type 316 stainless steel tubing by various degrees of cold working.^{13,14} In application to specimens from various suppliers, we demonstrated that within a batch, the error is about $\pm 0.25\%$ of the cold work. Recalibration will be necessary for different vendors and heats.

Under separate funding, we completed the design and testing of an induction probe to measure the level of molten bismuth in a chemical processing system. The probe will measure the level over a $13\frac{5}{8}$ -in. range with a resolution of 10 mils. The average temperature coefficient of the probe is less than 8 mils/ $^{\circ}\text{C}$ level change over a range of 550 to 700 $^{\circ}\text{C}$. The probe has a zero temperature coefficient from 600 to 625 $^{\circ}\text{C}$. There is excellent agreement between the calculated and experimental probe sensitivity and temperature coefficient. The associated phase-sensitive instrumentation can be adjusted to give direct level readings to within ± 0.01 in.

We completed both the ac and dc measurements on 13 different conductors. A statistical analysis on the measurements gave an estimated accuracy of the conductivity of $\pm 0.1\%$.

We improved the modular phase-sensitive eddy-current instrument. The temperature coefficient of the measurements of phase shift is now less than $0.01^{\circ}/^{\circ}\text{C}$. The chassis of the instrument was revised to allow multiple frequency measurements with analog computer corrections of variable parameters. Also, the instrument can make differential magnitude measurements. This allows highly accurate lift-off measurements to be made over a very wide range of lift-off.

ULTRASONIC INSPECTION METHODS

H. L. Whaley K. V. Cook Laszlo Adler⁸

Frequency Analysis

We continued studying the frequency effects in ultrasonic testing by means of spectral analysis, with emphasis on the use of frequency analysis for the

13. C. V. Dodd and W. A. Simpson, *Metals and Ceramics Division Annu. Progr. Rep. June 30, 1971*, ORNL-4770, pp. 100-101.

14. C. V. Dodd et al., *Fuels and Materials Development Program Quart. Progr. Rep. Sept. 30, 1971*, ORNL-TM-3550, pp. 168-69.

characterization of flaws. Several papers¹⁵⁻¹⁹ on this work have been prepared. The following two abstracts briefly describe the approach and some of the accomplishments:

A new method was developed for the characterization (determination of the size and orientation) of a reflector by ultrasonic spectral analysis. This technique can be used to determine nondestructively the nature of flaws detected in a material by means of ultrasonic examination. It is shown that it is feasible to characterize a flaw by this technique in spite of its composition (i.e., crack, void, or inclusion) or shape and without the need for a calibration standard. This technique is free of several limitations inherent in techniques based on amplitude. The results presented here are based on a series of reflection experiments in which the ends of solid rods immersed in water and machined discontinuities in metal samples were used as reflectors. Broad-band ultrasonic pulses were analyzed after reflection from the interface of interest. A physical and analytical model was developed based on an interference mechanism that results from the superposition of spherical wavelets emitted from opposing extremes of the reflector. This model explains very well the experimentally observed spectral variations in terms of size and three-dimensional angular orientation of the reflector, distance between the transducer and reflector, and displacement of the reflector from the axis of the transducer for a flat reflector of any composition. Based on this technique, a detailed procedure can be outlined for characterizing a randomly oriented natural flaw in a plate. The feasibility and practicality of using this technique to test various materials and in automated testing systems were considered.¹⁵

In an earlier paper, we have shown that the frequency analysis of a broad-band ultrasonic echo may be used to determine the size and orientation of flat circular reflectors. A single transducer was used as both source and receiver. The one-transducer is not completely satisfactory for the case of discontinuities having both random shape and orientation. Recently, we have used a second transducer to receive ultrasonic pulses scattered by a reflector. Defects in materials were simulated by irregularly shaped metal shims suspended with random orientation in water. The received frequency spectrum when analyzed shows characteristic maxima and minima, which depend on the shape, size, and orientation of the reflectors. A model – which assumes an interference pattern formation of the scattered spherical wavelets at the receiver – relates the spacing between frequency maxima and the positions of the two transducers to the size and orientation of the “discontinuities.” The measurement and the analysis are greatly simplified with the use of the second transducer, and size determination of the discontinuities can usually be made within 10–20%.¹⁹

We continued development of the two-transducer method²⁰ for ultrasonic frequency analysis because of its much greater simplicity for determining the size of a randomly oriented reflector (or flaw). An initial problem was encountered when the reflector was oriented to allow specular reflections to reach the receiving transducer. A method for avoiding this type of reflected energy was adopted. We wrote a computer program that determines the size of a randomly oriented reflector

from the spectral data obtained by the two-transducer method. Practical guidelines for obtaining optimum data by this technique were developed. The instruments used in this system were consolidated into a mobile rack mount to conserve space, simplify operation, and allow the system to be used conveniently at various places in the laboratory.²¹ Only two coaxial cable connections are required now to include the capabilities of frequency analysis in any ultrasonic test at any location in the laboratory. This mobile system was “debugged” by collecting detailed spectral data on reflections from a number of irregularly shaped and oriented brass shims. Computer analysis of these data yielded good determinations of the sizes of the reflectors. This would not have been possible with the one-transducer method. We can apparently tell the difference between spherical and cylindrical reflectors by the two-transducer method. The analysis of machined notches in metal blocks by the two-transducer and one-transducer methods indicates that notch (or crack) depth can be determined by spectral analysis of ultrasonic energy scattered from the notch. A physical model has been developed to describe the observed spectral variations. Spectra obtained with notches and side-drilled reference holes are also being compared.

Ultrasonic Imaging

We improved the ability of the schlieren system to effectively image ultrasound at higher frequencies (10 to

15. H. L. Whaley and L. Adler, “Flaw Characterization by Ultrasonic Frequency Analysis,” *Mater. Eval.* **25**, 182–88, 192 (1971).

16. H. L. Whaley and L. Adler, “A New Approach to the Old Problem of Determining Flaw Size,” *Int. J. Fract. Mech.* **8**, 112–13 (1972).

17. L. Adler and H. L. Whaley, “Interference Effect in a Multifrequency Ultrasonic Pulse Echo and Its Application to Flaw Characterization,” *J. Acoust. Soc. Amer.* **51**, part 2, 881–87 (1972).

18. H. L. Whaley and L. Adler, “Determining the Size of Flaws in Materials,” *Instrum. Contr. Syst.* **44**, 98–102 (1971).

19. L. Adler and H. L. Whaley “Advantages of a Two-Transducer Technique for Ultrasonic Frequency Analysis,” presented at 83rd meeting of the Acoustical Society of America, April 18–21, 1972, Buffalo, N.Y.; submitted for publication in *Journal of the Acoustical Society of America*.

20. H. L. Whaley, K. V. Cook, and L. Adler, *Fuels and Materials Development Quart. Progr. Rep. Dec. 31, 1971*, ORNL-TM-3703, p. 185.

21. H. L. Whaley, K. V. Cook, and L. Adler, *Fuels and Materials Development Program Quart. Progr. Rep. Mar. 31, 1972*, ORNL-TM-3797, pp. 173–77.

20 MHz).²² A second radio-frequency oscillator was obtained and modified for high-power applications, in which the transducers must be driven with large amplitude. The schlieren inspection of the stainless steel weld samples was completed.²² Several test configurations were employed at various ultrasonic frequencies to determine optimum conditions. These tests were recorded on video tape. Effects of known defect areas in the welds on the propagation of ultrasound in the specimens were observed, but interpretation was difficult. The optical table and equipment reserved for prototype optical systems were used to construct an experimental interferometric system for imaging ultrasound.²³ This method was successful in forming an image of the ultrasonic beam, but the optical system could not provide the stability necessary to maintain a setup. The same optical table and equipment were used to construct a Bragg diffraction imaging system. Necessary mechanical fixtures were designed and built, and rudimentary images of objects placed in the path of the ultrasound were obtained. Design of a larger, more versatile, sensitive, and stable system was undertaken. A pulsed laser and all other necessary optical components for this system have been ordered. We built and tested 1- and 2-in.² transducers for use with this system. Additional mechanical fixturing for this system has also been designed and built.

PENETRATING RADIATION INSPECTION METHODS

B. E. Foster S. D. Snyder

We continued our development of a closed-circuit television (CCTV) system²⁴⁻²⁶ for enhancing and interpreting radiographs. Tests were conducted to optimize the settings of the various controls for system response and sensitivity. A radiograph on a high-resolution plate of 400-mesh screen has been used as a standard for assessing resolution capability of the system. With an optical magnification of only 2.3X, we were able to image a crack or break in a single 30- μm -diam wire of the 400-mesh screen. The 2.3X optical magnification results in a total image enlarge-

ment of 40X when combined with the 17.5X from the Vidicon mosaic to the monitor screen.

The system allows selection of one or more of the 500 lines of video on the monitor for closer examination as well as any section of any of the lines. This selected region can be recorded on a strip chart or x-y recorder for further study. Any area of the image on the monitor screen can be selected and shaded (darkened or lightened) for more contrast and more comfortable viewing. This effect is quite similar to the split-screen viewing on a home television receiver, except in that case, the studio is using multiple cameras rather than a single camera.

The system is presently being applied to an intriguing problem on the heater bundle of the Fuel Failure Mockup (FFM). The engineering concern is possible movement of the heater elements during operation. The heater bundle was radiographed with a ⁶⁰Co source at conditions of (1) no load, (2) elevated temperature, and (3) flowing sodium. We are using the CCTV system to enlarge and enhance the region of interest on the radiograph. By selecting a portion of the proper scan line from the television raster we can produce an x-y recording from which we can measure the dimensions between a peripheral element and the surrounding clamp. Preliminary results are promising, with dimensional variations readily observable. We are calibrating the system to allow determination of accuracy and precision of the measurements.

22. H. L. Whaley, K. V. Cook, and L. Adler, *Fuels and Materials Development Program Quart. Progr. Rep. Sept. 30, 1971*, ORNL-TM-3550, pp. 171-72.

23. K. V. Cook, H. L. Whaley, and L. Adler, *Fuels and Materials Development Program Quart. Progr. Rep. Dec. 31, 1971*, ORNL-TM-3703, p. 186.

24. B. E. Foster and S. D. Snyder, *Fuels and Materials Development Program Quart. Progr. Rep. Sept. 30, 1971*, ORNL-TM-3550, pp. 173-74.

25. B. E. Foster and S. D. Snyder, *Fuels and Materials Development Program Quart. Progr. Rep. Dec. 31, 1971*, ORNL-TM-3703, p. 187.

26. B. E. Foster and S. D. Snyder, *Fuels and Materials Development Program Quart. Progr. Rep. Mar. 31, 1972*, ORNL-TM-3797, pp. 177-79.

Part III. Space Power Technology

21. Cladding Materials for Space Isotopic Heat Sources

R. G. Donnelly

The purpose of this program is to develop high-melting, oxidation resistant alloys for space applications of isotopic heat source capsules operating between 900 and 1300°C. This requires alloys exhibiting superior performance under operational, abort, reentry, earth impact, and postimpact conditions. Potential applications are as fuel containment materials in $^{238}\text{PuO}_2$ - and $^{244}\text{Cm}_2\text{O}_3$ -fueled thermoelectric generators, such as the Multihundred Watt (MHW) generator now under development and advanced versions of the SNAP-19 generator as used aboard the Pioneer space probe.

NEW PLATINUM-RHODIUM-TUNGSTEN ALLOYS FOR SPACE ISOTOPIC HEAT SOURCES¹

H. Inouye C. T. Liu
R. G. Donnelly

Multiple layers of refractory alloys clad with a platinum-rhodium alloy are now used as the capsulating materials for the fuel in isotopic heat sources. In this design one alloy compensates for the shortcomings of another. This method was developed because no single alloy of current manufacture can meet the severe service and safety requirements of thermoelectric generators for space power. However, improvements in oxidation resistance and compatibility with heat source environment over those obtainable with the refractory alloy components in such capsule assemblies are desired. The conventional platinum-rhodium alloy cladding, although possessing excellent fabricability and oxidation resistance, lacks the desired mechanical strength and high melting temperatures. Our program objective has been to develop fabricable alloys with

better strength, oxidation resistance, compatibility, and melting temperatures.

The new platinum-base alloys containing 25 to 30 Rh, 6 to 10 W, 0 to 1.0 Hf, and 0 to 0.5 Ti (wt %) can be fabricated by hot rolling in air between 1000 and 1250°C followed by cold working at room temperature with intermediate anneals. The formability is quite good: a 1¼-in.-diam hemisphere of the Pt-30% Rh-8% W-0.25% Hf-0.10% Ti alloy was made from a 0.030-in.-thick blank by cold forming over a mandrel, with two intermediate anneals at 1200°C.

The tensile properties of the new alloys were determined at temperatures to 1316°C. The tensile strengths increase with the tungsten content. Hafnium and titanium additions further improve the strength of the ternary alloy base, especially at the higher temperatures. Also, the hafnium and titanium additions inhibit grain growth and increase the 1-hr recrystallization temperature from 1050 to 1200°C. The new alloys are much stronger than Pt-30% Rh, iridium, and TZM at temperatures to 1093°C and are comparable to iridium and TZM at 1316°C. In terms of the impact resistance [defined as fracture strain \times (UTS + YS)/2] at 1316°C, the Pt-30% Rh-8% W-1.0% Hf-0.2% Ti is the best among all the candidate alloys (see Fig. 21.1).

To further qualify the use of Pt-Rh-W alloys as the capsulating material, sheet specimens were held at 1100°C in 1×10^{-5} torr oxygen. After 253 hr the alloy showed only a small reduction of the room-temperature ductility and no change in the 825°C ductility.

The oxidation behavior for these alloys was determined at 760, 1000, and 1200°C in air. Alloying with up to 10% W, 1% Hf, and 0.5% Ti did not impair the excellent oxidation resistance of the Pt-30% Rh base. The oxidation rates for the alloys are only 5 times those for unalloyed platinum but lower than those of

1. Summary of talk presented at ANS meeting in Las Vegas, Nevada, June 1972; ORNL-4813 (in press).

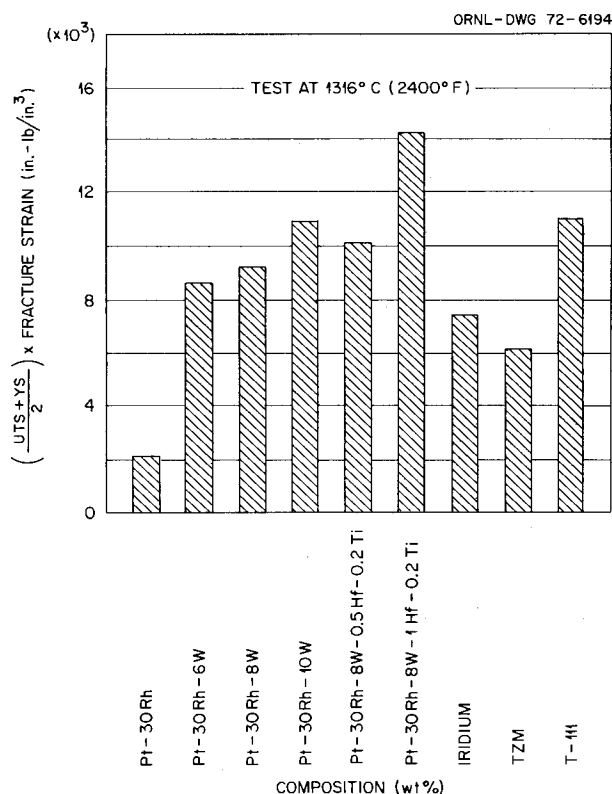


Fig. 21.1. Impact capabilities of cladding materials for isotopic heat sources.

molybdenum- and tantalum-base alloys by four orders of magnitude.

CHARACTERIZATION OF Pt-Rh-W ALLOYS

J. H. Erwin H. Inouye

A family of improved platinum alloys containing 26 to 30% Rh and 6 to 10% W as the principal alloying elements was recently developed for possible use in thermoelectric generators for space power. In a typical application, alloy sheet would be used to encapsulate the isotopic fuel in the heat source. The objective of this study is to fully characterize one or two alloys to qualify them for this application.

Four-pound ingots of Pt-2608 (nominal composition Pt-26% Rh-8% W) have been routinely hot rolled between 1000 and 1200°C in air to sheet 0.040 to 0.050 in. thick, then cold rolled to 0.030 in. at room

temperature. The formability of sheet thus produced and as determined by a modified Olsen cup test depends on the annealing temperature of the test blanks. Optimum formability as evidenced by the maximum in the cup height occurs in blanks annealed at approximately 1000°C. This temperature is at or just below the recrystallization temperature of this alloy.

Eddy-current inspection of sheet produced from several heats sometimes revealed isolated areas of inhomogeneity. Metallographic examination of these areas showed narrow stringers of a hard second phase, which was identified as unmelted tungsten by x-ray analysis. Segregated tungsten causes laminations in formed parts and low tensile properties. This problem has been overcome through the use of powdered tungsten and a modified melting procedure.

CHARACTERIZATION OF IRIIDIUM

C. T. Liu

The isotopic fuel in a heat source of an advanced radioisotope thermoelectric generator (RTG) for space power will be clad with iridium. One of the principal requirements of the cladding is to contain the fuel under accident conditions, such as a launch abort or unplanned reentry from earth orbit and subsequent earth impact. Tensile properties of iridium were determined at possible launch abort temperatures. No well-defined ductile-to-brittle transition temperature (DBTT) was observed in terms of the elongation. Reduction in area did increase significantly above 500°C, which is in agreement with the DBTT as reported in the literature.² The fracture surfaces showed a brittle-to-ductile transition between 500 and 760°C.

Iridium annealed at 1500°C and then subjected to a heat pulse of 2000°C for 5 min, which simulates reentry heating, has significantly lower yield strength than as-annealed specimens at room temperature and 1093°C. Most significant is the serious loss of ductility at 1093°C caused by the heat pulse. The tensile properties of iridium at 1316°C were unaffected by the heat pulse.

2. R. W. Douglas et al., *High Temperature Properties and Alloying Behavior of Refractory Platinum Group Metals*, NP-10939, Battelle Memorial Institute (August 1961).

22. Development of Uranium Nitride Fuels for NASA

J. L. Scott

A technology program for a compact fast reactor for space power is in progress at the NASA Lewis Research Center. The 2-MW reactor uses UN fuel clad in T-111 and is cooled with lithium.¹ Its lifetime is 50,000 hr with a coolant outlet temperature of 1220°K. In support of the program, we are conducting both irradiation tests of prototypic pins and basic fabrication studies on UN. These activities are a follow-on to a basic UN development program previously funded at ORNL by the AEC. One irradiation capsule, UN-6, contains UO₂, which is a backup to UN for the compact fast reactor.

IRRADIATION TESTING OF URANIUM NITRIDE

T. N. Washburn B. Fleischer K. R. Thoms²

The irradiation of capsules UN-4 and UN-5 in the ORR was continued during the last year, and a third capsule experiment, UN-6, containing UO₂ pellets was inserted August 3, 1971. Detailed descriptions of our capsule design³ and previous test results⁴⁻⁶ have been reported. After 1550 hr of operation at a cladding temperature of about 850°C, the heat rating of capsule UN-6 was increased to raise the middle pin cladding temperature to 925 to 960°C while limiting the maximum pin center line to 1600°C. The status of the three capsules as of May 1972 is given in Table 22.1.

Cladding thermocouple failure due to shorting, which forms a new junction, was the principal operational difficulty. Sufficient operating experience was obtained before failure of the thermocouples, however, to permit continued irradiation of the capsules. Capsule temperatures were inferred from calorimetric measurements.

In the NaK blanket gas ¹³³Xe was detected after about 6000 hr of irradiation of UN-4 and 8500 hr of irradiation of UN-5. The activity found was quite small, amounting to about 10⁻⁵ of the fission-product gas present in the capsules. The source of the activity will be determined by postirradiation examination.

1. M. H. Krasner, H. W. Davison, and A. J. Diaguila, *Conceptual Design of a Compact Fast Reactor for Space Power*, NASA-TMX-67859 (June 13, 1971).

2. Reactor Division.

3. V. A. DeCarlo, F. R. McQuilkin, R. L. Senn, K. R. Thoms, and S. C. Weaver, *Design of a Capsule for Irradiation Testing of Uranium Nitride Fuel*, ORNL-TM-2363 (February 1969).

4. T. N. Washburn, D. R. Cuneo, and E. L. Long, Jr., "Irradiation Performance of Uranium Nitride at 1500°C," *Amer. Ceram. Soc. Bull.* **50**, 427 (1971).

5. T. N. Washburn, K. R. Thoms, S. C. Weaver, D. R. Cuneo, and E. L. Long, Jr., "Examination of UN-Fueled Pins Irradiated at 1400°C Cladding Temperature," *Trans. Amer. Nucl. Soc.* **13**, 101 (1970).

6. S. C. Weaver, K. R. Thoms, and V. A. DeCarlo, "Irradiation Testing of UN in ORR," *Trans. Amer. Nucl. Soc.* **12**, 547 (1969).

Table 22.1. Status of capsules UN-4, UN-5, and UN-6

Capsule	Irradiation time (hr)	Current cladding temperature ^a (°C)	Average heat generation rate (kW/ft)	Estimated burnup (% FIMA)
UN-4	9310	976	9.9	2.52
UN-5	9000	991	9.6	2.37
UN-6	1550	845 ^b	4.6	
	6050	942	4.9	1.17

^aTemperature of cladding on middle of three pins in capsule.

^bTemperature of cladding for first 1550 hr of irradiation. The heat rating was then increased.

We made neutron radiographs to obtain data on the dimensional behavior of both fuel pins and pellets within each capsule. Very little change was found for any of the pins, but some pellets developed cracks and changed dimensions.

UN FABRICATION STUDIES

R. A. Potter V. J. Tennery

The basic objective of this study was to fabricate 85% dense UN pellets that are thermally stable to about 2300°C. We thermally conditioned powders of uranium nitride at several different temperatures in the range 1100 to 1500°C. The powders were characterized by particle size distribution measurements, specific surface area measurements, and chemical analysis.

Specimens prepared from the conditioned powders were sintered at four different temperatures in the

range 1700 to 2300°C and characterized by density measurements, metallography, porosimetry, and chemical analysis. Specimens prepared from powders conditioned at 1400°C for 3 hr and sintered at 2100°C resulted in microstructures of interest to NASA. They contained interlocking porosity and were about 85% of theoretical density. Specimens of 75% or greater density when thermally tested for 100 hr at 1365°C in vacuum were dimensionally and chemically stable. No change in crystal size was observed; however, some change in pore configuration was detected.

We also developed a process for synthesizing nitrogen-rich uranium sesquinitride powder. Uranium mononitride pellets made from $UN_{1.74}$ densified to approximately 85% of theoretical when sintered at 2300°C. Microstructures were comparable to those of specimens prepared from the 1400°C thermally conditioned powder.

23. Physical Metallurgy of Refractory Alloys

R. G. Donnelly

The program provides a base technology evaluation of materials for use in isotopic heat sources for space power applications. During this period these activities were aimed specifically at solving materials problems encountered in SNAP-19 radioisotope thermoelectric generators for use aboard the Pioneer space probe. These results have further impact because the SNAP-19 generator is also planned for use on the Viking mission to Mars.

EMBRITTLMENT OF T-111 PIONEER FUEL CAPSULES

C. T. Liu H. Inouye

The failure of the T-111 strength member in several test Pioneer heat sources in the summer of 1971 was traced to the embrittlement of the alloy by oxygen contamination. The source of the oxygen was the PuO_2 fuel, the graphite, and the MIN-K insulation. Although the degree of contamination could be reduced by the use of barriers, degassing of the components, and gettering of the noxious gases, oxygen contamination could not be entirely eliminated. Thus, the establishment of the relationship between the oxygen con-

tent and the ductility of T-111 was crucial to qualify the Pioneer heat source for flight by March 1972. The data obtained are shown in Fig. 23.1.

In addition to these vital data, ORNL established (1) that reentry heating can ductilize otherwise brittle T-111 containing up to 4000 ppm O, (2) that the ductility of oxygen-contaminated T-111 is fortuitously a maximum at the design temperature of 825°C, and (3) the reaction kinetic data necessary to estimate the extent of oxygen contamination between the time of fueling the launch.

Molybdenum-base alloys and molybdenum-coated T-111 were found to be suitable alternate "fixes" if the prime fix (method of reducing contamination) mentioned above failed.¹⁻⁴

EVALUATION OF PIONEER TEST CAPSULES

H. Inouye H. E. McCoy, Jr.
E. L. Long, Jr. R. W. Knight

Assistance to the Pioneer project in the fall-winter of 1971 consisted of measuring the mechanical properties of sections of the T-111 strength member cut from test capsules PF-3, PF-7, and PF-9. Tensile and bend tests were coupled with detailed scanning electron microscopic studies of the fracture surfaces to help evaluate the Pioneer "fix."

Consulting services were provided to the Space Nuclear Systems (SNS) Division of the AEC on a

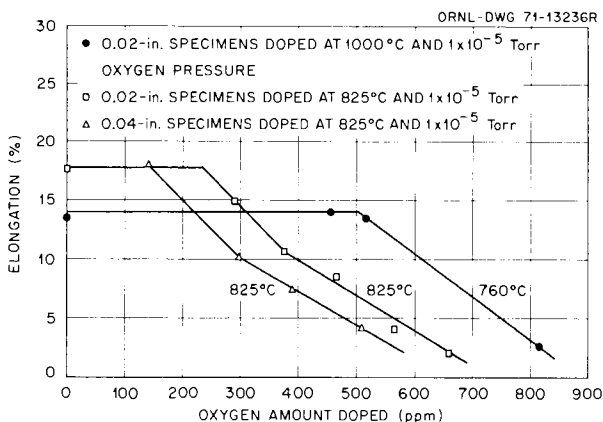


Fig. 23.1. High-temperature ductility of oxygen-doped T-111.

1. C. T. Liu, *Fuels and Materials Development Program Quart. Progr. Rep. Mar. 31, 1971*, ORNL-TM-3416, pp. 194-98.
2. R. G. Donnelly and P. Patriarca, *Fuels and Materials Development Program Quart. Progr. Rep. Sept. 30, 1971*, ORNL-TM-3550, pp. 224-34.
3. R. G. Donnelly and P. Patriarca, *Fuels and Materials Development Program Quart. Progr. Rep. Dec. 31, 1971*, ORNL-TM-3707, pp. 259-74.
4. C. T. Liu, H. Inouye, and R. W. Carpenter, "Mechanical Properties and Structure of Internally Oxidized Ta-8 W-2 Hf (T-111) Alloy," paper presented at AIME Spring Meeting, Boston, May 1972.

variety of problems related to the feasibility of using T-111 as the strength member. Consulting services to Teledyne Isotopes, and SNS subcontractor, were instrumental in salvaging one heat source that was accidentally exposed to air during assembly.

The Metals and Ceramics Division, in cooperation with the Plant and Equipment Division, fabricated palladium housings for the zirconium getters that were incorporated into the Pioneer generators as part of the "fix."

MECHANICAL PROPERTIES AND STRUCTURE OF INTERNALLY OXIDIZED

Ta-8% W-2% Hf (T-111) ALLOY⁵

C. T. Liu H. Inouye
R. W. Carpenter

Effects of internal oxidation on the mechanical properties and structure of Ta-8% W-2% Hf (T-111) alloy have been studied. Internal oxidation treatments

were performed on 0.02-in.-thick sheet material in a furnace at 1000°C and 1×10^{-5} torr dynamic oxygen pressure. After being doped, the specimens were heat treated at various temperatures. Calculations based on the lattice-parameter measurement indicate that the oxygen solubility in T-111 is around 100 ppm at 1700°C. The tensile properties of oxygen-contaminated specimens were determined in vacuum at temperatures to 1316°C (2400°F). The results for specimens with oxygen contents up to 3000 ppm heat treated at 1700°C show a slight increase in strength and a decrease in ductility. Beyond this level, the strength increases and ductility decreases sharply with oxygen contamination. Heat-treated T-111 loses its ductility completely when the oxygen content reaches 4000 ppm; in contrast, the as-doped T-111 is brittle at an oxygen level of only 800 ppm. Extremely fine, coherent precipitates were observed in electron micrographs of as-doped specimens. These coarsen upon annealing and eventually form discrete HfO₂ particles. With an increase of oxygen content, precipitate particles gradually appear on the grain boundaries and finally connect into a network at an oxygen level of 4000 ppm.

5. Summary of paper presented at AIME Spring Meeting, Boston, May 1972.

24. Tungsten Metallurgy

A. C. Schaffhauser

The objective of this program is to provide the base technology on tungsten alloys for advanced space-power and general reactor technology applications. We are developing fabrication processes for tungsten alloys based on modification of conventional extrusion, chemical vapor deposition, and welding techniques. Since the primary criterion for the use of tungsten alloys for these applications is based on the creep properties, we are conducting extensive long-time tests at the temperatures of interest. We are also determining the mechanisms that control the creep behavior and the effect of interactions with the vapor species from an isotope or reactor fuel. The behavior of tungsten alloys under fast-neutron irradiation is also being evaluated.

FABRICATION OF EXPERIMENTAL TUNGSTEN MATERIALS

J. I. Federer R. E. McDonald
A. C. Schaffhauser

We are developing fabrication techniques for experimental tungsten materials needed for the thermionic reactor project. The reference fuel cladding material for this application is chemically vapor deposited (CVD) tungsten. Previously we showed that the creep properties of CVD tungsten depend on the fluorine impurity content of the deposit, which can be controlled by adjusting the deposition parameters.¹ We fabricated a number of large sheet deposits of CVD tungsten having either low (5 to 10 ppm) or high (15 to 25 ppm) fluorine contents. The machining techniques and standard operating procedures have been established for consistently fabricating 12 to 16 creep specimens per deposit. Specimens have been supplied for our creep testing program (see the following section) and a cooperative creep testing program with NASA-Lewis Research Center.

1. R. L. Stephenson and J. I. Federer, "Creep Rupture Properties of CVD-Tungsten," pp. 90-94 in *IEEE Conference Record of 1970 Thermionic Convention Specialist Conference, October 26-29, 1970*, The Institute of Electrical and Electronics Engineers, New York, 1970.

We also developed fabrication techniques for alternate fuel cladding materials. Nominal 1-in.-diam \times 0.040-in.-wall thickness tubes of arc cast tungsten and W-2% ThO₂ machined from extruded tubing were supplied to Gulf General Atomic for thermionic fuel element irradiation testing.

THE HIGH-TEMPERATURE CREEP PROPERTIES OF CHEMICALLY VAPOR DEPOSITED TUNGSTEN²

H. E. McCoy, Jr. J. O. Stiegler
A. C. Schaffhauser

The creep-rupture properties of several deposits of chemically vapor deposited (CVD) tungsten were determined at 1650°C and stresses between 2000 and 10,000 psi. Above 3000 psi the creep-rupture properties could be correlated directly with the fluorine impurity content. Material containing 13 to 25 ppm F had 2 to 10 times longer rupture lives, $1/10$ to $1/100$ the minimum

2. Abstract of paper presented at Third International Conference on Chemical Vapor Deposition, Salt Lake City, Utah, April 24-27, 1972.

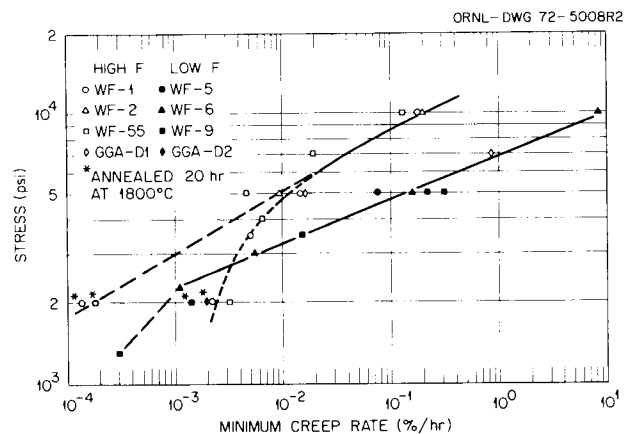


Fig. 24.1. Comparative creep rates of several lots of CVD tungsten at 1650°C. (Low F is 2-7 ppm, high F is 13-25 ppm.)

creep rate, and $\frac{1}{2}$ to $\frac{1}{10}$ the rupture ductility of material containing 2 to 7 ppm F. At stresses between 2000 and 3000 psi the minimum creep rate trend appears to reverse, and the purer material has a lower minimum creep rate (Fig. 24.1). However, annealing 20 hr at 1800°C before testing lowered the minimum creep rate of the high-fluorine material by a factor of 100 but had little effect on the low-fluorine material. This annealing treatment is typical of the thermal history of a thermionic diode during fabrication; therefore, the higher fluorine material appears to have a significant strength advantage for that application.

Electron microscopy of tested creep specimens has shown that the creep properties of CVD tungsten are controlled by fluorine impurities in the form of very small gas bubbles and the stress-induced growth of gas bubbles into grain boundary voids.

LOW-STRESS CREEP TESTING OF TUNGSTEN

A. C. Schaffhauser W. L. McCollough³

We are obtaining design-type creep data on CVD tungsten at stresses to produce 1% creep in 1000 to 50,000 hr. The strain measuring techniques used previously for obtaining creep-rupture data (see preceding section) are not sufficiently accurate at low stresses for design. Five ultrahigh-vacuum, high-temperature creep machines with optical extensometers are collecting the design data required for the thermionic reactor program. The optical strain measurement instrumentation and specimen targets are currently measuring strain to $\pm 3 \times 10^{-4}$ in. accuracy at 1650°C. Design changes in the instrumentation and specimen targets are in progress to obtain even greater accuracy.

A test matrix and cooperative creep testing program with NASA-Lewis Research Center has been established. The primary emphasis is on obtaining data at 1500, 1650, and 1800°C on low-fluorine duplex CVD tungsten,⁴ the reference material for thermionic fuel elements, and high-fluorine material that has greater creep strength.

Creep tests of CVD tungsten at 1650°C and 1000 and 2000 psi are in progress on a duplex deposit (GGA-D2) containing 5 ppm F and a fluoride deposit (WF-55) containing 20 ppm F. All specimens were annealed 20 hr at 1800°C before testing. The 2000-psi data for both deposits are plotted in Fig. 24.1 and confirm the previous results. The high-fluorine material has about $\frac{1}{10}$

the creep rate of the low-fluorine duplex material. Tests in progress at 1000 psi have produced 0.1% strain in 2400 hr for deposit WF-55 and 0.05% strain in 750 hr for deposit GGA-D2.

CREEP PROPERTIES OF W-3.8% ThO₂

H. E. McCoy, Jr.

The creep-rupture properties of W-3.8% ThO₂ have been determined under several conditions. The $\frac{1}{4}$ -in.-diam material was prepared by the Westinghouse Electric Corporation⁵ and had been cold worked 91%. Creep specimens having a gage section 1 in. long \times $\frac{1}{8}$ in. diam were prepared and tested in vacuum in the as-received condition.

The stress-rupture properties are compared in Fig. 24.2 with two previously reported⁶ curves for W-2% ThO₂. The limited number of data points at a given temperature makes it impossible to draw complete stress-rupture curves. The time to rupture at a given stress is not appreciably different for the two materials at 1650°C for rupture times up to 100 hr. For longer rupture times the W-2% ThO₂ deviates from linearity, but the W-3.8% ThO₂ does not appear to have this break. At 2200°C the rupture life of the W-3.8% ThO₂ is about 100 times that of W-2% ThO₂. However, the heat of W-3.8% ThO₂ that we are studying has shorter rupture lives than those reported by Westinghouse for a similar heat, which had 1-hr and 10-hr rupture stresses of 12,500 and 9500 psi respectively.⁷

The minimum creep rates were also measured in these tests. At 1650°C the strengths of the two materials are quite similar. At 2200°C the allowable stress for the W-2% ThO₂ is significantly lower than that for the W-3.8% ThO₂. The fracture strains at all temperatures were good, with the minimum being 7.5% at 2000°C.

EFFECT OF CARBURIZATION ON THE CREEP PROPERTIES OF TUNGSTEN ALLOYS

H. Inouye

The creep properties of 0.040-in. diam tungsten wire are being measured while it is being carburized with low-pressure CH₄ at thermionic temperatures. In tests

5. Westinghouse Electric Corporation, Lamp Division, Bloomfield, N.J.

6. H. E. McCoy, *Creep-Rupture Properties of Tungsten and Tungsten-Base Alloys*, ORNL-3992 (August 1966).

7. H. G. Sell, W. R. Morcom, and G. W. King, *Development of Dispersion Strengthened Tungsten Base Alloys*, AFML-TR-65-407, Part II (1966).

3. Consultant.

4. Supplied by Gulf General Atomic, San Diego, Calif.

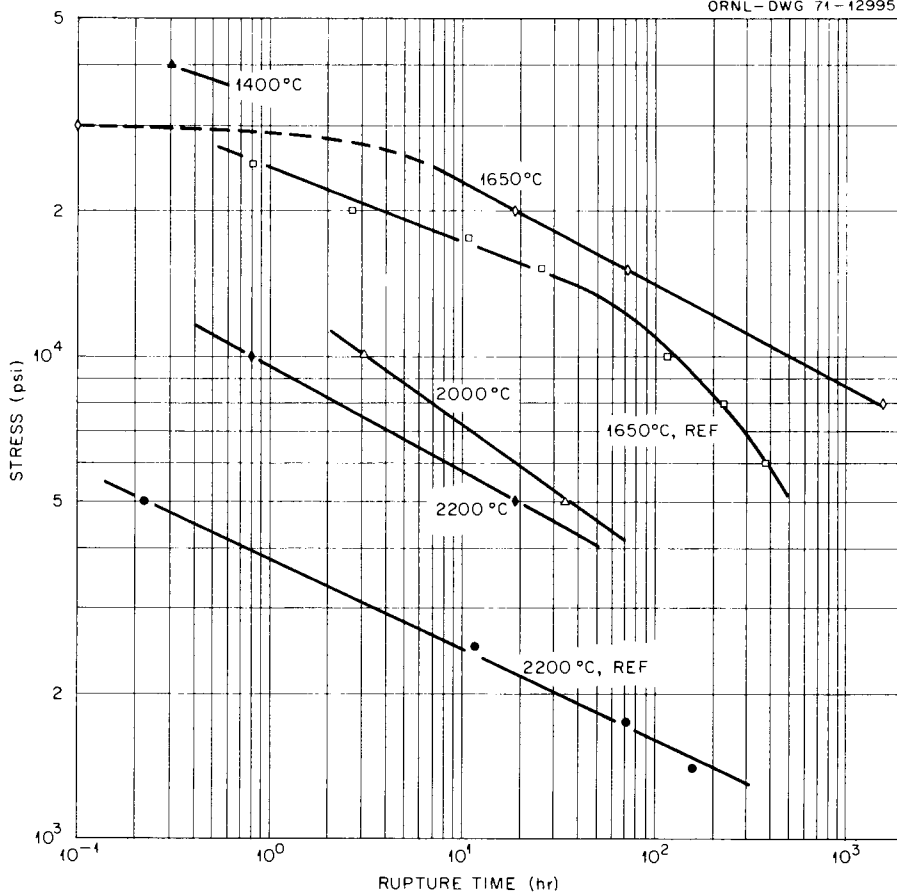


Fig. 24.2. Comparison of stress-rupture properties of W-3.8% ThO₂ with referenced W-2% ThO₂ properties. Ref: H. E. McCoy, *Creep-Rupture Properties of Tungsten and Tungsten-Base Alloys*, ORNL-3992 (1966).

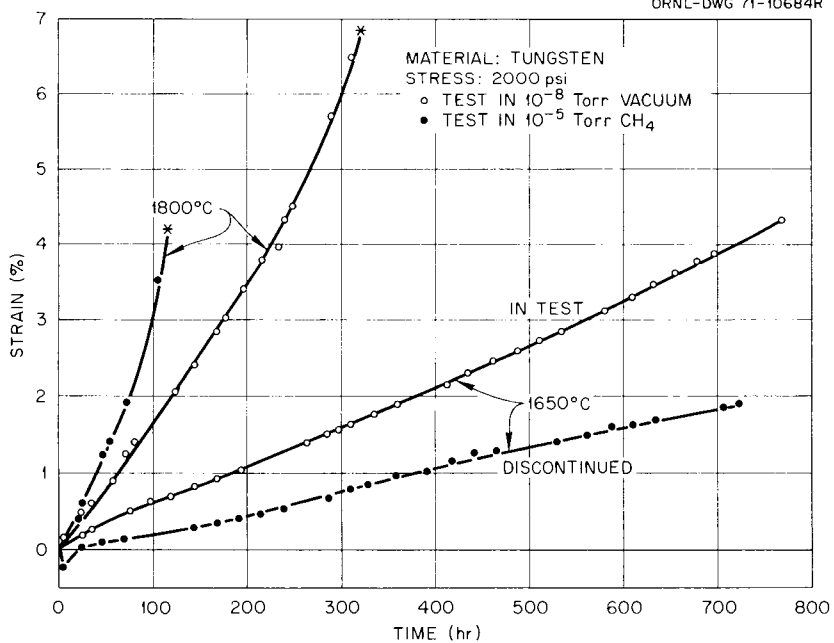


Fig. 24.3. Creep properties of tungsten in vacuum and low-pressure CH₄.

at 1800°C and a stress of 2000 psi, both the rupture ductility and rupture life progressively decreased with the CH₄ pressures; in contrast, tests at 1650°C show the opposite effect. Typical creep curves for tungsten tested in vacuum and in 10⁻⁵ torr CH₄ are shown in Fig. 24.3. X-ray analyses show W₂C on the surfaces of specimens exposed to CH₄ at 1650°C but not on specimens tested 1800°C. Chemical analyses show carbon contents ranging from 1100 to 1800 ppm independent of the CH₄ pressure.

RADIATION DAMAGE TO REFRACTORY METALS AS RELATED TO THERMIONIC APPLICATIONS⁸

F. W. Wiffen

The effects of fast neutron irradiation on the bcc refractory metals are reviewed with emphasis on materials and conditions typical of thermionic applications in space power systems. Changes produced in the microstructure are characterized as a function of irradiation temperature. The effects of fluence, alloying, and purity are examined where data are available. Swelling and changes in the mechanical and electrical properties produced by neutron irradiation are briefly reviewed. The major effects expected are in the collector and cooler portions of the emitter in a thermionic diode where swelling, increases in electrical resistivity, and losses of ductility are anticipated during reactor operation.

HIGH-TEMPERATURE FAST-NEUTRON IRRADIATION OF TUNGSTEN ALLOYS

F. W. Wiffen R. K. Williams

A single-capsule, high-temperature experiment⁹ was irradiated in the EBR-II to a total exposure of 6331

MWd. The calculated peak fluence was $7.8 \pm 2.0 \times 10^{21}$ neutrons/cm² (>0.1 MeV). The capsule contained five specimen holders designed to operate at irradiation temperatures ranging from 600 to 1500°C. The specimen holders contained rod specimens 0.10 in. in diameter, with 2-in.-long specimens for postirradiation resistivity measurements and 1-in.-long specimens for sectioning to provide electron microscopy samples. Sample materials include tungsten and tungsten-rhenium alloys prepared by powder metallurgy, arc melting, and CVD. Postirradiation examination of this experiment will include determination of swelling by measurements of geometry and immersion density, void classification by transmission electron microscopy, and measurements of electrical properties including low- and high-temperature resistivity.

Room temperature electrical resistivity (ρ) data were obtained on three tungsten and three W-25% Re samples that had been irradiated in EBR-II to a fluence of approximately 3.7×10^{22} neutrons/cm² (>0.1 MeV). The tungsten samples were irradiated at nominal temperatures of 800, 900, and 1000°C and the maximum increase in the ρ of those specimens was 17%. This result indicates that irradiation-induced damage at these temperatures does not have a large effect on the ρ of tungsten. The W-25% Re samples were irradiated at 700, 800, and 900°C and the respective changes were +6, -10, and -11%. These results indicate that irradiation induces a phase change or ordering in the alloy, and this possibility is being investigated.

8. Abstracted from ORNL-TM-3629 (February 1972).

9. F. W. Wiffen, *Fuels and Materials Development Program Quart. Progr. Rep. Mar. 31, 1972*, ORNL-TM-3797, pp. 263-66.

Previous reports in this series are:

ORNL-TM-920	Period Ending June 30, 1964
ORNL-TM-960	Period Ending September 30, 1964
ORNL-TM-1000	Period Ending December 31, 1964
ORNL-TM-1100	Period Ending March 31, 1965
ORNL-TM-1200	Period Ending June 30, 1965
ORNL-TM-1270	Period Ending September 30, 1965
ORNL-TM-1400	Period Ending December 31, 1965
ORNL-TM-1500	Period Ending March 31, 1966
ORNL-TM-1570	Period Ending June 30, 1966
ORNL-TM-1700	Period Ending September 30, 1966
ORNL-TM-1720	Period Ending December 31, 1966
ORNL-TM-1825	Period Ending March 31, 1967
ORNL-TM-1941	Period Ending June 30, 1967
ORNL-TM-2020	Period Ending September 30, 1967
ORNL-TM-2090	Period Ending December 31, 1967
ORNL-TM-2217	Period Ending March 31, 1968
ORNL-4330	Period Ending June 30, 1968
ORNL-4350	Period Ending September 30, 1968
ORNL-4390	Period Ending December 31, 1968
ORNL-4420	Period Ending March 31, 1969
ORNL-4440	Period Ending June 30, 1969
ORNL-4480	Period Ending September 30, 1969
ORNL-4520	Period Ending December 31, 1969
ORNL-4560	Period Ending March 31, 1970
ORNL-4600	Period Ending June 30, 1970
ORNL-4630	Period Ending September 30, 1970
ORNL-TM-3300	Period Ending December 31, 1970
ORNL-TM-3416	Period Ending March 31, 1971
ORNL-TM-3540	Period Ending June 30, 1971
ORNL-TM-3550	Period Ending September 30, 1971
ORNL-TM-3703	Period Ending December 31, 1971
ORNL-TM-3797	Period Ending March 31, 1972

INTERNAL DISTRIBUTION

(95 copies)

(3)	Central Research Library	E. L. Long, Jr.
	ORNL - Y-12 Technical Library	A. L. Lotts
	Document Reference Section	T. S. Lundy
(10)	Laboratory Records Department	R. E. MacPherson
	Laboratory Records, ORNL RC	W. R. Martin
	ORNL Patent Office	R. W. McClung
	G. M. Adamson, Jr.	H. E. McCoy, Jr.
	M. Bender	H. C. McCurdy
	S. E. Beall	W. T. McDuffee
	E. E. Bloom	D. L. McElroy
	J. A. Conlin	J. R. McGuffey
	W. B. Cottrell	C. J. McHargue
	J. A. Cox	L. C. Oakes
	R. S. Crouse	(20) P. Patriarca
	F. L. Culler, Jr.	S. Peterson
	J. E. Cunningham	P. L. Rittenhouse
	J. H. DeVan	M. W. Rosenthal
	R. G. Donnelly	A. C. Schaffhauser
	W. P. Eatherly	J. L. Scott
	D. E. Ferguson	J. D. Sease
	W. F. Ferguson	G. M. Slaughter
	M. H. Fontana	J. O. Stiegler
	J. H. Frye, Jr.	D. A. Sundberg
	R. J. Gray	D. B. Trauger
	B. L. Greenstreet	W. E. Unger
	W. R. Grimes	J. E. Van Cleve
	W. O. Harms	T. N. Washburn
(5)	M. R. Hill	J. R. Weir, Jr.
	F. J. Homan	G. D. Whitman
	H. Inouye	R. G. Wymer
	P. R. Kasten	H. L. Yakel

EXTERNAL DISTRIBUTION
(216 copies)

AEC DIVISION OF REACTOR DEVELOPMENT AND TECHNOLOGY, Washington, DC 20545

J. W. Bennett	W. H. McVey
M. Booth	J. J. Morabito
R. W. Cochran	E. C. Norman
J. W. Crawford	R. E. Pahler
G. W. Cunningham	D. Pollock
R. P. Denise	A. J. Pressesky
M. D. Dubrow	T. C. Reuther
H. N. Feinroth	M. A. Rosen
O. P. Gormley	S. Rosen
D. H. Groelsema	F. A. Ross
N. Grossman	M. Shaw
R. D. Hahn	G. L. Sherwood
P. A. Halpine	J. M. Simmons
W. H. Hannum	B. Singer
P. L. Havenstein	E. E. Sinclair
E. E. Hoffman	R. W. Sliger
K. E. Horton	J. F. Smith, Jr.
J. R. Hunter	R. F. Sweek
R. H. Jones	S. A. Szawlewicz
E. E. Kintner	A. N. Tardiff
R. E. Kosiba	A. Van Echo
(5) E. C. Kovacic	C. E. Weber
W. H. Layman	M. J. Whitman
J. E. McEwen	W. A. Williams

AEC DIVISION OF RESEARCH, Washington, DC 20545

L. C. Ianiello
P. W. McDaniel
D. K. Stevens

AEC DIVISION OF REACTOR LICENSING, Washington, DC 20545

(3) P. A. Morris

AEC DIVISION OF REACTOR STANDARDS, Washington, DC 20545

(2) E. G. Case

AEC TECHNICAL INFORMATION CENTER, Office of Information Services, P.O. Box 62,
Oak Ridge, TN 37830

(2) Manager
(17) Manager (for transmittal to members of ACRS)

AEC OAK RIDGE OPERATIONS OFFICE, P.O. Box E, Oak Ridge, TN 37830

Research and Technical Support Division

AEC-RDT SITE REPRESENTATIVES, Oak Ridge National Laboratory, P.O. Box X,
Oak Ridge, TN 37830

D. F. Cope
C. L. Matthews

AEC DIVISION OF NAVAL REACTORS, Washington, DC 20360

R. H. Steele

AEC HEADQUARTERS, Room G-049, Washington, DC 20545

Library

AIR FORCE MATERIALS LABORATORY, Wright-Patterson Air Force Base, OH 45433

C. H. Armbruster
H. M. Burte
I. Perlmutter

AMES LABORATORY, USAEC, Iowa State University, Ames, IA 50010

M. S. Wechsler

ARGONNE NATIONAL LABORATORY, 9700 S. Cass Avenue, Argonne, IL 60439

B.R.T. Frost
M. E. Jackson
J. H. Kittel
M. V. Nevitt
D. R. O'Boyle
P. G. Shewmon
R. C. Vogel

ARGONNE NATIONAL LABORATORY, USAEC, P.O. Box 2108, Idaho Falls,
ID 83401

D. A. Moss

ATOMIC POWER DEVELOPMENT ASSOCIATES, 1911 First Street, Detroit,
MI 48226

A. A. Shoudy, Jr.

ATOMICS INTERNATIONAL, P.O. Box 309, Canoga Park, CA 91304

J. G. Asquith
H. M. Diecamp
R. L. Morgan
T. A. Moss
H. Pearlman

ATOMICS INTERNATIONAL, LIQUID METAL ENGINEERING CENTER, P.O. Box 1449,
Canoga Park, CA 91304

K. L. Adler
E. Rodwell

BABCOCK & WILCOX COMPANY, Beaver Falls, PA 15010

G. F. Tisinai

BABCOCK & WILCOX COMPANY, Lynchburg, VA 24505

C. J. Baroch
S. P. Grant
C. R. Johnson
L. R. Weissert

BATTELLE COLUMBUS LABORATORIES, 505 King Avenue, Columbus, OH 43201

D. Keller
S. J. Paprocki
Defense Materials Information Center

BROOKHAVEN NATIONAL LABORATORY, 29 Cornell Avenue, Upton, Long Island,
NY 11973

D. H. Gurinsky
C. Klamut

BUREAU OF MINES, Albany Metallurgy Research Center, P.O. Box 70,
Albany, OR 97321

Haruo Kato

BUREAU OF MINES, Boulder City, NV 89005

T. A. Sullivan

COMBUSTION ENGINEERING, INC., 911 W. Main St., Chattanooga, TN 37402

R. C. Armstrong
D. Vandergriff
C. T. Ward
Librarian, Metallurgy Laboratory

COMBUSTION ENGINEERING, INC., P.O. Box 500, Windsor, CT 06095

M. Andrews
W. P. Chernock
W. P. Staker

FOSTER WHEELER CORPORATION, John Blizzard Research Center,
Livingston, NJ 07039

W. R. Apblett

GENERAL ELECTRIC COMPANY, P.O. Box 846, Pleasanton, CA 94566

H. W. Alter
Maurice Indig

GENERAL ELECTRIC COMPANY, 175 Curtner Avenue, San Jose, CA 95125

R. R. Asamoto
W. E. Bailey
R. Duncan
J. L. Krankota

GENERAL ELECTRIC COMPANY, 310 DeGuigne Drive, Sunnyvale, CA 94086

R. H. Ball
J. M. Case
R. E. Skavdahl
C. N. Spalaris
E. L. Zebroski
Technical Library

GEORGE C. MARSHALL SPACE FLIGHT CENTER, Huntsville, AL 35812

R. J. Schwinghamer

GULF GENERAL ATOMIC, P.O. Box 608, San Diego, CA 92112

A. J. Goodjohn
J. P. Howe
J. N. Lindgren
J. B. Radcliffe
D. Roberts
J. F. Watson
L. Yang

IDAHO NUCLEAR CORPORATION, P.O. Box 1845, Idaho Falls, ID 83401

W. C. Francis
W. W. Hickman
D. Kaiser
W. A. Yuill

KNOLLS ATOMIC POWER LABORATORY, P.O. Box 1072, Schenectady, NY 12301

R. F. Wojcieszak

LMFBR PROGRAM OFFICE, Argonne National Laboratory, 9700 S. Cass Avenue,
Argonne, IL 60439

A. Amarosi
G. A. Bennet
P. F. Gast
J. M. McKee
J. T. Venard

LOS ALAMOS SCIENTIFIC LABORATORY, P.O. Box 1663, Los Alamos, NM 87544

R. D. Baker

MINE SAFETY APPLIANCES COMPANY, J. T. Ryan Memorial Laboratory,
100 N. Braddock Avenue, Pittsburgh, PA 15208

Library

MOUND LABORATORY, P.O. Box 32, Miamisburg, OH 45342

W. T. Cave
R. E. Vallée

NASA HEADQUARTERS, Code RN, 600 Independence Avenue, Washington, DC
20545

J. J. Lynch

NASA-LEWIS RESEARCH CENTER, 21000 Brookpark Road, Cleveland, OH 44135

G. M. Ault
J.W.R. Creagh
F. E. Rom
L. Rosenblum
N. T. Saunders
C. M. Scheuermann
Roger Smith

NAVAL RESEARCH LABORATORY, Code 6390, Washington, DC 20360

J. R. Hawthorne

O'DONNELL & ASSOCIATES, INC., 5100 Centre Avenue, Pittsburgh, PA 15232

W. J. O'Donnell

PACIFIC NORTHWEST LABORATORIES, USAEC, P.O. Box 550, Richland, WA 99352

T. A. Nemzek

SANDIA CORPORATION, P.O. Box 5800, Albuquerque, NM 87115

J. R. Holland
P. D. O'Brian

SPACE NUCLEAR SYSTEMS OFFICE, AEC, Washington, DC 20545

R. E. Anderson
D. Beard
J. F. Griffo
H. Jaffe
C. E. Johnson
A. P. Litman
J. J. Lombardo
J. A. Powers
F. C. Schwenk

UNION CARBIDE CORPORATION, 270 Park Avenue, New York, NY 10017

J. A. Swartout

UNIVERSITY OF CALIFORNIA, LAWRENCE RADIATION LABORATORY, P.O. Box 808,
Livermore, CA 94550

W. R. Holman
L. W. Roberts
A. J. Rothman

U.S. NAVAL AIR SYSTEM COMMAND (AIR-52031B), Washington, DC 20360

I. Machlin

USAEC SCIENTIFIC REPRESENTATIVE, American Embassy, P.O. Box 40, FPO
New York, NY 09510

W.L.R. Rice

WESTINGHOUSE ADVANCED REACTORS DIVISION, Waltz Mill Site, P.O. Box 158,
Madison, PA 15663

E. C. Bishop
A. Boltax
Theodore Iltis
P. J. Levine
P. Murray
W. E. Ray
J. J. Taylor
G. A. Whitlow

WESTINGHOUSE ADVANCED REACTORS DIVISION, Cheswick Fuel Facility,
P.O. Box 217, Cheswick, PA 15024

P. M. French

WESTINGHOUSE ASTRONUCLEAR LABORATORY, P.O. Box 10864, Pittsburgh,
PA 15231

D. C. Goldberg

WESTINGHOUSE ATOMIC POWER DIVISION, P.O. Box 355, Pittsburgh, PA 15230

Technical Library

WESTINGHOUSE BETTIS ATOMIC POWER DIVISION, P.O. Box 79, West Mifflin,
PA 15122

R. H. Fillnow
P. N. Gustafson
W. Yenascavich
Technical Library

WESTINGHOUSE HANFORD COMPANY, P.O. Box 1970, Richland, WA 99352

E. A. Evans
(5) W. E. Roake
J. Sako
(5) W. F. Sheely

WESTINGHOUSE TAMPA DIVISION, Nuclear Energy Systems, P.O. Box 19218,
Tampa, FL 33616

M. E. Eilbeck
D. G. Harmon
B. King